DISSERTATION

FUNCTIONAL REDUNDANCY BETWEEN THE RAD51 ACCESSORY PROTEINS RAD51AP1 AND RAD54 IN HOMOLOGOUS RECOMBINATION DNA REPAIR

Submitted by

Platon Selemenakis

Graduate Degree Program in Cell and Molecular Biology

In partial fulfillment of the requirements

For the Degree of Doctor of Philosophy

Colorado State University

Fort Collins, Colorado

Spring 2021

Doctoral Committee:

Advisor: Claudia Wiese

Lucas Argueso
Takamitsu Kato
Seonil Kim

ABSTRACT

FUNCTIONAL REDUNDANCY BETWEEN THE RAD51 ACCESSORY PROTEINS RAD51AP1 AND RAD54 IN HOMOLOGOUS RECOMBINATION DNA REPAIR

Cancer is responsible for the death of millions of people annually. Factors that increase the risk of tumorigenesis are endogenous challenges and exogenous compounds. These insults are responsible for the generation of DNA lesions, the most toxic one of which is a DNA double-strand break (DSB). DSBs can be repaired by several different DNA repair pathways, among which homologous recombination (HR) is the least error prone. In HR, DNA strand exchange is mediated by the RAD51 recombinase which forms a nucleoprotein filament on single-stranded DNA for strand invasion. RAD51-mediated strand invasion is supported by the DNA motor protein RAD54 and by the RAD51-Associated Protein 1 (RAD51AP1). While the pre-synaptic steps of HR in human cells have been studied extensively, there are still extensive knowledge gaps with respect to the molecular mechanisms of synapsis and post-synapsis and the roles of RAD51AP1 and RAD54 in these later steps of HR.

Here, I hypothesized that RAD51AP1 and RAD54 may exhibit functional redundancy in human cells. Also, I speculated that *Rad51ap1* disruption in mice would be associated with an increased susceptibility of these mice to radiation carcinogenesis. Finally, I hypothesized that post-translational modification and, more specifically, phosphorylation may regulate the activity of human RAD51AP1.

To test for functional redundancy between RAD51AP1 and RAD54, we investigated the impact of simultaneous *RAD51AP1* and *RAD54* disruption in human cancer cell lines and in response to DNA-damaging agents in cell survival and DNA replication assays. We found that cells lacking both *RAD51AP1* and *RAD54* (*i.e.*, double KO cells) are more sensitive to the cytotoxic effects of mitomycin C (MMC) or olaparib exposure than cells lacking either *RAD51AP1* or *RAD54*. Accordingly, double KO cells exhibit a more pronounced G2/M arrest, higher levels of chromosomal aberrations and increased sensitivity to DNA

replication stress as determined by DNA combing experiments. These results show that RAD51AP1 and RAD54 can compensate for each other in human cancer cell lines.

To investigate the consequences of RAD51AP1 loss in mice we utilized a novel mouse model that lacks *Rad51ap1* and determined the susceptibility of these mice to radiation carcinogenesis. We found that compared to wild type mice, loss of *Rad51ap1* does not affect the survival of mice after whole body IR. We speculate that functional redundancy between RAD51AP1 and RAD54 may also exist in mice, and that *Rad51ap1*$^{-/-}$ *Rad54*$^{-/-}$ double KO mice may exhibit pronounced susceptibility to radiation carcinogenesis.

Finally, we sought to characterize the regulation of RAD51AP1 activity by post-translational modification. To achieve this objective, we identified two critical residues in RAD51AP1 that appear to be regulated by phosphorylation, S277 and S282. We found that mutation of these residues to the non-phosphorylatable S277A and S282A compromises RAD51AP1 function as measured by DNA replication and cell survival assays. These results suggest that phosphorylation of S277 and/or S282 is crucial for RAD51AP1 function.

Collectively, our studies clarify one aspect of functional redundancy within the HR pathway, and the role of post-translational modification of RAD51AP1. Our results provide new insights on the mild phenotypes associated with RAD51AP1 or RAD54 deficiency in human cells and mice. Our findings highlight the importance of development of personalized approaches for cancer treatment.

ACKNOWLEDGEMENTS

Throughout my research over the past 4 years and during the writing of this dissertation, I have received great support and assistance from colleagues, friends, and family.

First and foremost, I would like to express my sincere gratitude to my advisor, Dr. Claudia Wiese for funding my research and the support I received these years. I could not have asked for a better mentor to guide and encourage me to become the scientist I am today. I am really grateful for the insightful feedback and advice I received that pushed me to think critically and become more self-confident and proficient as a scientist. I would also like to extend my gratitude to my committee members Drs. Lucas Argueso, Takamitsu Kato and Seonil Kim for their valuable time, guidance, and constructive feedback.

The completion of this dissertation was also made possible thanks to past and present labmates. I would like to thank Dr. David Maranon for the time and effort he put into my training when I first joined the lab. Also, I would like to thank Dr. Neelam Sharma for all her support, advice, and technical assistance. A big thank you to Mollie for her amazing work in the lab and for the immense help that I received that made this dissertation possible. Additionally, I would like to thank Kriti for her valuable help and Elena for going through the PhD experience together.

I am also thankful for the CMB program and the great experiences and education I received. Most importantly, I want to thank the past and present CMB directors, Drs. Howard Liber and Carol Wilusz, and of course Charlene Spencer for always being there when I needed assistance.

My appreciation also goes to my parents and family in Greece for being on my side every moment, even from far away. Also, I would like to thank all my friends and family in Fort Collins for the amazing years of new fun experiences. Lastly and most importantly, I would like to whole-heartedly express my appreciation to my caring partner Alina, for her great support through this journey.

TABLE OF CONTENTS

LIST OF TABLES

LIST OF FIGURES

CHAPTER ONE

CHAPTER TWO

CHAPTER THREE

CHAPTER FOUR

LIST OF ACRONYMS

ALT	Alternative lengthening of telomeres
ATM	Ataxia telangiectasia mutated kinase
BRCA1/2	Breast cancer protein 1/2
CDK	Cyclin dependent kinase
CldU	Cloro-deoxyuridine
D-loop	Displacement loop
DSB	Double-strand break
DSBR	DSB repair
dsDNA	Double-stranded DNA
EdU	5-ethynyl-2′-deoxyuridine
HJ	Holiday junctions
HR	Homologous recombination
HRD	Homologous recombination deficiency
HU	Hydroxyurea
IdU	Iodo-deoxyuridine
IR	Ionizing radiation
MMC	Mitomycin C
NHEJ	Non-homologous end joining
PARPi	PARP inhibitor
RAD51PA1	RAD51 associated protein 1
RPA	Replication protein A
SDSA	Synthesis-dependent DNA strand annealing
ssDNA	Single-stranded DNA

LIST OF PUBLICATIONS

1. Maranon DG, Sharma N, Huang Y, **Selemenakis P**, Wang M, Altina N, Zhao W, Wiese C. 2020. NUCKS1 promotes RAD54 activity in homologous recombination DNA repair. *J Cell Biol* **219**.

2. Pires E, Sharma N, **Selemenakis P**, Wu B, Huang Y, Zhao W, Wiese C. 2020. RAD51AP1 mediates RAD51 activity through nucleosome interaction. *bioRxiv*: 2020.2012.2017.421636.

CHAPTER ONE

Introduction

1.1. Genomic instability and cancer

Cancer is the second leading cause of death in the United States (Center for Disease Control and Prevention), and it is estimated that almost 1.9 million new cases will be diagnosed, and more than 600,000 Americans will succumb to the disease in 2021 (American Cancer Society). While there is no single cause for cancer, there are several factors known to increase the risk for developing the disease, the most common of which include exposure to environmental carcinogens, such as ionizing radiation (IR), stress to DNA replication forks and inherited mutations. These factors can promote genome instability and initiate cancer development processes.

Genomic instability is one of the enabling hallmarks of cancer (Hanahan and Weinberg 2011) and, as mentioned above, can arise after exposure to endogenous challenges as well as exogenous compounds. These insults can lead to the induction and propagation of mutations through the generation of multiple DNA lesions, the most toxic one of which is a DNA double-strand break (DSB) (**Figure 1.1**). DSBs can be repaired by two major DNA repair pathways, homologous recombination (HR) or non-homologous end joining (NHEJ), with HR being the least error prone. HR is considered the more faithful DSB repair pathway, and this is because it involves the exchange of genetic material between the DNA containing the damaged site and the sister chromatid (Kadyk and Hartwell 1992; Takata et al. 1998).

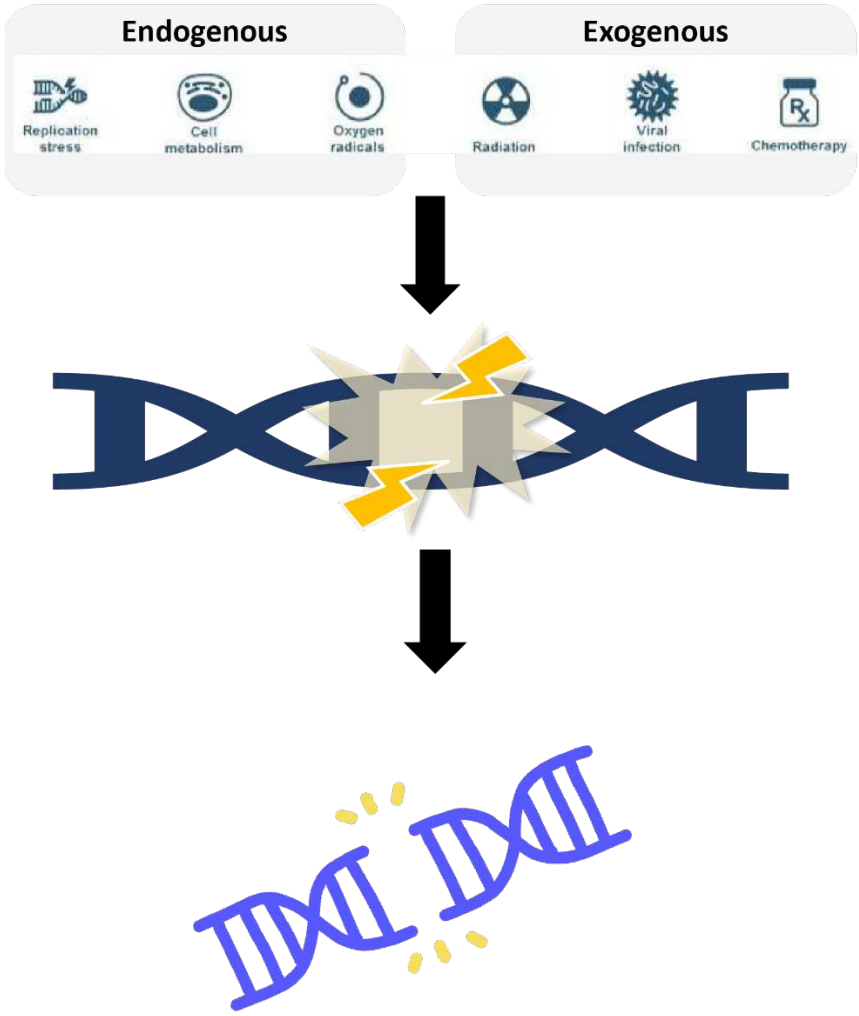

Figure 1.1. Endogenous and exogenous factors that can lead to DNA damage and genomic instability. [Modified by Sierra oncology].

1.2. DSB repair by homologous recombination

DSB detection and early steps of homologous recombination

Once a DSB is induced, for example after exposure to IR (**Figure 1.2**, **step a**), one of the earliest cellular responses is the localization of the MRN complex to the damaged site. The complex consists of the MRE11 nuclease, the RAD50 ATPase and the NBS1 protein (Maser et al. 1997; Lisby et al. 2004; Yuan and Chen 2010; Reginato and Cejka 2020). Next, the ataxia-telangiectasia-mutated (ATM) kinase associates with the MRN complex and gets activated and autophosphorylated at S1981, which is critical

for its activity (Lee and Paull 2005). Once ATM is activated, it phosphorylates many downstream protein targets, and thus initiates a sequence of events important for the processing of DSBs. One of the downstream targets of ATM is mammalian H2AX which gets phosphorylated at S139 residing on the C-terminus of the protein, and the modified histone is denoted as γH2AX (Rogakou et al. 1999; Paull et al. 2000; Mah et al. 2010). This modification is important for chromatin modification as well as recruitment of downstream mediators involved in the repair of DSBs (Foster and Downs 2005; Mah et al. 2010).

HR pathway starts with DNA end resection to produce 3′-single-stranded DNA (ssDNA) overhangs and it includes a two-step process (**Figure 1.2**, **step b**). First, CtIP (in humans, Sae2 in yeast), after activation by ATM, binds to NBS1 of the MRN complex and promotes the endonucleolytic cleavage of the 5′-terminated DNA strand (Sartori et al. 2007; Wang et al. 2013; Wang et al. 2017b). The short-range resection by MRN-CtIP is promoted by breast cancer protein 1 (BRCA1) (Bunting et al. 2010). Following the short-range resection, exonuclease EXO1 and nuclease DNA2 are recruited to perform long-range resection and produce a 3′-overhang. EXO1 possesses a 5′-3′ exonuclease activity that resects DNA within double-stranded DNA (dsDNA) (Lee Bi et al. 2002; Mimitou and Symington 2008; Zhu et al. 2008). In contrast, DNA2 possesses an endonuclease activity and can degrade ssDNA with the help of the helicase BLM (Bae et al. 1998; Masuda-Sasa et al. 2006; Zhu et al. 2008). Once the 3′-ssDNA overhang is produced, replication protein A (RPA) binds to ssDNA to protect the DNA from degradation and prevent the formation of inappropriate hairpin structures (Robison et al. 2007; Chen et al. 2013) (**Figure 1.2**, **step b**).

The RPA bound to ssDNA is a barrier for the recruitment of the RAD51 recombinase, the central protein of HR. However, RAD51 can form a filament on the ssDNA with the help of breast cancer protein 2 (BRCA2) and other recombination mediators (**Figure 1.2**, **step c**). BRCA2 physically interacts with RAD51 through the BRC repeats and facilitates the displacement of RPA from the ssDNA (Yuan et al. 1999; Yu et al. 2003; Galkin et al. 2005; Davies and Pellegrini 2007; Wiwanitkit 2007; Jensen et al. 2010). In addition to BRCA2, BRCA1 also binds to RAD51 along with its interacting partner BARD1 to enhance RAD51 activity during strand invasion (Zhao et al. 2017). Here, several other RAD51 accessory factors

also enhance the activity of RAD51, and these will be introduced below. A more detailed summary of their functional roles in HR, as known to date, will be given in **Section 2.1**.

RAD51 accessory factors

RAD51AP1

RAD51 associated protein 1 (RAD51AP1) is found in all vertebrates (Parplys et al. 2014). Orthologs of RAD51AP1 are also found in some invertebrates, but RAD51AP1 is absent in some of the most common laboratory model organisms, such as *S. cerevisiae, C. elegans* and *D. melanogaster* (Parplys et al. 2014). There are 3 mapped and 6 potential isoforms of RAD51AP1 (https://www.uniprot.org/; human RAD51AP1 Uniprot ID: Q96B01), with Isoform 2 (335 aa) being predicted the most prevalent in humans (Kovalenko et al. 1997; Dray et al. 2011). Isoform 2 is highly hydrophilic, consisting of a third of arginine, glutamic and aspartic acid residues (Kovalenko et al. 1997).

RAD51AP1 was first discovered as interacting partner of RAD51 by using the yeast two-hybrid system and initially named Pir51 and RAB22 for the human protein and the mouse homologue, respectively (Kovalenko et al. 1997; Mizuta et al. 1997). The high affinity interaction between the two proteins has been shown in yeast two-hybrid and co-immunoprecipitation experiments (Kovalenko et al. 1997; Mizuta et al. 1997; Henson et al. 2006). In support of this, the colocalization of spontaneous and damage-induced RAD51 and RAD51AP1 foci has been reported in human cells and the CHO cell line (Mizuta et al. 1997; Modesti et al. 2007; Wiese et al. 2007; Obama et al. 2008). Based on mapping experiments, RAD51 interacts with RAD51AP1 through a domain that is composed of the last 26 residues in human RAD51AP1 (Kovalenko et al. 2006) . This interaction is crucial for the enhancement of RAD51 activity during the displacement-loop (D-loop) reaction which involves the formation of a joint structure between the ssDNA and the homologous template dsDNA (Modesti et al. 2007; Wiese et al. 2007; Dunlop et al. 2012) (**Figure 1.2**, **step d and e**). Truncated RAD51AP1 in which the RAD51 binding domain was absent and thus the interaction with RAD51 was impaired, failed to stimulate the D-loop reaction (Modesti et al. 2007; Wiese et al. 2007).

RAD54 and RAD54B

RAD54 is found in all eukaryotes, is highly conserved, and is a member of the *RAD52* epistasis group. RAD54 is member of a group of ATPases/DNA helicase-related proteins of the SNF2/SWI2 family (Calderon et al. 1983; Heyer et al. 2006; Mazin et al. 2010; Ceballos and Heyer 2011). RAD54 was first discovered by screening different mutants in *S. cerevisiae* for sensitivity to X-rays (Snow 1967; Game and Mortimer 1974). Later, the *ScRAD54* gene was isolated and characterized along with other DNA repair genes (Calderon et al. 1983; Perera et al. 1988). RAD54 possesses ATPase activity that is dependent on dsDNA (Petukhova et al. 1998; Swagemakers et al. 1998). The core motor domain of RAD54 is constituted of seven common motifs (I, Ia, II-VI) and is responsible for ATP hydrolysis (Singleton et al. 2007). RAD54-mediated ATP hydrolysis is dependent on the presence of dsDNA (Petukhova et al. 1998; Swagemakers et al. 1998; Mazina et al. 2007). RAD54 shows higher affinity to branched DNA and with preference for Holiday junctions (Bugreev et al. 2006; Mazina et al. 2007). Moreover, RAD54 while bound to dsDNA can translocate by introducing topological changes with energy from ATP hydrolysis (Petukhova et al. 1999; Tan et al. 1999; Van Komen et al. 2000; Ristic et al. 2001; Bianco et al. 2007) (**Figure 1.2**, **step e**). RAD54 as other members of the SNF2/SWI2 family contain sequence motifs found in all DNA helicases, however RAD54 does not exhibit any helicase activity and thus is unable to unwind dsDNA (Bugreev et al. 2006; Mazina et al. 2007).

S. cerevisiae possesses a RAD54 paralogue, Rdh4, which exhibits functional similarities to Rad54 (Klein 1997; Petukhova et al. 2000; Shinohara et al. 2000). Mammalian cells as well hold a RAD54 paralogue, RAD54B, that shares functional similarities with RAD54. However, its biochemical properties are different from Rdh54 (Tanaka et al. 2000; Tanaka et al. 2002).

Homologous recombination-mediated pathways

HR contains two main sub-pathways: Canonical DSB repair (DSBR) and synthesis-dependent DNA strand annealing (SDSA). Following end resection and strand invasion of the 3′-ssDNA overhang into the template molecule, the invading 3′-OH end is extended via DNA repair synthesis (Sung and Klein

2006). In DSBR, the second DNA end is captured to form an intermediate structure with two Holiday junctions (HJs). Resolution of HJs can lead to either non-crossover or crossover of genetic material between the sister chromatids (Collins and Newlon 1994; Schwacha and Kleckner 1995; Sung and Klein 2006) (**Figure 1.2**, **step f**). In SDSA, the invading DNA strand, after strand invasion and DNA synthesis, is released and ligated to the other DSB end. Then gap-filling DNA synthesis occurs, leading to non-crossover events (Allers and Lichten 2001; Sung and Klein 2006; Wesoly et al. 2006) (**Figure 1.2**, **step f**).

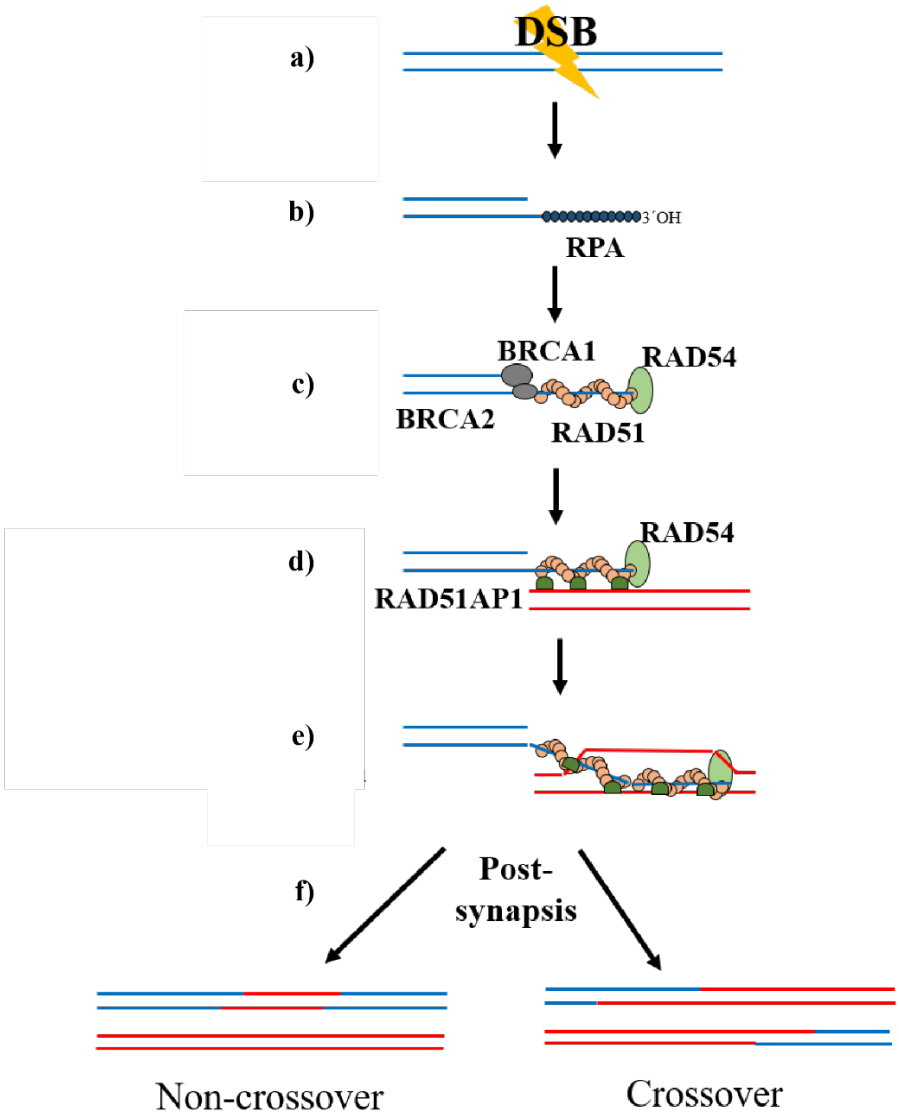

Figure 1.2. Steps and proteins involved in the homologous recombination DNA repair pathway. a) Generation of DSB. **b)** DNA end resection and recruitment of RPA. **c)** Recruitment of RAD51 by BRCA1 and BRCA2 and

binding of RAD54 to RAD51. **d)** Binding of RAD51AP1 to RAD51 and synaptic complex formation. **e)** D-loop formation. **f)** Post-synaptic stage of HR leading to no-crossover or crossover of genetic material.

1.3. Regulation of homologous recombination

The efficiency of HR relies on the accessibility of the sister chromatid. Therefore, it is not surprising that HR mainly functions during the S and G2 stages of the cell cycle (Kadyk and Hartwell 1992; Takata et al. 1998). On the other hand, NHEJ functions throughout the cell cycle, and therefore the two pathways can compete for the same DSBs (Takata et al. 1998). On this note, the regulation of DSB repair choice is very important for the maintenance of genomic integrity.

Cell cycle progression is actively regulated by cyclin-dependent kinases (CDKs), and HR is regulated by CDK activity. The yeast CDK1 homologue (cdc28) is activated at G1 and promotes the progression through S phase (Toone et al. 1997). Studies have found that Cdc28 is important for initiation of DNA end resection and for RPA and Rad51 loading on ssDNA (Aylon et al. 2004; Ira et al. 2004). In yeast, phosphorylation of Rad51 by Cdc28 (in mammalian cells, CDK1) is critical for its DNA binding affinity (Lim et al. 2020). In mammalian cells, CDKs can regulate HR at many steps and also by phosphorylation of BRCA2, blocking its interaction with RAD51 (Esashi et al. 2005).

1.4. Homologous recombination and cancer

Homologous recombination and tumorigenesis

HR is fundamental for cancer avoidance, and a defect in HR will lead to genomic instability. Therefore, it is not surprising that tumorigenesis can be a consequence of homologous recombination deficiency (HRD) (Ali et al. 2020). Next generation sequencing revealed that alterations in HR genes exist in ~17% of tumors across 21 cancer lineages (Heeke et al. 2018). Moreover, a pan-cancer analysis that looked at The Cancer Genome Atlas (TCGA) data set showed that over 5% of all cancers exhibit bi-allelic pathogenic variant of genes that are involved in HR, and that the pathway is altered in ~25% of ovarian and ~10% of breast cancers (Riaz et al. 2017). HRD can lead to chromatid type aberrations that occur during

defective repair in S and G2 phase. Chromatid breaks and gaps are often produced after IR in HR-deficient human cells with BRCA2 mutation (Conrad et al. 2011). Metaphases of *Brca1*-mutant B cells, which are deficient for HR, are found with increased percentage of radial chromosome structures generated by NHEJ (Bunting et al. 2010). In addition, spectral karyotyping analysis of BRCA1- and BRCA2-mutant cell lines has revealed that these cells contain heavily rearranged karyotypes, suggesting that mutations in *BRCA1* or *BRCA2* and concomitant HRD lead to increased chromosome instability (**Figure 1.3**, **compare B to normal karyotype in A**).

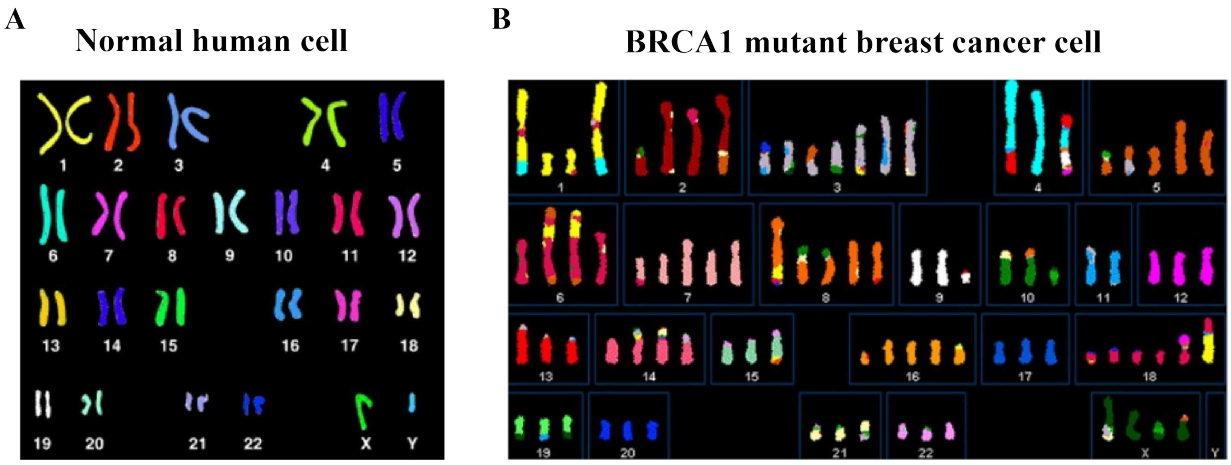

Figure 1.3. Homologous recombination deficiency increases genomic instability. **A)** Spectral karyotyping analysis of a normal human cell. **B)** Spectral karyotyping analysis of a BRCA1-mutant breast cancer cell. [Adopted from Grigorova M. et al. 2004].

RAD54 has also been found to be mutated in several different cancer types (https://www.cbioportal.org/). Early studies have shown that *RAD54* can be deleted as a consequence of loss of heterozygosity in breast tumors (Rasio et al. 1997; Gonzalez et al. 1999). Point mutations found in functional regions of *RAD54* are observed in several primary cancers including breast, colon cancer and lymphoma (Matsuda et al. 1999). *RAD54B* gene, a RAD54 paralogue, is also found to contain mutations in primary lymphoma and colon cancer, which suggests that *RAD54B* mutations could be involved in the development of cancer (Hiramoto et al. 1999). Overall, the different mutational profiles that tumors exhibit

may lead to new ways of therapeutic intervention and a more personalized approach in treating cancer patients with tumors that are HRD.

Therapy for tumors defective in homologous recombination

Normal cells employ two major pathways to repair DSBs, HR and NHEJ, and the balance of the usage of these two pathways is very crucial (**Figure 1.4A**). Any imbalance between the utilization of the two pathways can lead to chromosome instability and eventually to carcinogenesis. Once cancer is established, the type of genotoxic agents used in anti-cancer therapy and the outcome of treatment is greatly affected by the status of HR capability. Cancer cells deficient in HR are greatly sensitive to chemotherapeutic agents (**Figure 1.4B**) and one of the most promising strategies to treat breast tumors that exhibit HRD is inhibition of PARP-1 (Keung et al. 2019). In the clinical setting, most commonly, tumors that exhibit *BRCA*-deficiency, or so called "BRCAness", are treated with PARP inhibitors (PARPi) (Helleday 2010; Faraoni and Graziani 2018). The first time that it was suggested to treat HRD tumors with PARPi was when a group found that *BRCA2*-deficient cancer cells are hypersensitive to PARP-1 inhibition (Bryant et al. 2005). Following that study, multiple PARPi have been developed and used in the clinical setting or are in clinical trials to treat breast cancer patients (Farmer et al. 2005; Wang et al. 2017a; Keung et al. 2020). Olaparib is the very first PARPi to be approved for cancer therapy following a Phase I study showing its antitumor activity in ovarian and breast cancer patients with *BRCA1* or *BRCA2* mutations (Fong et al. 2009; Keung et al. 2019).

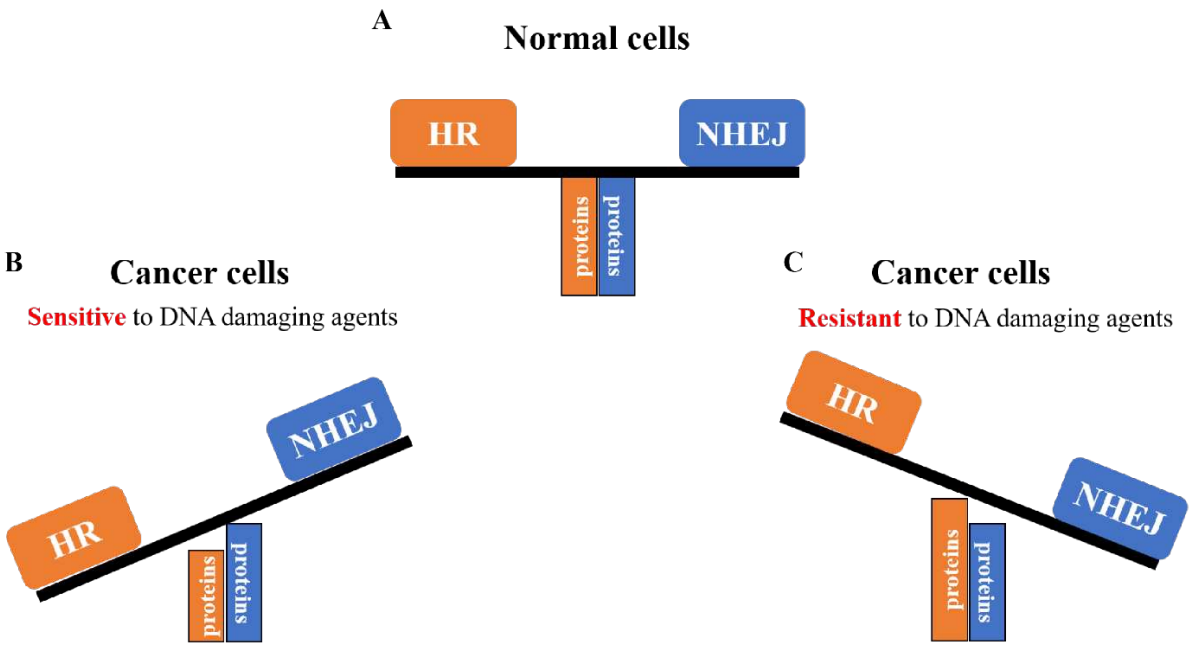

Figure 1.4. Schematic to show that the status of HR capability may affect the outcome of therapy. A) Utilization of HR and NHEJ is balanced in normal cells. **B)** Cancer cells with HRD are sensitive to DNA damaging agents. **C)** Cancer cells with upregulated HR are resistant to DNA damaging agents.

Aberrant expression of Homologous Recombination proteins in cancer

In some tumor types, the HR pathway is upregulated (Song et al. 2004; Pathania et al. 2016; Feng et al. 2019; Bridges et al. 2020), rendering these tumors more resistant to chemotherapy and radiation therapy (**Figure 1.4C**). As mentioned above, *BRCA*-deficiency leads to HRD that renders cancer cells sensitive to chemotherapeutic agents (**Figure 1.5A**). However, in many instances resistance to therapy has been correlated with reversion mutations in *BRCA1* or *BRCA2* (Edwards et al. 2008; Sakai et al. 2008; Swisher et al. 2008). Other RAD51 accessory proteins also have been found to be overexpressed in several different tumor types and are described below (**Figure 1.5B**).

The *RAD51AP1* gene is overexpressed in many different tumor types (https://www.cbioportal.org/). Microarray and/or qPCR data have shown that *RAD51AP1* expression is significantly higher in ovarian, breast, lung adenocarcinoma, esophageal and hepatocellular cancer. High

expression of *RAD51AP1* in the tumors of these patients correlates with poor survival (Pathania et al. 2016; Chudasama et al. 2018; Li et al. 2018; Bridges et al. 2020; Zhao et al. 2020; Zhuang et al. 2020).

RAD54 rarely is found to be amplified in human cancers. However, one study using mRNA microarray datasets of cervical cancer samples revealed that *RAD54* is highly expressed and that elevated *RAD54* expression correlates with better survival outcome in these patients (Qiu et al. 2020). The paralogue of RAD54, RAD54B, is overexpressed in many tumor types (https://www.cbioportal.org/) (McAndrew and McManus 2017). RAD54B is upregulated in late clinical tumor stages of breast cancer and high levels of the protein correlates with worse survival (Feng et al. 2019). Moreover, RAD54B protein is found to be upregulated in lung adenocarcinoma and high levels of RAD54B correlate with poor prognosis and survival (Hwang et al. 2015).

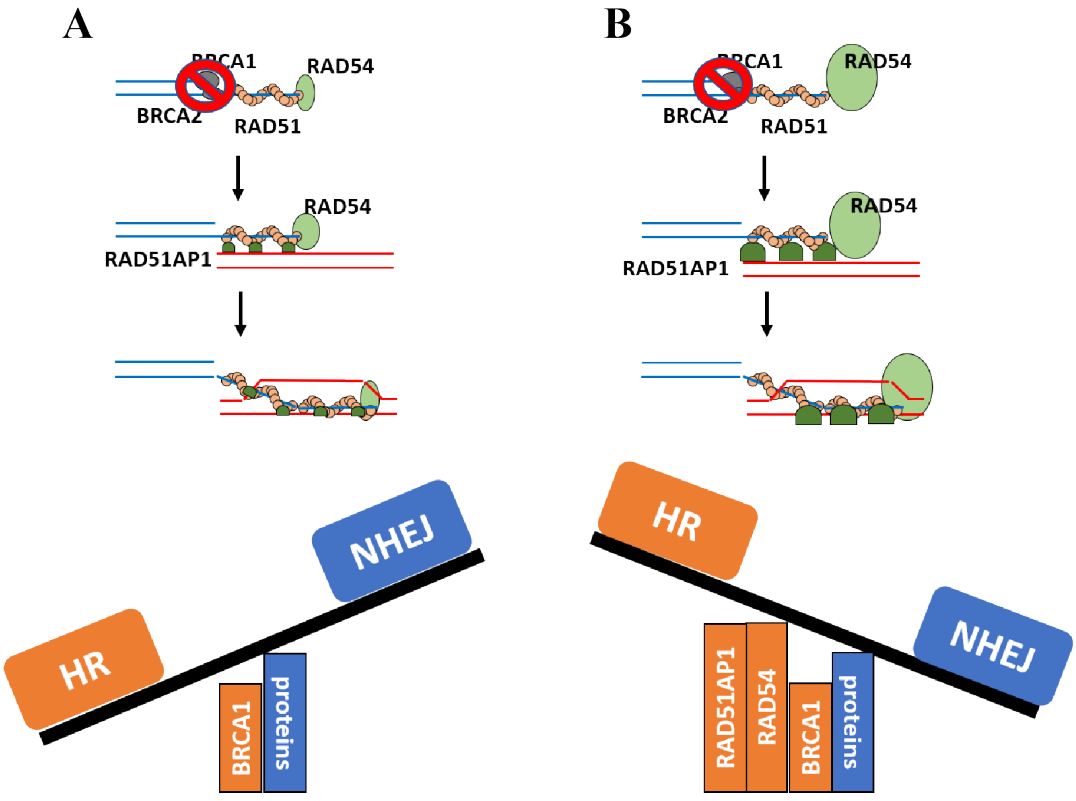

Figure 1.5. Schematic depiction of the consequences of RAD51AP1 and/or RAD54 overexpression in BRCA1-mutant breast cancers. A) BRCA1 or BRCA2-mutant cancer cells exhibit HRD. **B)** Overexpression of RAD51AP1 and/or RAD54 (as indicated by the enlarged symbols for either protein) leads to upregulated HR.

1.5. Summary and knowledge gap

The HR pathway is a multi-step and a very complex DNA repair pathway that involves the action of many proteins. Among these, RAD51AP1 and RAD54 are of great interest due to their shared role in enhancing the activity of the RAD51 recombinase. While RAD54 has been studied abundantly, literature on the involvement of RAD51AP1 in HR is limited. Moreover, there is lack of information concerning the functional overlap between these two key players in the HR reaction in cells. Also, the exact role of RAD54B in human cells is not yet understood. Moreover, it is unclear how RAD51AP1 may be regulated during the cell cycle and after DNA damage induction, and if post-translational modifications may play a role. Finally, a mouse model with disrupted *Rad51ap1* was not available until recently, and no data were available with respect to the susceptibility of such mice to radiation carcinogenesis.

1.6. Hypothesis and Specific Aims

Given the importance of HR in the maintenance of genomic integrity and cancer avoidance and as a promising target of anti-cancer therapy, there is a clear need to fully understand the pathway's molecular details. While the pre-synaptic steps of HR have been investigated in great detail, there is a conceptual gap in our understanding of the roles of RAD51 accessory proteins RAD51AP1 and RAD54 in later stages of the pathway that include synapsis and post-synapsis.

I hypothesized that functional redundancy exists between RAD51AP1 and RAD54, and that this could explain the mild phenotypes of HR deficiency observed for loss of either protein alone. To test this hypothesis, first I investigated the phenotypic consequences of *RAD51AP1* and/or *RAD54* loss in human cancer cell lines. Secondly, I tested *Rad51ap1* knockout (KO) mice for their susceptibility to radiation carcinogenesis, and I compared the response of *Rad51ap1* KO mice to the available published reports for *Rad54* KO mice. Last, I identified two critical residues in the human RAD51AP1 protein that appear to be regulated by phosphorylation.

Specific Aim 1: Characterize the phenotype of human cancer cell lines deleted for *RAD51AP1* and/or *RAD54.*

RAD51AP1 and RAD54 function at similar stages during the HR pathway, and loss of either protein is associated with a mild HR defect in human cells. I hypothesize that simultaneous inactivation of both RAD54 and RAD51AP1 may lead to synthetic phenotype in human cells.

Specific Aim 2: Characterize the susceptibility to radiation carcinogenesis of *Rad51ap1* KO mice.

The consequences of organismal *Rad51ap1* loss had not been investigated due to the lack of an appropriate model system in vertebrates. However, a *Rad51ap1* KO mouse has recently become available. This mouse is viable and fertile and will be characterized here for its susceptibility to radiation carcinogenesis. I hypothesize that *Rad51ap1* loss in mice is associated with an increased susceptibility to radiation carcinogenesis.

Specific Aim 3: Characterize the regulation of RAD51AP1 activity.

RAD51AP1 is post-translationally modified upon exposure to DNA damaging agents. In a phospho-proteomic study, serines 277 and 282, two residues located within RAD51AP1's C-terminal DNA binding domain, were found to be phosphorylated. I hypothesize that phosphorylation of Ser-277 and Ser-282 regulates RAD51AP1 function in human cells.

CHAPTER TWO

RAD51AP1 substitutes for RAD54 in human cancer cell lines

2.1. Introduction

HR is a multistep pathway that ensures genomic integrity and can conceptually be separated in three different stages: the pre-synaptic, the synaptic, and the post-synaptic stage. In each of these stages, critical proteins are involved to ensure the stringent regulation of the pathway and the precise repair of damaged DNA. As described in **Section 1.2**, the first step during the pre-synaptic stage of HR is DNA end resection to produce a ssDNA overhang (Lee Bi et al. 2002; Mimitou and Symington 2008; Zhu et al. 2008). Then, the produced ssDNA is protected by RPA that forms a nucleoprotein filament (Robison et al. 2007; Chen et al. 2013). RPA is displaced by RAD51 to form the RAD51-ssDNA nucleoprotein filament. Following the pre-synapsis, RAD51 interacts with several accessory proteins to proceed to synapsis.

During the synaptic stage, one of the critical proteins that interacts with RAD51 to enhance its function is RAD51AP1 (Kovalenko et al. 1997; Mizuta et al. 1997). More specifically, the interaction between RAD51AP1 and RAD51 enhances the RAD51-mediated DNA strand pairing reaction (Modesti et al. 2007; Wiese et al. 2007; Dray et al. 2010; Dunlop et al. 2012) (**Figure 1.2**, **step d**). More recently, our group found RAD51AP1 bridges the dsDNA with the RAD51-ssDNA nucleoprotein filament through its affinity for the nucleosomes of the template (Pires et al. 2020). RAD51AP1 also assists with RAD51-mediated strand invasion, generating the D-loop (Modesti et al. 2007; Wiese et al. 2007; Dray et al. 2010; Dunlop et al. 2012) (**Figure 1.2**, **step e**).

The RAD51 recombinase also interacts with the DNA motor protein RAD54 which stabilizes the RAD51 filament, and this function of RAD54 is independent of its ATPase activity (Mazin et al. 2003) (**Figure 1.2**, **step c**). Moreover, RAD54 assists with the formation of the synaptic complex (Petukhova et al. 1999; Solinger and Heyer 2001; Solinger et al. 2001; Van Komen et al. 2002; Jaskelioff et al. 2003) (**Figure 1.2**, **step d)**). RAD54 also translocates on dsDNA and uses energy from ATP hydrolysis to facilitate strand

invasion (Zhang et al. 2007; Wright and Heyer 2014) and homology search (Mazin et al. 2000; Crickard et al. 2020) (**Figure 1.2**, **step e**). Efficient strand invasion and homology search is supported by the ability of RAD54 to remodel nucleosomes and make the template accessible to the invaded RAD51-ssDNA filament (Zhang et al. 2007). Following homology search, RAD51 is removed from the heteroduplex by RAD54 in an ATPase-dependent manner, in order to make the invaded 3´ DNA end accessible to DNA polymerases that will initiate DNA repair synthesis (Ceballos and Heyer 2011; Wright and Heyer 2014; Liu et al. 2017). Finally, at the post-synaptic stage, RAD54 can displace nucleosomes on the homologous DNA target (Alexeev et al. 2003) to promote branch migration of Holiday Junctions (Bugreev et al. 2006; Goyal et al. 2018) (**Figure 1.2**, **step f**). RAD54's branch migration activity is stimulated by RAD51 (Rossi and Mazin 2008). Most recently, it was also shown that both RAD54 and RAD51AP1 are very important for maintaining telomere length through their involvement in the HR-mediated alternative lengthening of telomeres (ALT) mechanism (Barroso-Gonzalez et al. 2019; Mason-Osann et al. 2020).

RAD51AP1 and RAD54 are structurally different proteins and either one assists the HR reaction in human cells. Cells deficient for either RAD51AP1 or RAD54 show a mild sensitivity upon exposure to DNA damaging agents (Modesti et al. 2007; Wiese et al. 2007; Maranon et al. 2020; Zhou et al. 2020). So far, there is no evidence of a synergistic relationship between RAD51AP1 and RAD54. However, since both proteins function at similar stages within the HR pathway, I hypothesized that functional redundancy may exist between the two proteins.

A third protein that is involved in the synaptic stages of the HR is RAD54B, a RAD54 paralogue (Hiramoto et al. 1999). RAD54B shares functional similarities with RAD54, however its ATPase activity is less prominent compared to that of RAD54 (Tanaka et al. 2002). As RAD54, RAD54B interacts with RAD51 through its N-terminal domain (Tanaka et al. 2000; Sarai et al. 2008). Furthermore, as RAD54, RAD54B promotes D-loop formation and assists with strand invasion into the donor DNA (Wesoly et al. 2006; Sarai et al. 2008). A function of RAD54B, that RAD54 is lacking, is that it enhances the MDM2-MDMX-mediated ubiquitination of p53 and subsequent degradation. This suggests that RAD54B also has

HR-unrelated roles during the DNA damage response (Yasuhara et al. 2014). Cells deficient for both *RAD54* and *RAD54B* show accumulation of non-damage associated RAD51 foci, which leads to proliferation defects, slower progression of DNA replication forks and mitotic defects (Mason et al. 2015). Mouse embryonic stem cells deleted for both *Rad54* and *Rad54b* are more sensitive to IR and mitomycin C (MMC) compared to single knockout cells (KO) and the survival of mice lacking both proteins is significantly lower after treatment with MMC compared to single KO mice (Wesoly et al. 2006). In addition, mice lacking both proteins are more prone to increased chromosomal aberrations in spermatocytes after exposure to IR (Russo et al. 2018). However, while there is clear evidence of some functional overlap between RAD54 and RAD54B in mice and mouse cells, the exact role and importance of RAD54B in HR in human cells remains to be determined.

In this chapter, we show that RAD51AP1 and RAD54 exhibit a synergistic interaction and have overlapping roles in HR. Tested in two different human cancer cell lines, both RAD51AP1 and RAD54 are important for survival upon exposure of cells to DNA-damaging agents. However, cells that lack both proteins show further increased cellular sensitivity and also a more pronounced G2/M arrest. Compared to single *RAD51AP1* or *RAD54* KO cells, double *RAD51AP1/RAD54* KO (DKO) cells also are significantly impaired in overcoming replication stress. These results show that RAD51AP1 and RAD54 largely can compensate for each other in human cancer cell lines and that inactivation of both proteins may open new avenues in treatment options of cancer patients. Overall, these findings provide new knowledge on the importance of inhibiting RAD51AP1 in combination with RAD54 to effectively target tumors proficient or overactive in HR.

2.2. Materials and Methods

Cell culture

The human cervical cancer cell line, HeLa, was obtained from ATCC and maintained in Eagle's Minimum Essential Medium (Genesee Scientific) supplemented with 10% Fetal Bovine Serum (FBS) (Sigma) and 1× of a mix of antibiotic (penicillin and streptomycin) and antimycotic (amphotericin B) drugs

(Gibco). U2OS cells, a human osteosarcoma cell line with integrated a DR-GFP HR reporter acquired from Dr. Maria Jasin's lab and HEK293FT cells, an immortalized human embryonal kidney cell line obtained from ATCC were maintained in Dulbecco's Modified Eagle medium (Genesee Scientific) supplemented with 10% FBS and 1× of antibiotic and antimycotic solution. The human lung cancer cell line, A549, was kindly provided by Dr. Jac Nickoloff. A549 cells were maintained in RPMI medium 1640 supplemented with 10% FBS and 1× of antibiotic and antimycotic solution.

Transfections, and siRNAs

To knockdown RAD54, RAD51AP1, RAD54B and BRCA1 small interfering RNAs (siRNA) were purchased from Qiagen and the target sequences used are: 5′-AAGCATTTATTCGAAGCATTT-3′, 5′-AACCTCATATCTCTAATTGCA - 3′, 5′ - ACCCAAGAAATTATAAATAAA - 3′ and 5′ - AAGCTCCTCTCACTTCAGT - 3′ (Modesti et al. 2007; Wiese et al. 2007; Zafar et al. 2010; Parplys et al. 2015) respectively. As a non-targeting negative control siRNA, the following sequence was used: 5′-GATTCGAACGTGTCACGTCAA-3′ (Zafar et al. 2010; Parplys et al. 2015). Transfections were performed using lipofectamine RNAiMAX (Invitrogen) and 20 nM siRNAs diluted in Opti-MEM reduced serum medium (Thermo Fisher Scientific). Cells were seeded in antibiotic-free medium in a 6-well tissue culture plate at a density of 1×10^5 cells per well and incubated for 24 hours before transfection on two consecutive days. Lipid-siRNA complex was formed in a 1:1 ratio according to the manufacturer's instructions (Invitrogen). After transfection, cells were re-seeded and incubated for 48 hours before treatment.

Gene conversion assay

The gene conversion assay using U2OS DR-GFP cells was performed as previously described (Parplys et al. 2015; Liang et al. 2016; Liang et al. 2020). Briefly, 1.5×10^5 cells per well were seeded in a 6-well tissue culture plate, 24 hours prior to transfection in antibiotic free media. Transfection was carried out with siRNA against RAD51AP1 and/or RAD54 for two consecutive days. The cells were then transfected with HA tagged I-SceI expression vector (4 μg, pCBASce) using Lipofectamine 2000. After 72

hours, cells were processed for flow cytometry analysis in CyAn ADP cell analyser (Beckman Coulter). To fit the data for GFP positive cells, FlowJo version 10.7 (BD Biosciences) was used.

Generation of KO cell lines

The *RAD54* KO and *RAD51AP1* KO cell lines were generated as described (Liang et al. 2019; Maranon et al. 2020).

Double KO (for *RAD51AP1* and *RAD54*) cell lines were generated by using the *RAD51AP1* KO cell line. *RAD51AP1* KO cells were transfected with a cocktail of 2 sgRNA-containing plasmids for *RAD54*, using our published procedures (Maranon et al. 2020). Genomic DNA was isolated from all edited and non-edited control HeLa cell derivatives using DNeasy Blood & Tissue Kit (Qiagen). Genomic DNA flanking the sgRNA target sites (

Table S2.1) was amplified by PCR using the primer pairs listed in **Table S2.2**. PCR products were gel purified and cloned into pCR 4-TOPO vector (Invitrogen), transformed into DH5α competent *E. coli*, and plasmid DNA was prepared using ZR Plasmid Miniprep-Classic Kit (Zymo Research) and submitted for Sanger sequencing.

Cloning and generation of RAD54-HA expressing cells

The full length RAD54 cDNA with C-terminal HA-tag was digested from pCDNA3.1-RAD54-HA and cloned from *KpnI* to *NotI* into pENTR1A (Gateway system; Invitrogen). RAD54-HA was introduced to pLenti CMV/TO DEST #2 (Campeau et al. 2009) by Gateway LR Clonase II reaction (Invitrogen).

To ectopically express RAD54 in DKO, *RAD54* KO and *RAD51AP1* KO cells, replication-incompetent lentivirus was produced in HEK 293T cells. HEK 293FT cells were plated in 10 cm dishes at a density of 3×10^6 cells per dish and transfected on the next day with Lipofectamine 2000, a cocktail of plasmids consisting of the virus packaging genes, pLP1 (5 μg), pLP2 (2 μg), and pVSV-G (2.6 μg) and the pLenti vector containing *RAD54*-HA (3 μg). Fourty-eight hours post transfection, the supernatant was removed, centrifuged and filtered, and then used for transduction of HeLa cell derivatives. After 48 hours, cells were trypsinized and replated in 96-well tissue culture plates at a density of 0.5 cells per well in the

presence of 0.75 µg/ml puromycin. Puromycin-resistant clones were isolated, expanded and were further screened for the expression of RAD54 protein by western blot. Clones were also tested for the formation of RAD54 foci after DNA damage and by immunocytochemistry.

Exposure to genotoxic agents

Cell survival assays after MMC (Sigma) were performed as described (Maranon et al. 2020). Briefly, exponentially growing cells were acutely exposed to graded doses of MMC at 37ºC for 1 hour in regular growth medium. Cells were washed twice in warm 1×PBS, counted, and plated in regular growth media for 12 days for colony formation. To assess cellular sensitivity to olaparib (AZD2281 (KU-0059436); Selleck Chemicals), cells were chronically exposed to olaparib in regular growth medium for 12 days (Spies et al. 2016).

Protein extraction and protein estimation

To prepare whole cell lysates, cells were trypsinized and washed with ice-cold 1×PBS. After washing, the cell pellet was resuspended in lysis buffer (50mM Tris-HCl, 300mM NaCl and 0.5% NP-40). Cells were left on ice to lyse for 5 min and then centrifuged at 4º C at 14,000 rpm for 20 minutes. The supernatant consisting of the proteins was saved and transferred to a pre-chilled tube. Samples were snap-frozen in liquid nitrogen and stored at -80ºC. For isolation of subcellular protein fractions, the Subcellular Protein Fractionation kit (Thermo Fisher Scientific) was used and the protocol from the manufacturer was followed. Samples from the subcellular fractions were saved, snap-frozen in liquid nitrogen and stored at -80ºC.

Protein concentration was estimated using the DC Protein Assay and followed the manufacturer's instructions (Bio-Rad).

Western blot analysis

Isolated proteins were resolved by sodium dodecyl sulphate-polyacrylamide gel electrophoresis (SDS-PAGE) and then transferred to a polyvinylidene difluoride (PVDF) membrane overnight at 4ºC in cold 1×transfer buffer (25 mM Tris-base, 190 mM glycine) with 10% methanol. Membranes were dried for 30 minutes and then reactivated in methanol, washed in ddH2O and 1×TBS-T (20mM Tris base, 150mM NaCl, 0.05% Tween-20). Membranes were blocked for 2 hours at room temperature in 5% m/v non-fat milk in 1×TBS-T. To detect proteins of interest the following primary antibodies were used: α-RAD51AP1 (our own α-RAD51AP1 antibody (1:6,000), as previously described (Dray et al. 2010), α-RAD54B (homemade antibody acquired from Dr. Patrick Sung at University of Texas Health San Antonio (1:1,000), as previously described (Wesoly et al. 2006)), α-RAD54 (F-11; sc-374598; Santa Cruz Biotechnology; 1:1,000), α-BRCA1 (C-20; sc-642; Santa Cruz Biotechnology; 1:500), α-RAD51 (Ab-1; EMD Millipore; 1:2,000), α-PARP1 (ab6079; Abcam; 1:2,000), and α-β-actin (ab8226; Abcam; 1:1,000). HRP-conjugated goat anti-rabbit or goat anti-mouse IgG (Jackson ImmunoResearch Laboratories; 1:10,000) were used as secondary antibodies. For detecting the signals, SuperSignal West Pico or Femto Chemiluminescent Substrate was used. Western blot signals were acquired using a Chemidoc XRS+ Gel Imaging System and images were analyzed in the Image Lab software version 5.2.1 (BioRad).

Cell growth assay

Cells were seeded in 6-well tissue culture plates at a density of 1.21×10^4 cells per well and cell growth was monitored by trypsinizing the cells and counting every 24 hours for 8 consecutive days. Cell counts from each day were plotted using nonlinear regression and population doubling times (PDL) were calculated using the following equation (https://www.coriell.org):

$$\mathbf{PDL = 3.32 \times (log(\frac{total\ viable\ cells\ at\ harvest}{total\ viable\ cells\ at\ seed}))}$$

Cell cycle analysis and flow cytometry

Cell cycle analysis and flow cytometry was performed according to the method described in Maranon et. al. (Maranon et al. 2020) Briefly, exponentially growing cells were treated with 0.5 μM MMC for 1 hour, washed twice with warm 1×PBS and incubated in fresh media. At indicated time points, cells were pulse-labelled with 5-ethynyl-2′-deoxyuridine (EdU)-containing media (10 μM) for 20 minutes. Cells were then trypsinized, washed in ice-cold 1×PBS, fixed by adding 3 ml of ice-cold 70% ethanol in 1×PBS and stored at 4°C for at least 2 days. Fixed cells were rehydrated at room temperature for 1 hour in 2 ml of 1×PBS and permeabilized in 1×PBS with 0.25% Triton X-100 at room temperature for 30 minutes. The Click-iT EdU Alexa Fluor-488 reaction was carried out as described by the manufacturer (Thermo Fischer Scientific). Cells were washed once in 1×PBS with 1% BSA and then 0.5 ml prepared Click-iT reaction cocktail (1×TBS, 2 mM $CuSO_4$, 10 mM sodium ascorbate and Alexa Fluor 488 azide) was added to each sample. Samples were incubated at room temperature in the dark for 30 minutes. Cells were washed three times to gradually reduce the BSA and Triton X-100 concentration to 0.25% (BSA) and 0.025% (Triton X-100). Cells were pelleted and resuspended in 0.5 ml of 1×PBS containing 1 μl/ml SYTOX Red (Invitrogen) and 100 μg/ml RNase A (Invitrogen), stored in dark for 1 hour and then overnight at 4°C. Data acquisition was conducted using a CyAn ADP cell analyser (Beckman Coulter) with a 488 nm laser with a 530/40 nm band pass filter to detect EdU and a 635 nm laser with a 665/20 nm band pass filter to detect SYTOX. The analysis of cell cycle data was performed in FlowJo version 10.7 (BD Life Sciences).

Indirect immunostaining, microscopy and image analysis

Indirect immunostaining was performed according to our standard protocols (Maranon et al. 2020). Cells were seeded in four-chamber slides in a 20,000 cells per chamber density and incubated for 48 hours prior to exposure to 8Gy of γ-rays. After treatment, cells were fixed, permeabilized and incubated with primary antibodies in 1×PBS with 1% BSA overnight at 4°C. The primary antibody used was α-RAD54 (F-11; sc-374598; Santa Cruz Biotechnology; 1:1,000). Slides were then washed twice in 1×PBS and incubated in mouse AlexaFluor-488 goat secondary antibody (Thermo Fisher Scientific; 1:750) in 1×PBS

with 1% BSA for 45 minutes at room temperature. Finally, slides were mounted in ProLong gold antifade with DAPI (Molecular Probes).

A Zeiss Axio-Imager.Z2 microscope equipped with Zen Blue software (Carl Zeiss Microscopy) was used to take images using a 63× oil objective. In each channel, 18 Z-stacks were obtained as 0.2 µm slices. Images were processed in Fiji (https://imagej.net/Fiji), separating the channels and producing maximum projection files.

Metaphase spreads

For chromosomal aberrations, 2×10^5 cells were seeded in 6-well tissue culture plates and incubated at 37°C for 24 hours before treated with 4 mM hydroxyurea (HU; Sigma) for 5 hours at 37°C (Schlacher et al. 2011). After HU treatment, cells were washed in warm 1×PBS and treated with 0.1 µg/ml colcemid (SERVA) for 24 hours (Schlacher et al. 2011). To produce metaphase spreads we followed our standard protocols described previously (Wiese et al. 2007). Briefly, following the colcemid treatment, mitotic cells were shaken off and transferred to a clean tube. Attached cells were trypsinized and combined with mitotic cells. Cells were allowed to swell in 0.075 M KCl at 37°C for 30 minutes and fixed in methanol:acetic acid (3:1). Cells were dropped on slightly tilted ice-cold slides, air dried and stained in 0.2 M Sorensen buffer pH = 7.3 (0.2 M Na_2HPO_4•2H2O and 0.2 M NaH_2PO4•H_2O) with 3% Giemsa for 10 minutes at room temperature. Images were acquired using Zeiss Axio-Imager.Z2 microscope equipped with Zen Blue software (Carl Zeiss Microscopy) using a 63× oil objective. One hundred metaphases per sample per experiment were scored for chromosomal aberrations. In each metaphase the number of different chromosomal aberrations (radial chromosomes, chromatid breaks and chromatid gaps) was recorded and the number of mean aberrations per metaphase was analyzed.

DNA Fiber assay

DNA replication progression was assessed by DNA fiber assay (Schlacher et al. 2011; Taglialatela et al. 2017). Exponentially growing cells were pulse-labelled with chloro-deoxyuridine (CldU) (25 µM) for

20 minutes and then treated with or without 4 mM HU for 5 hours. Cells were washed with warm 1×PBS and pulse-labelled with iodo-deoxyuridine (IdU) (250 μM) for 20 minutes. Fiber spreads were prepared on slides from 0.5×10^6 cells/ml. Slides were allowed to air dry and fixed in methanol:acetic acid (3:1) for 10 minutes. Slides were rehydrated in 1×PBS for 10 minutes and denatured with 2.5 M HCl for 50 minutes. Fibers were blocked in 1×PBS with 5% BSA and 0.1% Triton X-100 for 1 hour and then incubated with primary antibodies in blocking solution. Rat α-BrdU (1:150; AbD Serotec) was used to detect CldU and mouse α-BrdU (1:100; Becton Dickinson) to detect IdU. Goat anti-rat AlexaFluor 594 (1:300; Molecular Probes) and goat anti-mouse AlexaFluor 488 (1:300; Molecular Probes) were used as secondary antibodies. Slides were mounted with Prolong Gold antifade (Molecular Probes) and images were acquired using a 63× oil objective on the microscope described above. Approximately 200 fibers were scored per condition per experiment. Both IdU and CldU tract lengths were recorded and the median tract lengths were plotted in Prism 8 GraphPad Software.

Statistical analyses

Prism 8 GraphPad Software was used to perform statistical analysis. Data obtained are from at least 2 independent experiments, unless stated otherwise. To assess statistical significance two-way ANOVA, or one-way ANOVA was performed, as indicated. A p value of ≤ 0.05 was considered significant.

2.3. Results

Simultaneous knockdown of both RAD51AP1 and RAD54 synergistically impairs gene conversion

In human cells, RAD51-mediated HR is supported by RAD51AP1 and RAD54. We and others have previously shown that knockdown of RAD51AP1 by shRNA leads to decreased HR DNA repair as determined by gene conversion at DR-GFP (Wiese et al. 2007; Liang et al. 2016). To test if HR DNA repair is affected after depletion of both RAD51AP1 and RAD54, we utilized the DR-GFP recombinational reporter incorporated in U2OS human osteosarcoma cells. In accord with our previous study, we find that knockdown of RAD51AP1 leads to a ~50% decrease in gene conversion (**Figure 2.1A and B**). A similar decrease was observed when RAD54 was depleted by siRNA. However, simultaneous depletion of both

RAD51AP1 and RAD54 exhibited a much greater effect with gene conversion levels dropping to ~5% (**Figure 2.1A and B**). These results show that both RAD51AP1 and RAD54 support gene conversion at DR-GFP in U2OS cells, and suggest that either protein can compensate for the other to some extent.

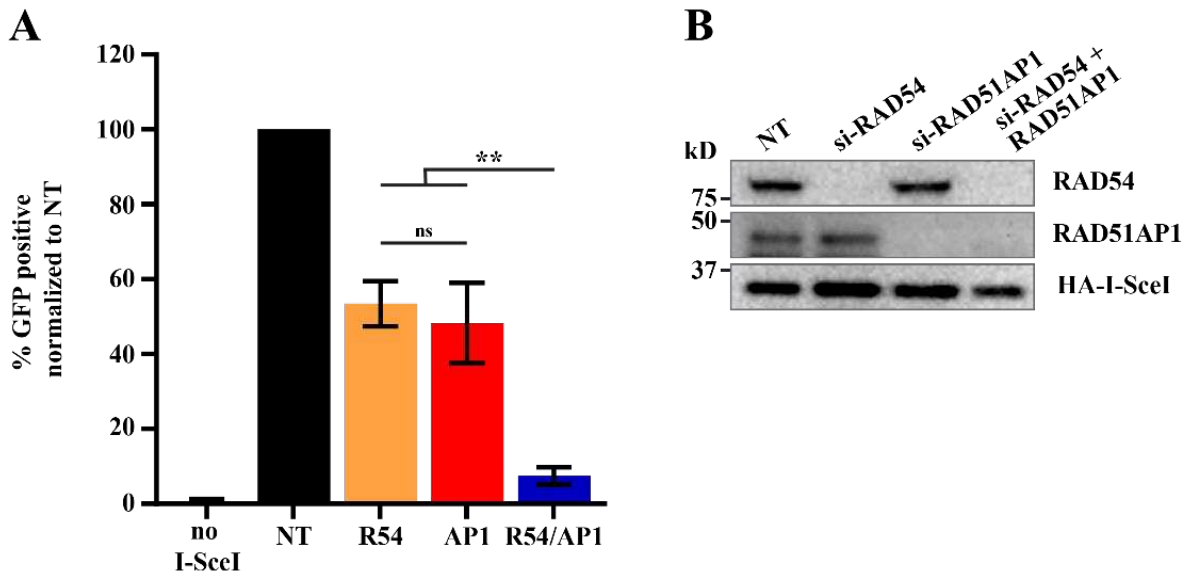

Figure 2.1. Depletion of RAD51AP1 and RAD54 synergistically affects gene conversion in U2OS-DRGFP cells. **(A)** Average percentage of GFP positive cells normalized to non-targeting control siRNA (NT) after RAD51AP1 (here: AP1) and/or RAD54 (here: R54) knockdown. Bars are the means from 3 independent experiments ±1SD. **, $p<0.01$, ns, not significant; one-way ANOVA analysis (Tukey's multiple comparisons test). **(B)** Western blots of whole extracts confirming the knockdown of RAD54 and RAD51AP1 in DR-GFP U2OS cells. The signal for HA-I-SceI serves as a transfection control.

Generation and characterization of RAD51AP1/RAD54 double knockout cells

To further investigate a synergistic relationship between RAD51AP1 and RAD54, we generated single *RAD51AP1* or *RAD54* and double *RAD51AP1/RAD54* knockout (KO) HeLa cell lines using CRISPR/Cas9 technology. The sgRNAs used, target the Cas9-nic to produce single-strand breaks in the complementary DNA strands and within the catalytic site, the ATPase domain, of RAD54 and result in the introduction of a small deletion (**Figure S2.1A**). To verify the disruption of *RAD54* alleles and loss of RAD54 expression, 5 single *RAD54* KO and 3 double *RAD51AP1/RAD54* KO (DKO) promising clonal

isolates were screened by WB analysis of prepared nuclear extracts (**Figure 2.2A**). From these clones, two *RAD54* KO (**Figure 2.2A, lanes 3 and 4**) and two DKO clones (**Figure 2.2A**, **lanes 5 and 6**) were selected for further studies. In both DKO clones, we detected less nuclear RAD51 protein expressed compared to single *RAD51AP1* or *RAD54* KO and HeLa control cell lines (**Figure 2.2A**, **compare lanes 5-6 and 1-4**). To verify loss of RAD54 foci formation by ICC, cells were exposed to 8 Gy γ-rays, fixed and stained at 4 hours after treatment (**Figure S2.1B**). RAD54 foci are visible in RAD54 expressing cells, but absent in *RAD54* KO and DKO cells, as expected. Clones with abrogated RAD54 expression were then sequenced across the Cas9-nic cleavage sites to confirm sequence loss. The KO clones produced smaller amplicons confirming deleted sequences (**Figure S2.1C**). We then purified all specific bands of 597 bp and shorter and proceeded to sequencing. The schematic in **Figure S2.1D** shows the type of deletions in KO cell lines. In the tested *RAD54* KO cell line only one allele could be detected, while in DKO cell lines all three alleles were detected. The RAD54 gene is located on the short arm of chromosome 1 and it has been shown that in HeLa cells the short arm of chromosome 1 has 3 copies (Landry et al. 2013). Therefore, we speculate that in *RAD54* KO cells we could not detect the other two edited alleles due to generation of larger deletions that may include the binding sequences for the primers P1 and P2.

Next, we sought to investigate if loss of RAD51AP1 and/or RAD54 would affect the growth rates of the KO cell lines. We found no significant difference between growth rates and the doubling times for single *RAD51AP1* or *RAD54* KO and DKO cells when compared to HeLa cells (**Figure S2.1E**). This indicates that the cells lacking RAD51AP1 and/or RAD54 overall replicate similar to Hela cells.

Deletion of RAD54AP1/RAD54 sensitizes HeLa cells to DNA damaging agents

To phenotypically characterize the single *RAD51AP1* or *RAD54* KO and DKO cell lines for their sensitivity to DNA damaging agents, we performed mitomycin C (MMC) cell survival assays. Cells were treated with or without MMC for 1 hour and plated for colony formation. In accord with our previous studies (Liang et al. 2019), we show that *RAD51AP1* KO cells are more sensitive to MMC than wild type cells (**Figure 2.2B, orange line**). Compared to *RAD51PA1* KO cells, both clones of *RAD54* KO cell lines

show very similar sensitivity to MMC (**Figure 2.2B, red lines**). Interestingly, DKO cells are considerably more sensitive to MMC exposure compared to single *RAD51AP1* or *RAD54* KO cells (**Figure 2.2B, blue lines**). To confirm that the observed phenotype is not a cell type-specific effect only observed in the HeLa cell line, we tested A549 cells with RAD51AP1 and/or RAD54 depletion. We observed comparable degrees of sensitization for A549 cells with RAD51AP1 or RAD54 knockdown. A549 cells depleted for both RAD51AP1 and RAD54 showed the highest sensitivity to MMC (**Figure S2.1F and G**), similar to what we observed for DKO HeLa cells (**Figure 2.2B**). These results suggest some degree of functional redundancy between RAD51AP1 and RAD54 in both HeLa and A549 cells.

In addition to MMC sensitivity, we pursued to examine the sensitivity to a different DNA-damaging agent and specifically the PARP1/2 inhibitor, olaparib. PARP inhibitors are commonly used as chemotherapeutic agents to treat patients with BRCA-mutant tumors (Wang et al. 2017a; Bochum et al. 2018; Faraoni and Graziani 2018). Olaparib works by trapping PARP-1 on the DNA and the PARP-1-DNA complexes then interfere with DNA replication. *RAD54* KO cells show a more pronounced sensitivity to olaparib than *RAD51AP1* KO cells (**Figure S2.1H**). Interestingly, synergistic effects are observed for DKO cells in response to olaparib (**Figure S2.1H**). These results further support the notion of a functional redundancy between RAD51AP1 and RAD54. Also, the difference in sensitivity between *RAD51AP1* KO and *RAD54* KO cells suggests that RAD51AP1 and RAD54 exhibit a different degree of dependence on PARP-1.

Cells lacking both RAD51AP1 and RAD54 show a more pronounced G2/M arrest after MMC treatment

To further elucidate the impact of RAD51AP1 and/or RAD54 loss in cells exposed to MMC, we assessed cell cycle progression of DKO and single *RAD51AP1* or *RAD54* KO cells by flow cytometry and compared the results to HeLa cells. In the absence of MMC, all cell lines proceed similarly through the cell cycle (**Figure 2.2C and Figure S2.2A**). At 24 hours post release from MMC exposure, all cell lines arrested in G2/M phase (**Figure 2.2D and Figure S2.2A**). However, at 72 hours post-treatment, HeLa and single *RAD51AP1* or *RAD54* KO cells were able to proceed through mitosis and enter the following cell cycle,

while DKO cells remained arrested in G2/M-phase (**Figure 2.2E and Figure S2.2A**). These results show that in response to MMC treatment the cell cycle progression of cells lacking both RAD51AP1 and RAD54 is impaired, likely resulting from the higher fraction of sustained DNA damage in these cells.

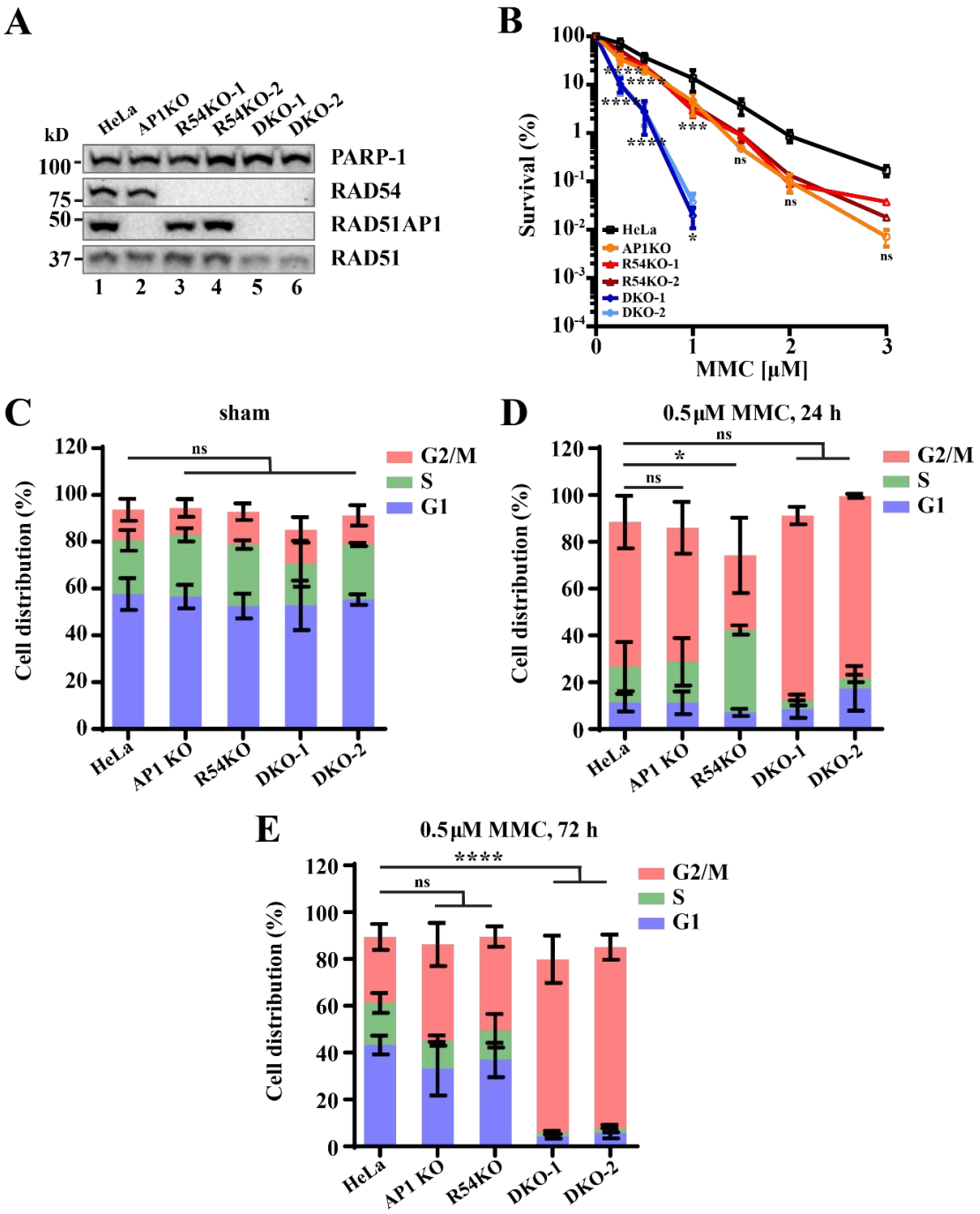

Figure 2.2. Deficiency of both *RAD51AP1* and *RAD54* synergistically affects sensitivity to MMC and cell cycle progression. (A) Western blots of nuclear extracts. The signal for PARP-1 serves as loading control. **(B)** Results from

clonogenic cell survival assays of HeLa, single *RAD51AP1* or *RAD54* KO and DKO cells after MMC. Data points are the means from 3 independent experiments ± 1SD. ***, $p<0.001$, ****, $p<0.0001$, ns, not significant; two-way ANOVA analysis (Dunnett's multiple comparisons test). **(C)** Average percentage of cells in G1, S and G2/M cell cycle phases without MMC treatment. **(D)** As described in panel **(C),** 24 hours after treatment with 0.5 μM MMC for 2 hours. **(E)** As described in panels **(C)** and **(D),** 72 hours after treatment with MMC. Bars are the means from 3 independent experiments ± 1SD. *, $p<0.05$, ****, $p<0.0001$, ns, not significant; one-way ANOVA analysis (Dunnett's multiple comparisons test).

RAD54 deficiency in RAD54 KO and DKO cells is rescued by ectopic expression of RAD54-HA

To ascertain that the sensitivity observed in single *RAD51AP1* or *RAD54* KO and DKO cells truly is a consequence of the loss of *RAD54*, we ectopically expressed RAD54-HA and monitored these cells for their response to MMC in cell survival assays. The expression of ectopic RAD54-HA in *RAD54* KO and DKO cells was first evaluated by western blot analysis and compared to endogenous RAD54 levels in HeLa cells (**Figure S2.2B and Figure S2.2C**). Compared to the level of endogenous RAD54 protein in HeLa cells, we found that the expression of the ectopic RAD54 is slightly higher in DKO cells (**Figure S2.2B, lane 6 compared to 5 and 1**) and similar to that of HeLa cells in *RAD54* KO cells (**Figure S2.2C lane 3 compared to 1**). We also performed ICC to monitor the ability of the ectopic protein to accumulate into IR-induced protein foci. We found that after 8 Gy γ-rays, in *RAD54* KO and DKO cells the ectopic RAD54 protein could successfully form foci similar to what is observed in HeLa cells (**Figure S2.2D and Figure S2.1B)**.

HeLa, *RAD54* KO and DKO cells with and without RAD54-HA were then challenged with MMC in clonogenic cell survival assays. In DKO+RAD54-HA cells (**Figure 2.3A**) the *RAD54* deficiency is rescued by ectopic RAD54, and now comparable to that of *RAD51AP1* KO cells. DKO cells expressing RAD54-HA also were evaluated for their cell cycle profile after MMC treatment. Without any damage, the cell cycle profile of DKO+RAD54-HA cells (**Figure 2.3B and Figure S2.2A, sham**) is similar to that of single *RAD51AP1* or *RAD54* KO and HeLa cells (**Figure 2.2C**). At 24 hours post release from MMC, DKO+RAD54-HA cells are arrested at G2/M phase (**Figure 2.3B and Figure S2.2A, 24 hours**), as seen for

single *RAD51AP1* or *RAD54* KO and HeLa cells (**Figure 2.2D**). At 72 hours post release from MMC, DKO+RAD54-HA cells could proceed with the cell cycle and enter G1 phase (**Figure 2.3B and Figure S2.2A, 72 hours**), similar to what is observed for single *RAD51AP1* or *RAD54* KO and control HeLa cells (**Figure 2.2E**). In addition, we found that *RAD54* deficiency is also rescued by ectopic RAD54 in *RAD54* KO cells undergoing MMC cell survival assays, and that the phenotype of *RAD54* KO cells expressing RAD54-HA is comparable to that of HeLa cells (**Figure 2.3C).** These results support the notion that the phenotypes associated with *RAD54* loss in single *RAD54* KO and DKO cells stem from the loss of RAD54.

We sought to investigate if ectopic RAD54 could also rescue *RAD51AP1* KO cells. The expression of ectopic RAD54-HA in *RAD51AP1* KO cells was confirmed by western blot and expression level was determined. We selected two different *RAD51AP1* KO clones that overexpressed the ectopic protein in comparison to HeLa cells (**Figure S2.2B, lanes 3 and 4 compared to 2 and 1**). In one clone the expression of RAD54-HA was found to be ~8-fold higher than that of endogenous RAD54 in HeLa cells (**Figure S2.2B, lane 3 compared 1**). In the second clone, the expression of RAD54-HA was ~4-fold higher than that of RAD54 in HeLa cells (**Figure S2.2B, lane 4 compared 1**). When these two clones were challenged with

MMC, no rescue of MMC sensitivity was observed (**Figure 2.3C**). These results show that overexpression of RAD54 in *RAD51AP1* KO cannot override the lack of RAD51AP1 protein.

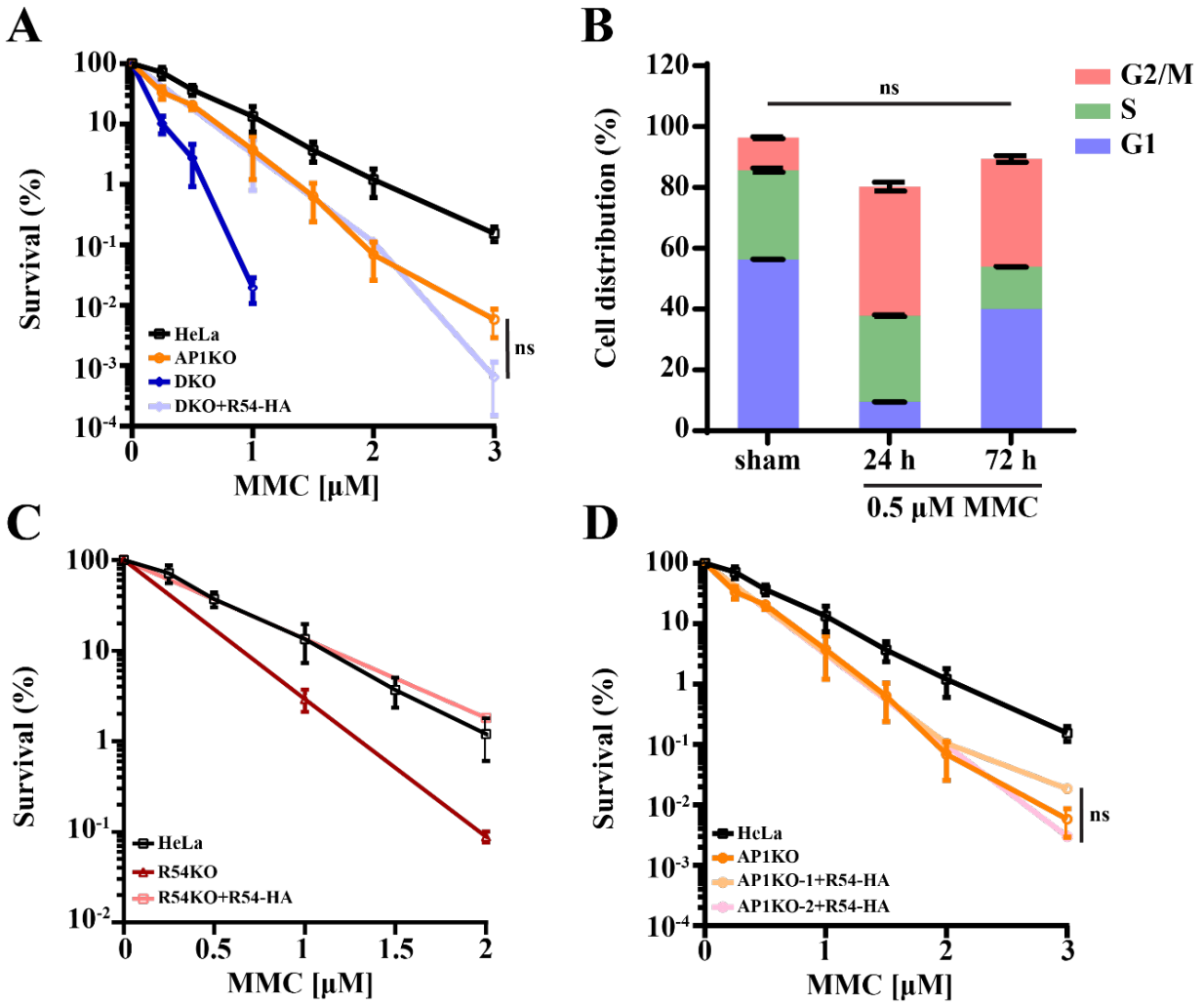

Figure 2.3. Ectopic RAD54 expression can rescue *RAD54* deficiency. (A) Results from clonogenic survival assays after MMC treatment of *RAD51AP1* and *RAD54* deficient cells with and without ectopic RAD54-HA. Data points are the means from 2 independent experiments ± 1SD. ns, not significant; two-way ANOVA analysis (Sidak's multiple comparisons test). **(B)** Average percentage of DKO cells with ectopic RAD54-HA in G1, S and G2/M cell cycle phases without MMC (sham), 24 and 72 hours after MMC treatment. Bars are the means from 2 technical replicates ± 1SD. ns, not significant compared to HeLa cells; one-way ANOVA analysis (Dunnett's multiple comparisons test). **(C)** Results from clonogenic survival assays after MMC treatment of *RAD54*-deficient cells with and without ectopic RAD54-HA. Data points are the means from 3 technical replicates. **(D)** Results from clonogenic survival assays after

MMC treatment of *RAD51AP1* deficient cells with different levels of ectopic RAD54-HA. For AP1KO+R54-HA #1 data points are the means of 2 independent experiments ± 1SD. ns, not significant; two-way ANOVA analysis (Sidak's multiple comparisons test). For AP1KO+R54-HA #2 data points are the means of 3 technical replicates.

Deletion of both RAD51AP1 and RAD54 exacerbates genomic instability

To investigate if loss of both *RAD51AP1* and *RAD54* renders the cells more prone to genomic instability, metaphase spreads were prepared after treatment with hydroxyurea (HU). HU is a cytostatic agent that inhibits the ribonucleoside phosphate reductase, depleting the deoxyribonucleoside pool and immediately stalls replication forks (Bianchi et al. 1986).The schematic of the experimental design is shown in **Figure 2.4A**. In **Figure 2.4B**, representative images are shown for 3 types of chromosomal aberrations scored (radial chromosomes, black arrow; chromatid breaks, red arrow; chromatid gaps, blue arrow). Comparing the mean number of aberrations per metaphase, DKO cells have a significantly higher number of aberrations than single *RAD51AP1* or *RAD54* KO or HeLa cells (**Figure 2.4C**). These results suggest that compared to single *RAD51AP1* or *RAD54* KO cells, DKO cells exhibit higher levels of unrepaired or unfaithfully repaired DNA damage, in accord with their more pronounced G2/M arrest and our results described above (**Figure 2.2**).

Replication fork restart is slower in cells deleted for RAD51AP1 and RAD54

Next, we sought to examine the roles of RAD51AP1 and RAD54 in DNA replication and their impediments to replication fork progression. To this end, we used the single-molecule DNA fiber assay and labeled exponentially growing cells first with CldU, treated cells with HU, and then – upon removal of HU - labeled cells with IdU (**Figure 2.4D)**. Replication fork restart was determined by measuring the tract lengths of IdU labeled fibers in HeLa and KO cell lines. In **Figure 2.4E,** representative images are shown for a restarted fork (**Figure 2.4D, i**), a fork that restarted with delay (**Figure 2.4D, ii**) and a fork that failed to restart (**Figure 2.4D, iii**). Without HU treatment, DKO cells have significantly shorter IdU tracts compared to the single *RAD51AP1* or *RAD54* KO (*RAD51AP1* KO, $p<0.0001$; *RAD54*KO, $p=0.0002$) and HeLa cells ($p<0.0001$) (

Table S2.3), indicating that replication fork progression may be hindered by endogenous DNA damage in DKO cells (**Figure 2.4F**). Following HU, replication fork restart is similarly impaired in both HeLa and *RAD51AP1* KO cells. In *RAD54* KO cells, however, replication forks progress faster post-HU release when compared to HeLa cells. Remarkably, after HU treatment, replication fork restart in DKO cells is greatly impaired in comparison to single *RAD51AP1* or *RAD54* KO ($p<0.0001$) and HeLa cells ($p<0.0001$) (

Table S2.4 and Figure 2.4G). These results show that, in comparison to single *RAD51AP1* or *RAD54* KO cells, DKO cells are significantly more sensitive to replication stress.

Previous studies have described the function of HR proteins in the protection of stressed replication forks (Bugreev et al. 2011; Schlacher et al. 2011; Schlacher et al. 2012). For example, when replication is stalled by HU in *BRCA2*-deficient cells, newly synthesized DNA is rapidly degraded (Schlacher et al. 2011). To assess if deletion of RAD51AP1 and/or RAD54 affects the degradation of nascent DNA at stalled replication forks, we measured the lengths of the CldU tracts in cells treated with and without HU. Our results show that while in single *RAD51AP1* or *RAD54* KO, DKO and HeLa cells CldU tracts are significantly shorter after treatment with HU compared to non-treatment (sham) (p<0.0001), all cell lines exhibit CldU tracts of similar lengths after HU (**Table S2.5 and Figure S2.2D**). These results suggest that RAD51AP1 and RAD54 have no role in the stabilization of stressed forks and protection of the DNA from the spurious attack of unregulated or false activity of nucleases.

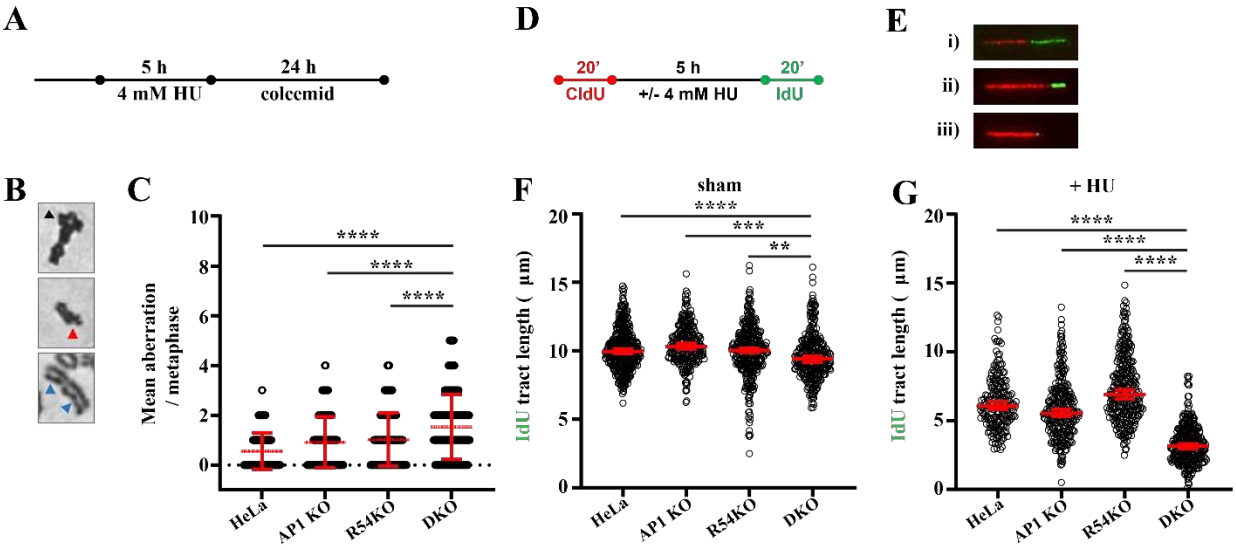

Figure 2.4. Concomitant loss of *RAD51AP1* and *RAD54* results in increased genome instability and replication stress. (A) Schematic of experimental protocol for chromosomal aberration analyses. **(B)** Representative images of chromosomal aberrations after HU; radial chromosomes (black arrow), chromatid breaks (red arrow) and chromatid gaps (blue arrow). **(C)** Mean number of chromosomal aberrations per metaphase. Bars are the means from 2 independent experiments ± 1SD. ****, p<0.0001; one-way ANOVA analysis (Tukey's multiple comparisons test).

(D) Schematic of experimental protocol for DNA fiber analyses. **(E)** Representative images of fiber tracts; i) restarted, ii) delayed, and iii) failed to restart replication fork. **(F)** Median IdU (green) tract length in cells without treatment. Per experiment and condition 100-150 fibers were analyzed. **(G)** As described in panel **(F),** after treatment with 4mM HU. Data points are the medians from 2 independent experiments ±95% CI. ****, $p<0.0001$; Kruskal-Wallis test (Dunn's multiple comparisons test).

Depletion of RAD54B in RAD54 KO renders cells more sensitive to MMC

The synergistic relationship between RAD54 and RAD54B has been shown in mice *in vivo* and *in vitro* (Wesoly et al. 2006). However, the activity of RAD54B in HR in human cells is less well understood. Hence, we wanted to investigate if RAD54B contributes to the repair of MMC-induced DNA damage in single *RAD51AP1* or *RAD54* KO and DKO cells. We depleted RAD54B by siRNA in HeLa, single *RAD51AP1* or *RAD54* KO and DKO cells and performed MMC survival assays (**Figure 2.5**). Depletion of RAD54B in HeLa and *RAD51AP1* KO cells had no effect on the survival of cells after exposure to MMC (**Figure 2.5B**). Likewise, in DKO cells depletion of RAD54B had no effect on the survival. Interestingly, after RAD54B depletion, *RAD54* KO cells exhibited a small but significantly increased sensitivity to MMC (p=0.044). These results support within-pathway redundancy between RAD54 and RAD54B in HeLa cells, and show that RAD54B apparently has no role in protecting HeLa cells from MMC-induced DNA damage in the presence of RAD54. Hence, RAD54B partially can compensate for the loss of RAD54 in human cells.

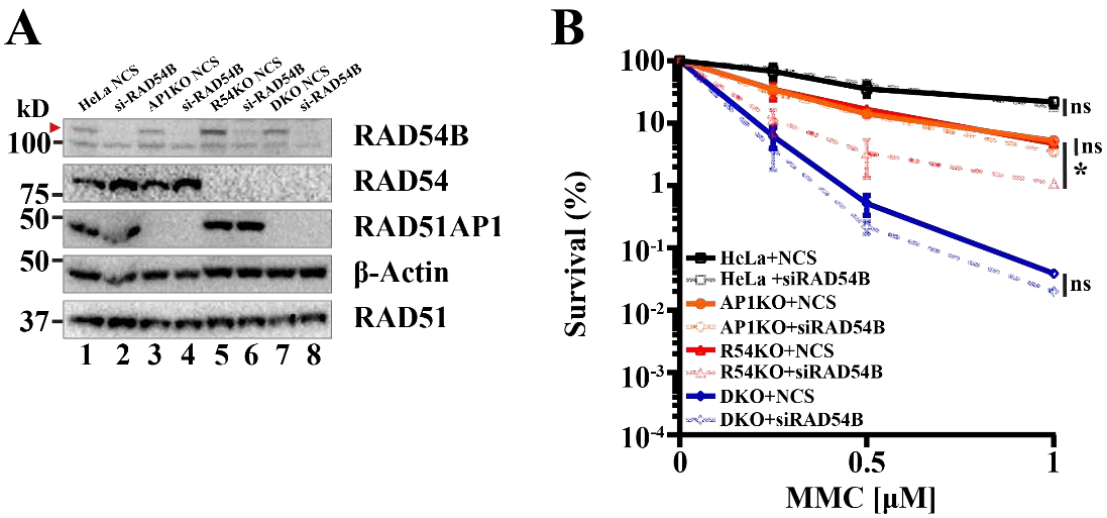

Figure 2.5. RAD54B depletion in *RAD54* KO leads to increased MMC sensitivity. (A) Western blots of whole extracts confirming the knockdown of RAD54B in HeLa, *RAD51AP1* KO, *RAD54* KO and DKO cells. The signal of β-actin serves as a loading control. **(B)** Results from clonogenic survival assays of HeLa, *RAD51AP1* KO, *RAD54* KO and DKO cells with NCS (a non-depleting control siRNA) or RAD54B siRNA. Data points are the means from 2 independent experiments ± 1SD. ns, not significant, *, $p<0.05$; two-way ANOVA analysis (Sidak's multiple comparisons test).

DKO cells depleted for BRCA1 show further increased cellular sensitivity to MMC

BRCA1 functions early in the HR pathway by counteracting the inhibitory effect of 53BP1 during DNA end resection (Bunting et al. 2010). In addition, at the synaptic stage, BRCA1 binds to RAD51 and enhances its activity in strand invasion (Scully et al. 1997; Silver and Livingston 2012; Zhao et al. 2017). Compromised HR activity is observed in many breast cancer patients with *BRCA1* deficiency, as they express BRCA1 protein with missense mutations or truncations (Elstrodt et al. 2006). It has also been shown that some breast cancer cells with *BRCA1* mutations overexpress RAD51AP1 and/or RAD54 (Song et al. 2004; Martin et al. 2007; Pathania et al. 2016; Bridges et al. 2020), by which they may regain HR functionality and limit genome instability. Therefore, we questioned if the phenotype that is described for BRCA1 mutant cells was comparable to that of DKO cells simulating the hypomorphic mutant BRCA1 condition by BRCA1 knockdown, and if BRCA1 depletion in DKO cells would render these more sensitive to MMC. To this end, HeLa and DKO cells were depleted for BRCA1 by siRNA and challenged with MMC

(**Figure 2.6**). BRCA1 depletion in HeLa cells increased their sensitivity to MMC, as expected, although not to the degree of DKO cells transfected with a non-depleting negative control siRNA. Moreover, compared to DKO cells transfected with negative control siRNA, DKO cells depleted for BRCA1 exhibited further increased sensitivity to MMC (**Figure 2.6B**). Overall, these results could suggest that targeted inactivation of both *RAD51AP1* and *RAD54* may further increase the sensitivity to chemotherapy of HR-compromised cancer cells that express mutant BRCA1.

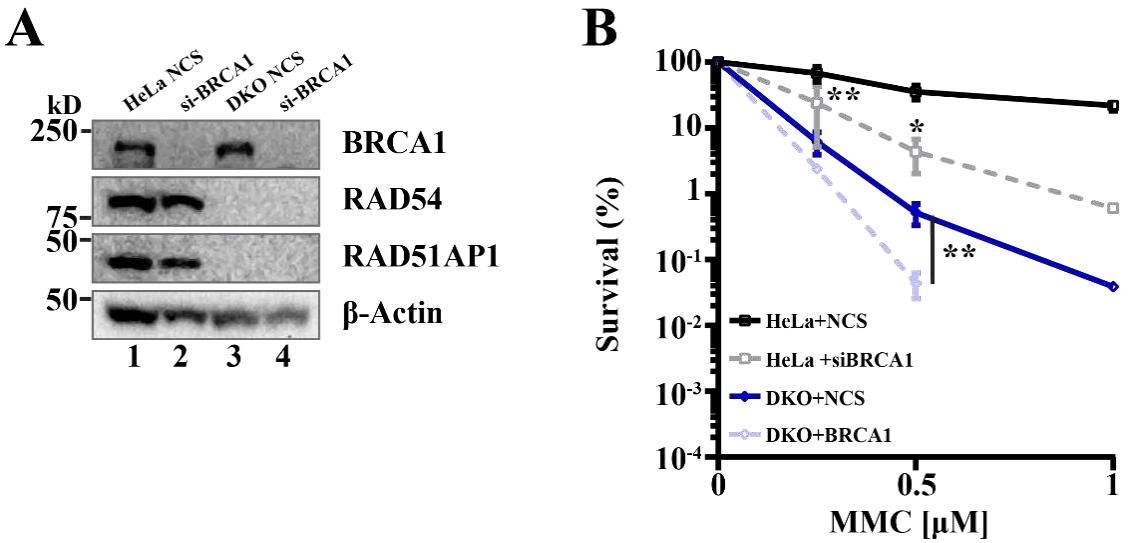

Figure 2.6. BRCA1 depletion in HeLa leads to increased MMC sensitivity. (A) Western blots of whole extracts confirming the knockdown of BRCA1 in HeLa and DKO cells. The signal of β-actin serves as a loading control. **(B)** Results from clonogenic survival assays after MMC treatment in HeLa and DKO cells with NCS or siRAD54B. Data points are the means from 2 independent experiments ± 1SD. **, $p<0.01$, ****, $p<0.0001$; two-way ANOVA analysis (Sidak's multiple comparisons test).

2.4. Discussion

Previous studies have shown that loss of *RAD51AP1* leads to a moderate phenotype in human cells after treatment with DNA damaging agents (Modesti et al. 2007; Wiese et al. 2007; Liang et al. 2019; Olivieri et al. 2020). Similarly, other studies and this study show that cells with *RAD54* deficiency exhibit mild sensitivity to DNA damaging agents (Maranon et al. 2020; Olivieri et al. 2020; Zhou et al. 2020). In our study, for the first time, we show that cells with simultaneous deletion of both *RAD51AP1* and *RAD54*

are hypersensitive to MMC and more prone to genome instability compared to cells with single deletion of either *RAD51AP1* or *RAD54*. Taken together, our results suggest that the two proteins largely can compensate for each other in HR in human cells. On the other hand, the moderate phenotype that is observed after loss of either RAD51AP1 or RAD54 suggests that these two proteins also have distinct roles in HR. Both RAD51AP1 and RAD54 can enhance the activity of RAD51 and assist with the formation of the synaptic complex as well as the D-loop (Jaskelioff et al. 2003; Modesti et al. 2007; Wiese et al. 2007; Wright and Heyer 2014). During these steps, when one protein is absent the other may compensate. What functionally separates the two proteins is the ATPase activity of RAD54, that RAD51AP1 is lacking (Petukhova et al. 1998). The ATPase domain is responsible for ATP hydrolysis which produces the needed energy for RAD54 to facilitate homology search, branch migration and finally the disruption of the D-loop (Mazin et al. 2000; Wright and Heyer 2014; Crickard et al. 2020). At these very late stages of HR, RAD54 may work independently of RAD51AP1.

Similar to the response observed after MMC, DKO are hypersensitive to olaparib. However, while we noticed comparable sensitivities to MMC for single *RAD51AP1* or *RAD54* KOs, surprisingly their response to olaparib was different, and *RAD51AP1*-deficient cells are less sensitive than *RAD54* KO cells. While the reasons for this are not known at this point, our observation is supported by the *in vivo* results of Tanori et al. (Tanori et al. 2017). This group has shown that in mice disruption of both *Rad54* and *Parp-1* leads to synthetic lethality and nonviable double mutants. Cell-based studies have also shown that depletion of RAD54 and treatment with PARPi leads to synthetic phenotype (Gottipati et al. 2010; Spies et al. 2016; Poti et al. 2019). A recent study performed a CRIPSR/Cas9 screen in an hTERT-immortalized RPE1 cell line and identified genes, deletion of which increases sensitization to different genotoxic agents. Among the multiple hits, deficiency of RAD51AP1 leads to a very mild sensitivity to olaparib, that is less prominent than what is observed in *RAD54*-deficient cells (Olivieri et al. 2020). Taken together, our results and those of others could suggest that RAD51AP1 and PARP-1 have a more epistatic relationship while PARP-1 may work independently from RAD54. In this regard, it is interesting to note that GFP-RAD51AP1 and PARP-

1 co-precipitate in U2OS cells (Wagner et al. 2016). Therefore, we speculate that PARP-1 and RAD51AP1 could function together in HR or within the same sub-pathway, while RAD54 and PARP-1 are part of distinct pathways.

When we looked at the impact of loss of both RAD51AP1 and RAD54 on the replication fork restart we found that in DKO replication forks are stalled longer after HU. A remarkable observation was the fact that replication fork restart after HU of *RAD54* KO cells was faster than in all other cell lines tested. The DNA replication machinery of eukaryotic cells can be challenged by accumulated ssDNA gaps at the replication fork leading to its stall (Budzowska and Kanaar 2009; Prado 2018). The cell has developed several mechanisms to rescue stalled replication forks. Replication fork regression which leads to a formation of a DNA junction called the "chicken foot" is one of such mechanisms (Meng and Zhao 2017). *In vitro*, RAD54 is one of the proteins that can catalyze the regression of stressed forks to allow their restoration and progression at a later time (Bugreev et al. 2011). We speculate that, when RAD54 is absent, replication fork regression is diminished and replication forks progress past their lesions, and that is why we observe longer IdU tracts in *RAD54* KO cells after HU treatment. Looking at the DNA degradation after HU treatment, we found that RAD51AP1 and RAD54 are not involved in the protection of ssDNA from nucleases, suggesting that the non-canonical role of HR proteins at replication forks is not directly affected by loss of RAD51AP1 and RAD54.

RAD54B, while sharing functional similarities with RAD54, seems to not majorly contribute to the HR reaction in human cells when RAD54 is present. We found that only in the absence of RAD54, RAD54B depletion renders cells more sensitive to MMC. This indicates that the RAD54B can partially substitute for the function of RAD54 in human cells. While the depletion of RAD54B in *RAD54* deficient cells leads to increased MMC sensitivity, it is milder compared to what is observed for DKO cells. This could be due to the partial, incomplete depletion of RAD54B by siRNA. Another explanation may be that there is another, yet unidentified translocase that can compensate for the loss of both RAD54 and RAD54B. In *RAD51AP1* KO cells, RAD54B depletion has no effect and this is probably because these cells fully rely on the activity

of RAD54. We also found no effect of RAD54B depletion in DKO cells. One interpretation of this result could be that RAD54B activity requires RAD51AP1 to be present.

Overall, we suggest that there is functional redundancy within the HR pathway between RAD51AP1 and RAD54, and between RAD54 and RAD54B. Firstly, when RAD51AP1 or RAD54 are deleted individually, cells exhibit moderately impaired HR, likely because RAD51AP1 and RAD54 can compensate for each other to large extents (**Figure 2.7A**). In addition, RAD54B can partially compensate for loss of RAD54 (**Figure 2.7A**). Simultaneous deletion of both *RAD51AP1* and *RAD54* renders cells very sensitive and leads to cell death after chemotherapeutic drugs. In addition, RAD54B in a *RAD51AP1*/*RAD54* KO background seems to not compensate the loss of RAD54, possibly because it requires RAD51AP1 presence (**Figure 2.7B**). It is also possible that upon removal of both RAD54 and RAD54B, a third translocase and member of the SWI2/SNF2 protein family may step in to assist with branch migration (**Figure 2.7C**).

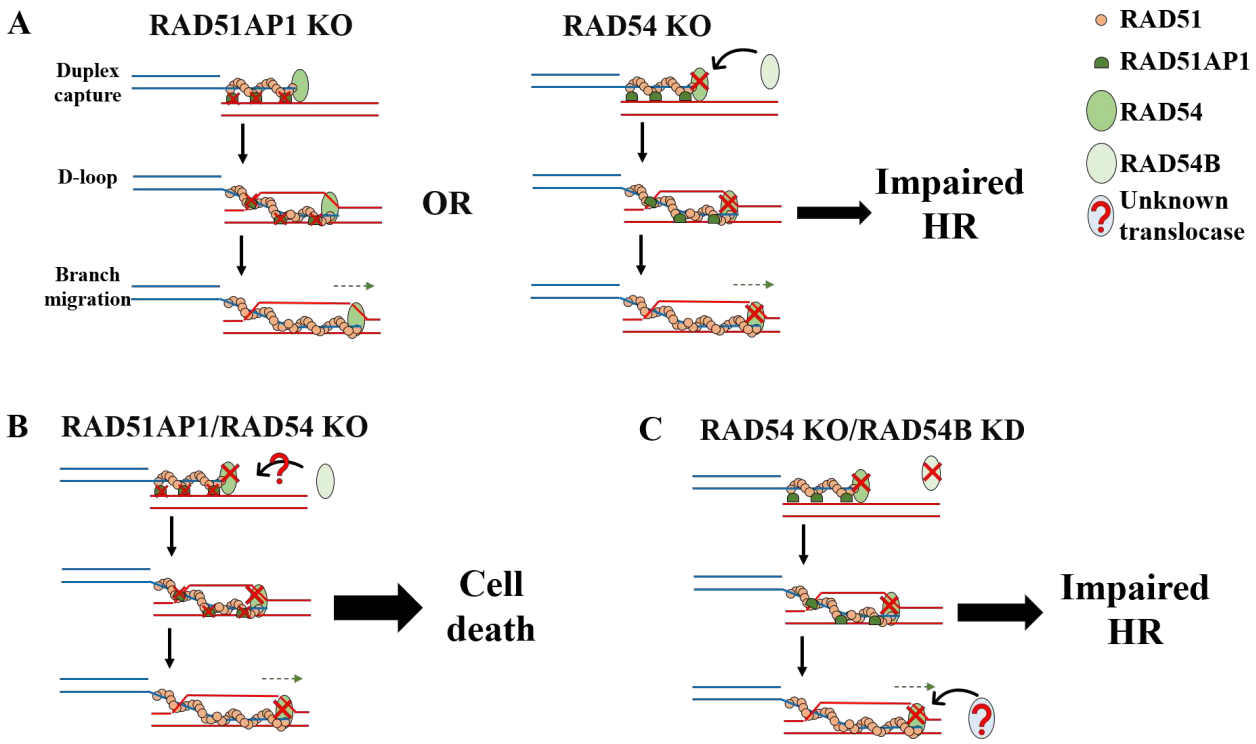

Figure 2.7. Model to explain the functional redundancy between RAD51AP1 and RAD54, and between RAD54 and RAD54B. (A) In *RAD51AP1*-deficient cells, synaptic and post-synaptic stages of HR rely on RAD54 activity (and possibly also on RAD54B). In *RAD54* KO cells both RAD51AP1 and RAD54B can compensate for loss of RAD54 (albeit possibly to different degrees). Both single *RAD51AP1* or *RAD54* KO cell lines exhibit impaired HR. **(B)** Loss of both *RAD51AP1* and *RAD54* leads to greatly impaired HR and cell death. **(C)** Depletion of RAD54B in *RAD54* KO cells can further impair HR. Duplex capture and D-loop formation is supported by RAD51AP1. However, branch migration may be assisted by a third translocase that remains to be identified.

HeLa cells, upon depletion of BRCA1, exhibit moderately increased sensitivity to MMC. However, breast cancer cell lines with defective *BRCA1* exhibit hypersensitivity to MMC (Hill et al. 2014). An explanation may be that HeLa cells are more resistant to MMC compared to breast cancer cells. Another explanation might be partial BRCA1 depletion by siRNA and this could be related to the importance of BRCA1 in early stages of HR (Bunting et al. 2010). Finally, we found that depletion of BRCA1 in DKO renders the cells more sensitive to MMC and this might be due to the role of BRCA1 later within the pathway, where it enhances RAD51 activity (Zhao et al. 2017). Taken together, I believe that both

RAD51AP1 and RAD54 are great candidates to further sensitize BRCA1-mutant tumors to chemotherapeutic agents. Importantly, my results suggest that the simultaneous inactivation of both RAD51AP1 and RAD54 may be a promising new strategy in the development of more effective anti-cancer therapy in tumors with proficient/overactive HR.

2.5. Future Directions

Our findings support the notion that within the HR pathway there is functional redundancy between several proteins: RAD51AP1, RAD54 and RAD54B. Here we found that RAD51AP1 and RAD54 display a synergistic interaction in HR, in which they exhibit overlapping as well as distinct functions. Considering that RAD51AP1 and RAD54 might also work together at some distinct steps of the HR reaction in cells, and considering that both interact with RAD51, one should investigate if RAD51AP1 and RAD54 physically interact and try and map their binding domains by using different truncation mutants.

We also found that gene conversion is significantly impaired after simultaneous depletion of both RAD51AP1 and RAD54. It would be interesting to further investigate if disruption of both proteins will affect HR progression by analyzing RAD51 foci formation kinetics. It has been previously shown that depletion of RAD51AP1 in DT40 cells impairs the resolution of DNA damage induced RAD51 foci after exposure of cells to IR (Parplys et al. 2014). Therefore, we hypothesize that in HeLa cells deleted for both RAD51AP1 and RAD54 resolution of RAD51 foci will be dramatically impaired after IR treatment.

To follow up on our results regarding the increased sensitivity to MMC after depletion of RAD54B in *RAD54* KO cells, it would be interesting to produce double *RAD54* and *RAD54B* KO cell lines and monitor their sensitivity to MMC. We speculate that the phenotype could be similar to that of *RAD51AP1 RAD54* DKO cells. To confirm such an effect in a double KO of *RAD54* and *RAD54B*, we would further investigate the phenotype of such cells by analyzing their response to replication stress in the DNA fiber assay. Should *RAD54/RAD54B* DKO cells exhibit the same phenotype as *RAD51AP1/RAD54* DKO cells, it would be interesting to test if RAD51AP1 and RAD54B can function together. However, if the observed

phenotype is similar to the one seen in **Figure 2.5** in *RAD54* KO after RAD54B depletion, it would be exciting to try and screen for a different translocase within the SNF2/SWI2 family, that may be able to compensate for loss of both RAD54 and RAD54B.

Finally, it would be interesting to investigate where the difference in olaparib sensitivity between *RAD51AP1* KO and *RAD54* KO cells stems from. We could reaffirm the association of RAD51AP1 with PARP-1 and that RAD54 is unable to associate with PARP-1. That would partially explain the difference between the two phenotypes.

CHAPTER THREE

RAD51AP1 is not required for the protection of mice from radiation carcinogenesis

3.1. Introduction

Organisms can get exposed to a plethora of DNA damaging agents, producing DNA lesions that can lead to genomic instability and the propagation of mutations. Fortunately, cells have developed different processes to repair such DNA lesions, with the HR pathway considered as one of the most faithful DSB repair pathways. The core proteins involved in HR, such as RAD51 and the majority of RAD51 mediators, have been widely studied (Scully et al. 2019). To better understand the significance of the HR pathway in the organismal protection against genomic instability, there is a need to study the biological impact of the disruption of HR genes in animal models.

Throughout the years, several mouse models have been developed to study homologous recombination deficiency phenotypes. Many of the mouse models containing mutations in essential HR genes are embryonic lethal. *RAD51* is one of the essential genes of HR that when disrupted in vertebrate cells leads to cellular death (Sonoda et al. 1998). Even though loss of *RAD51* is a cellular lethal, several efforts have been made to produce a mouse model with *Rad51* disruption. Homozygous disruption of *Rad51* in mice is embryonically lethal and embryos die at 8.5 days post coitum (dpc) (Tsuzuki et al. 1996). Another study produced a mouse model expressing a mutant RAD51 and embryos homozygous for the RAD51 mutant die *in utero* (Lim and Hasty 1996). A paralogue of RAD51, RAD51C also was found to cause embryonic lethality when disrupted in mice (Kuznetsov et al. 2009). Other mouse models that are hard to phenotypically characterize because of the associated embryonic lethality phenotypes are *Brca1*- and *Brca2*-deficient mice (Evers and Jonkers 2006). Mice with mutated or disrupted *Brca1* die early in embryonic development (Ludwig et al. 1997), but the embryonic lethality of the *Brca1*-deficient mice can be rescued by disruption of *53BP1* (Bunting et al. 2012). *Brca2* deficiency in mice also leads to an embryonic lethal phenotype and embryos are hypersensitive to γ-rays (Sharan et al. 1997). The embryonic

lethal phenotype that is observed in mice with these genes disrupted suggests that the proteins encoded are essential for the development of the embryo.

Several other mouse models that were established and used to investigate the consequences of HR deficiency in an organism, do not exhibit embryonic lethality. For example, *Rad52*-deficient mice are viable and fertile, and isolated *Rad52*$^{-/-}$ ES cells are not hypersensitive to MMC or IR (Rijkers et al. 1998). In addition, *Rad54*-deficient mice are viable and fertile (Essers et al. 1997; Messiaen et al. 2013). ES cells isolated from *Rad54*$^{-/-}$ mice exhibit moderate sensitivity to IR, UV light, MMC and MMS (Essers et al. 1997). Likewise, disruption of *Rad54b* in mice leads to viable and fertile offspring. Mice disrupted for *Rad54b* or *Rad54b/Atm* exhibit reduced survival after treatment with MMC or IR, respectively (Wesoly et al. 2006; Kirshner et al. 2009). In addition, ES cells isolated from *Rad54b*$^{-/-}$ mice are moderately sensitive to MMC and IR (Wesoly et al. 2006; Kirshner et al. 2009). Finally, a mouse model with disrupted *Rad51ap1* was recently developed. *Rad51ap1*$^{-/-}$ mice are viable and fertile as observed by us and another group (Bridges et al. 2020).

Here, we used *Rad51ap1*$^{-/-}$ mice and sought to investigate if RAD51AP1 is required to protect mice from radiation carcinogenesis. We found that the majority of both wild type and *Rad51ap1*$^{-/-}$ mice survived 4 Gy whole-body IR until the study was terminated at 500 days post exposure. Of the mice that succumbed to disease, both wild type and *Rad51ap1*$^{-/-}$ mice developed hematological malignancies, such as thymic and splenic lymphoma. From the limited number of animals investigated here, we conclude that loss of *Rad51ap1* does not affect the susceptibility to radiation carcinogenesis in mice.

3.2. Materials and Methods

Animals

Adult heterozygous *Rad51ap1*$^{tm1.1(KOMP)Vlcg}$ mice were purchased from the University of California Davis. The mice are of a pure C57BL/6N genetic background and were produced by the partnership of Jackson Laboratory and the NIH funded Knockout Mouse Project at University of California Davis. The

mice were maintained under controlled conditions in cages housed at the Lab Animal Resources Painter building at CSU, with free access to food and water. The protocol was approved by the Institutional Animal Care and Use Committee at CSU.

Genotyping

Tail snips and/or ear punch biopsies from each animal were sampled ~21 days after birth and used to isolate total DNA. The genotypes were confirmed by polymerase chain reaction (PCR) using two primer sets, one for the wild type allele (wt) and one for the knockout allele (KO) (

Table S3. 1) (**Figure S3.1A**). PCR products were resolved on a 1.5% agarose gel. A 693 bp product was observed for the KO allele with the Reg-LacF/geneR primer set (**Figure S3.1B)**, and a 111 bp product was observed for the wt allele with the wt Fw/Rv primer set (**Figure S3.1C)**. Samples with both products amplified were considered heterozygous for the disrupted *Rad51ap1* allele (*Rad51ap1*$^{+/-}$), while samples with either the 693 bp or the 111 bp product amplified were considered *Rad51ap1*$^{-/-}$ or *Rad51ap1*$^{+/+}$, respectively.

Animal treatment

Rad51ap1$^{+/+}$ (7 females, 7 males) and *Rad51ap1*$^{-/-}$ (6 females, 8 males) mice were exposed to 4 Gy of total body γ-irradiation (TBI) at 5-7 weeks of age and their health was monitored ~twice a week for the occurrence of any signs of disease. Behavioral observations of diseased mice consisted of rapid breathing, hunched posture, poor grooming and lethargy.

Necropsy

Necropsy was performed once mice showed severe signs of disease. Tissues were collected for histopathological evaluation and fixed in 10% Neutral Buffered Formalin. Fixed tissues were embedded in paraffin, sectioned, and stained with hematoxylin and eosin at the Veterinary Diagnostic Laboratories at CSU. Stained tissues were analyzed with a 20× magnification with an EVOS Cell Imaging System. Blood was also collected via cardiac puncture immediately after mice were euthanized for blood smears.

Blood smear staining

Blood smears were fixed in 100% methanol for 10 minutes at room temperature. Slides were air-dried and stained in 1×PBS with 5% Giemsa stain for 10 minutes. Slides were destained in deionized water and air-dried before observing under the microscope. Stained blood smears were analyzed with a 20× magnification with an EVOS Cell Imaging System.

Statistical analyses

Prism 8 GraphPad Software was used to perform the statistical analysis. To evaluate the significance of survival between *Rad51ap1*$^{+/+}$ and *Rad51ap1*$^{-/-}$, the Log-rank test was performed. A p value of ≤ 0.05 was considered significant.

3.3. Results

Rad51ap1*$^{+/+}$ *and Rad51ap1*$^{-/-}$ *exhibit the same probability of survival after γ-ray exposure

We tested for the consequences of 4 Gy TBI on wild type and *Rad51ap1*$^{-/-}$ KO mice. In this study we included 14 mice of each genotype, of which ~half were female and half were male. After 4 Gy TBI, 4/14 wild type and 5/14 *Rad51ap1*$^{-/-}$ mice died within 500 days post IR exposure. To determine the probability of tumor-free survival, Kaplan-Meier survival curves for *Rad51ap1*$^{+/+}$ and *Rad51ap1*$^{-/-}$ were prepared. From these Kaplan-Meier survival curves we infer that there is no difference in the probability of survival after 4 Gy TBI between *Rad51ap1*$^{+/+}$ and *Rad51ap1*$^{-/-}$ mice (**Figure 3.1**).

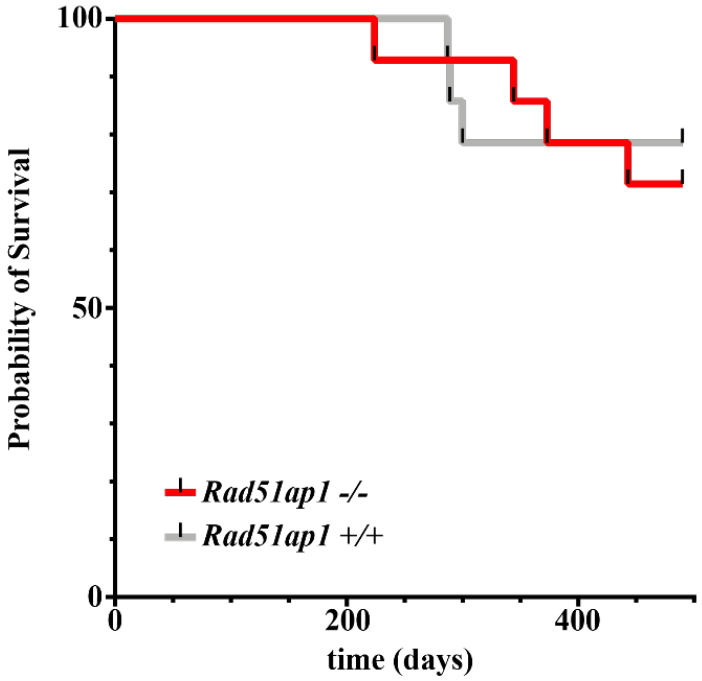

Figure 3.1. Kaplan Meier survival curve of *Rad51ap1*$^{+/+}$ (n=14) and *Rad51ap1*$^{-/-}$ (n=14) mice. $\chi^2(1, N=28) = 0.1084$, ns, p=0.7420; Log-rank (Mantel-Cox) test.

Excess lymphocytes in the blood of both Rad51ap1*$^{+/+}$ *and Rad51ap1*$^{-/-}$ *after γ-ray exposure

Blood smears from one *Rad51ap1*$^{+/+}$ (#93) and three *Rad51ap1*$^{-/-}$ mice (#115, #133, and #193) were analyzed for lymphocyte density. Mice #93 (**Figure 3.2A, i**), #115 (**Figure 3.2A, ii**), #133 (**Figure 3.2A, iii**) exhibited excess number of lymphocytes in their blood smears. However, the blood smear of the KO mouse #193 (**Figure 3.2A, iv**) appeared to be normal with a typical number of lymphocytes.

Infiltrating lymphocytes in tissues of both Rad51ap1*$^{+/+}$ *and Rad51ap1*$^{-/-}$ *after γ-ray exposure

Liver, lung, spleen and thymus tissues were analyzed from one *Rad51ap1*$^{+/+}$ and three *Rad51ap1*$^{-/-}$ mice by Mollie Uhrig. The liver tissue from wild type mouse #93 was highly infiltrated with lymphocytes (**Figure 3.2B, i**). Similar degree of infiltrated lymphocytes was observed for the KO mice #115 and #133. In contrast, the liver of KO mouse #193 appeared normal (images not shown). Infiltrating lymphocytes were also observed within the spleens of all four mice, and these spleens were deficient of any clear differentiation between the red and white pulp (**Figure 3.2B, ii; image for #115 only**). Similarly, the lungs

of all four mice were infiltrated by lymphocytes (**Figure 3.2B, iii; image for #133 only**). Finally, comparing the thymi of the four mice, mouse #93 appeared with moderately increased levels of lymphocytes (image not shown), while in the thymi of all KO mice lymphocytes were abundantly present (**Figure 3.2B, iv; image for #193 only**).

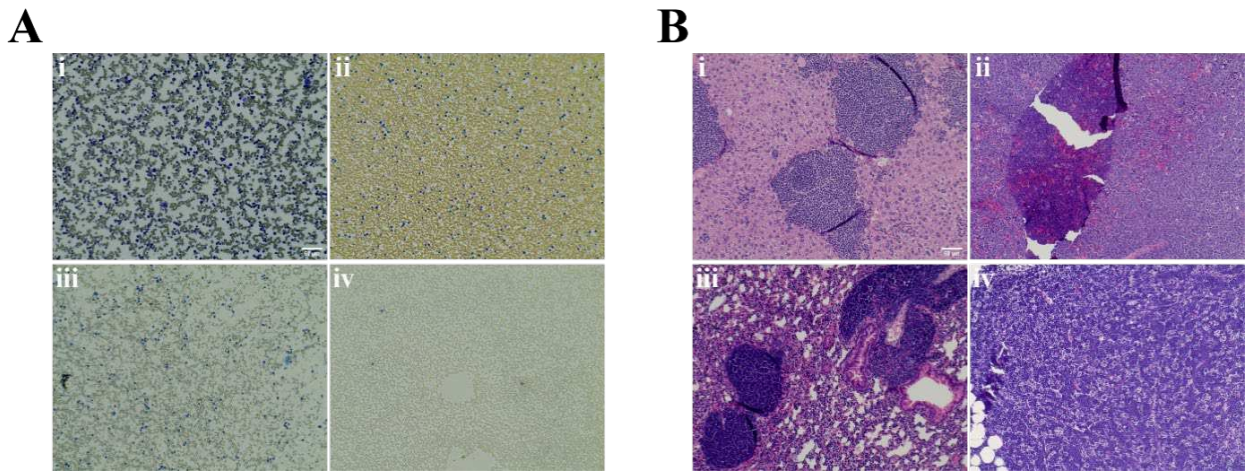

Figure 3.2. Histopathological evaluation. (A) Representative micrographs of blood smears stained with Giemsa from mouse #93-wt (i), #115-KO (ii), #133-KO (iii), and #193-KO (iv). **(B)** Representative micrographs of hematoxylin-eosin stained sections of liver tissue from mouse #93-wt (i), spleen tissue from #115 mouse (ii), lung tissue from #133 mouse (iii), and thymus tissue from #193 mouse (iv). [Data by Mollie Uhrig].

3.4. Discussion

In accordance with what is described by the International Mouse Phenotyping Consortium (https://www.mousephenotype.org) and others (Bridges et al. 2020), we find that *Rad51ap1*$^{-/-}$ mice are viable and fertile. Moreover, in our study, most of *Rad51ap1*$^{-/-}$ and wild type mice survived 4 Gy TBI and lived up to 500 days post IR exposure, at which time the study was terminated. These results show that *Rad51ap1* deficiency is not associated with an increased susceptibility to radiation carcinogenesis in mice. These results are somewhat reminiscent of what has been described for *Rad54*$^{-/-}$ mice exposed to 4 Gy TB X-irradiation, which similarly show survival rates comparable to that of wild type mice, while the combined deficiencies of both *Rad54* and *Rad54b* led to an increase in radiosensitization (Kirshner et al. 2009). We

conclude that, if deleted singly, the RAD51 accessory proteins RAD51AP1, RAD54 and RAD54B play no major role in the repair of IR-induced DNA damage in mouse tissues.

Rad54$^{-/-}$ mice, however, are sensitive to MMC, as previously shown (Wesoly et al. 2006; Kirshner et al. 2009). Moreover, the combined loss of both *Rad54* and *Rad54b* further increases the sensitivity of mice to MMC exposure (Wesoly et al. 2006; Kirshner et al. 2009). These studies defined the synergistic interaction between RAD54 and RAD54B in mice, similarly to what has been described in mouse cells (Kirshner et al. 2009). Since our experiments in human cancer cell lines also uncovered synergism between RAD51AP1 and RAD54, we speculate that mice disrupted for both *Rad51ap1* and *Rad54* may exhibit some sensitivity to IR and likely hypersensitivity to MMC.

From our histopathological analyses we observed that loss of *Rad51ap1* does not exacerbate development of disease after IR, since the select number of mice that we investigated succumbed to disease at similar times. Blood smears from all diseased wild type and KO mice, with the exception of one KO mouse, exhibited elevated lymphocytes. This is a direct sign of an arising hematological malignancy such as leukemia or lymphoma (Hamad and Mangla 2020). We also found that several tissues in mice from both genotypes were infiltrated with lymphocytes. Finally, all four mice tested here were found with enlarged thymi (images not shown).

IR-induced cancers have been investigated in different strains of mice commonly used in research. Among these, the cancers that are most commonly induced are leukemias and lymphomas, and tumors in the breast and lung (Rivina et al. 2016). The mouse strain that we used in this study, C57BL/6N, is found to be prone to IR-induced thymic lymphoma (Rivina et al. 2016). Our results are in support of this observation, although our study is limited by the small number of mice that succumbed to disease.

3.5. Future Directions

Since we do not observe any phenotype after treatment with IR, it would be interesting to expose the mice to a different DNA damaging agent that introduces DSBs that more directly affect DNA

replication. Such a DNA damaging agent is MMC, and MMC has been previously used to investigate the sensitivity of *Rad54*$^{-/-}$ mice (Wesoly et al. 2006). Another advantage of MMC use over IR is that the length of the study is much shorter, and disease occurs much quicker compared to disease observed after IR (Wesoly et al. 2006).

According to our results described in **Section 2.3**, RAD54 can partially compensate for the loss of RAD51AP1 in HeLa cells and loss of both proteins renders the cells more sensitive to MMC and prone to genomic instability. Therefore, it would be interesting to cross *Rad51ap1*$^{-/-}$ with *Rad54*$^{-/-}$ mice, expose the double *Rad51ap1*$^{-/-}$*Rad54*$^{-/-}$ KO mice to IR or MMC, and observe the consequences on survival and tumor development. However, it is also possible, that *Rad51ap1*$^{+/-}$*Rad54*$^{-/-}$ or *Rad51ap1*$^{-/-}$*Rad54*$^{+/-}$ mice may suffer from defects in meiosis, which may impede the availability of double KO mice.

CHAPTER FOUR

S277 and S282 phosphorylation sites of RAD51AP1 are essential for protein function

4.1. Introduction

RAD51AP1, during the formation of the synaptic complex and D-loop reaction, binds to DNA. RAD51AP1 binds ssDNA as well as dsDNA, however it exhibits a higher affinity to dsDNA (Kovalenko et al. 1997; Modesti et al. 2007; Wiese et al. 2007). Yet, RAD51AP1 shows higher preference for branched DNA molecules and D-loops over dsDNA (Modesti et al. 2007; Wiese et al. 2007). The DNA binding ability of RAD51AP1 is essential for the stimulation of the D-loop reaction mediated by RAD51 (Modesti et al. 2007; Dunlop et al. 2012). RAD51AP1 binds to DNA via two distinct domains, one lies at the N-terminus of the protein (Isoform 2, residues 30-49), while the second one resides in the C-terminal domain of the protein and upstream of the RAD51 binding site (Isoform 2, residues 226-290) (Modesti et al. 2007; Dunlop et al. 2012). Both DNA-binding domains are needed for the activity of RAD51AP1 to promote D-loop formation by RAD51 (Dunlop et al. 2012). RAD51AP1 upon damage by IR or MMC is recruited to chromatin and forms foci that colocalize with RAD51 foci as seen by ICC (for review see (Pires et al. 2017)).

Previous studies have shown that RAD51AP1 is heavily modified upon DNA damage, and that some of the post-translational modifications occurring in RAD51AP1 are phosphorylation, acetylation and ubiquitination (Beli et al. 2012; Elia et al. 2015; Wagner et al. 2016). HR proteins can be cell-cycle regulated by CDK phosphorylation. More specifically, CDK1 is important during the DNA end resection, the initial step of HR (Aylon et al. 2004; Ira et al. 2004). Phosphorylation of Rad51 by CDK1 is crucial for its DNA binding affinity (Lim et al. 2020). BRCA2 is also phosphorylated at residue S3291 by CDK1 after treatment with nocodazole, leading to blockage of interaction with RAD51 (Esashi et al. 2005). Proteomic studies have identified multiple residues in RAD51AP1 that can be phosphorylated. Residue S120 is phosphorylated by ATM or ATR following exposure of human cells to X-rays or γ-rays (Matsuoka et al. 2007; Bennetzen et al. 2010; Beli et al. 2012; Elia et al. 2015; Wagner et al. 2016) and after etoposide (Beli

et al. 2012). S19, S21, S294 and S299 (in Isoform 1) are phosphorylated after IR exposure (Beli et al. 2012; Elia et al. 2015). The two latter phosphorylation sites, S277 and S282 (in isoform 2), lie within the C-terminal portion of RAD51AP1 protein and near critical residues of its essential DNA-binding domain (Dunlop et al. 2012). Therefore, we speculated that phosphorylation of S277 and S282 may impact RAD51AP1's function and regulation during HR.

RAD51AP1 is ubiquitinylated at K93, K123 and K156 residues upon treatment with UV or IR, while ubiquitination of residues K138 and K169 are specific to IR (Elia et al. 2015). The impact of ubiquitination of these residues on RAD51AP1 regulation has not yet been explored. Residue K269 also is found to be ubiquitinated, as U2OS cells expressing mutant RAD51AP1-K269R showed significantly reduced ubiquitination of RAD51AP1 (Barroso-Gonzalez et al. 2019). Another ubiquitin-like post-translational modification that proteins undergo is SUMOylation. Unlike ubiquitination, that frequently targets proteins for degradation, SUMOylation plays an essential role in the regulation of many cellular processes, including DNA repair. Multiple proteins involved in several steps of HR, such as RAD51, are sumoylated to facilitate their recruitment to the damaged site (Dhingra and Zhao 2019). Recent proteomic studies have shown that RAD51AP1 can be sumoylated at residue K269 (isoform 1) upon proteasome inhibition and heat stress (Hendriks et al. 2017; Lamoliatte et al. 2017). Residue K269 of RAD51AP1 has also been found to be sumoylated in a study that looked at the role of RAD51AP1 in the ALT pathway (Barroso-Gonzalez et al. 2019). In this study, the same residue (K269) is a target of both SUMO and ubiquitin E3 ligases, with SUMOylation protecting RAD51AP1 from ubiquitin-mediated degradation.

In this chapter, we show that in RAD51AP1 residues S277 and S282 and their modification are crucial for cell survival against induced DNA damage. We found that mutation of S277 and S282 to S277D and S282D (S2D) has no negative effect on the function of the RAD51AP1 protein, as the phenotype of the *RAD51AP1* KO cells ectopically expressing the S2D mutant is essentially identical to that of *RAD51AP1* KO cells ectopically expressing the wild type protein. In contrast, expression of RAD51AP1-S277A/S282A (S2A) compromises RAD51AP1 function as measured by DNA replication

and cell survival assays. Based on these and other findings, I suggest that phosphorylation of S277 and/or S282 is critical for RAD51AP1 function, including its ability to form foci in response to DNA damage.

4.2. Materials and Methods

Cloning and generation of wild-type and mutant RAD51AP1 and expression in RAD51AP1 KO cells

The full length wild-type RAD51AP1 cDNA with N-terminal Flag-tag included in pENTR1A was subjected to site-directed mutagenesis (NEB) to generate two different RAD51AP1 mutants: the non-phosphorylatable RAD51AP1-S2A mutant and phosphorylation mimetic RAD51AP1-S2D mutant. Apart from the double S2A mutant, we also generated single mutants that contain either the S277A or S282A amino acid change. The coding sequence for the wild-type RAD51AP1 protein and the RAD51AP1 mutants were introduced into pLenti CMV/TO DEST #2 using the Gateway LR Clonase II technology (Invitrogen).

To ectopically express wild-type or mutant RAD51AP1 in *RAD51AP1* KO cells, a lentivirus delivery system was used, and the method is described in **Section 2.2**. The transduced cells were trypsinized and replated in a 96-well tissue culture plate at a density of 0.5 cells per well in the presence of 2mg/ml G418. G418 resistant clones were isolated, expanded and were further screened for the expression of RAD51AP1 protein by western blot, as described in **Section 2.2**.

Methods similar to Section 2.2

The human cervical cancer cell line, HeLa, was used as described in **Section 2.2** "Cell culture". Cell sensitivity assays to mitomycin C and olaparib were performed as described in **Section 2.2** "Exposure to genotoxic agents". Cell growth was monitored according to the protocol followed in **Section 2.2** "Cell growth assay". Cell cycle analysis was performed as described in **Section 2.2** "Cell cycle analysis and flow cytometry". DNA replication progression was assessed by DNA fiber assays as described in **Section 2.2** "DNA Fiber assay". Statistical analyses were performed in Prism 8 as described in **Section 2.2** "Statistical analyses".

4.3. Results

Characterization of cells expressing RAD51AP1 phospho-mutants

In order to investigate the biological impact of S277 and S282 in RAD51AP1 (isoform 2) we ectopically expressed the RAD51AP1 wild-type (WT), RAD51AP1-S2D (S2D) and RAD51AP1-S2A (S2A) proteins in *RAD51AP1* KO cells. Clonal isolates were screened by Neelam Sharma by WB analysis of nuclear protein extracts and the clones that exhibited approximately equal expression of the ectopic RAD51AP1 proteins were picked (**Figure 4.1A**).

We first sought to investigate if the phospho-mutants would affect cellular growth. *RAD51AP1* KO cells stably expressing RAD51AP1-S2D (AP1KO-S2D) exhibited similar growth characteristics as *RAD51AP1* KO cells expressing wild type RAD51AP1 (AP1KO-WT). However, ectopic expression of RAD51AP1-S2A in *RAD51AP1* KO cell (AP1KO-S2A) was associated with a slightly reduced growth rate (**Figure 4.1B**). These results suggest that phosphorylation of RAD51AP1 at S277 and S282 may promote RAD51AP1 function in the context of spontaneous damage.

We also evaluated if the ectopically expressed RAD51AP1 proteins bind to proteins that RAD51AP1 is known to associate with (Kovalenko et al. 2006; Dray et al. 2011; Cukras et al. 2016; Wagner et al. 2016; Liang et al. 2019; Liang et al. 2020). We found that all ectopically expressed RAD51AP1 proteins bind RAD51, UAF1 and PARP-1 to similar extent (data not shown). This strongly suggests that ectopic RAD51AP1, RAD51AP1-S2D and RAD51AP1-S2A sustain wild type conformation.

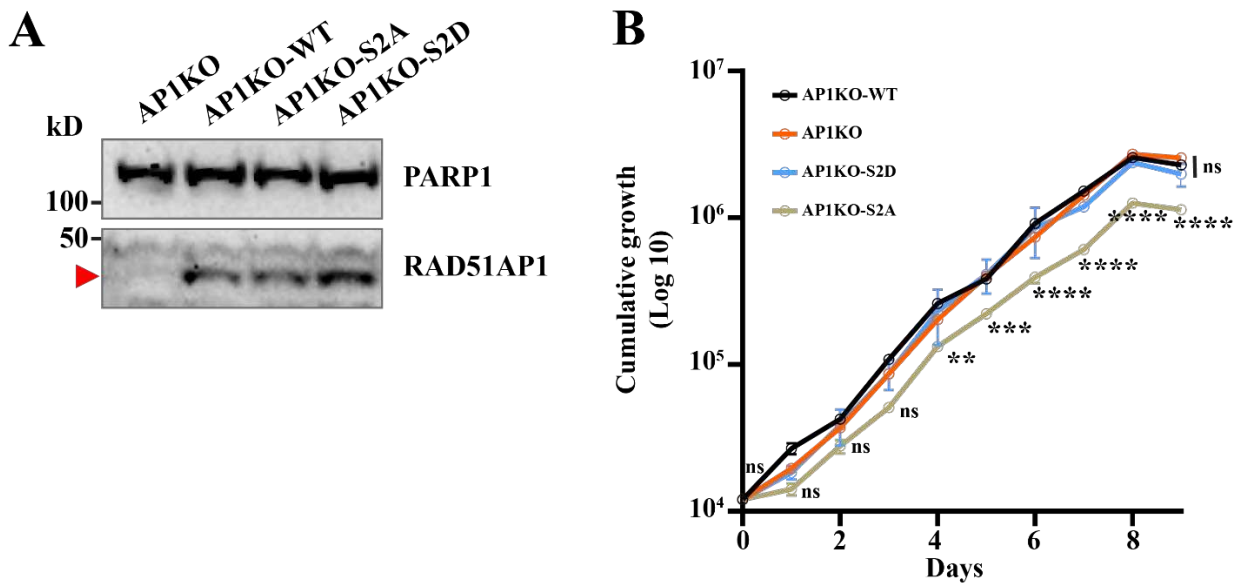

Figure 4.1. Characterization of *RAD51AP1* KO cells and *RAD51AP1* KO cells expressing wild-type RAD51AP1 or RAD51AP1 mutants. (A) Western blots of whole cell protein extracts. Red arrow indicates the specific RAD51AP1 band. The signal of PARP-1 serves as loading control. **(B)** Results from cell growth assays of untreated cells. Data points are the means from 3 independent experiments ±1SD. ****, $p<0.0001$, **, $p<0.01$, ns, not significant; two-way ANOVA analysis (Sidak's multiple comparisons test). [Panel A, data by Neelam Sharma; Panel B, data by Neelam Sharma and Platon Selemenakis.]

RAD51AP1 KO cells expressing RAD51AP1-S2A show increased sensitivity to MMC

To assess the sensitivity to MMC of *RAD51AP1* KO cells expressing RAD51AP1 phospho-mutants, we performed MMC cell survival assays. Cells were treated as described in **Section 2.3** and plated for colony formation. In accord with a previous study (Liang et al. 2019) and as shown in **Figure 2.2B**, *RAD51AP1* KO cells are more sensitive to MMC than HeLa cells. AP1KO-WT cells exhibit the same sensitivity as HeLa cells (**Figure 4.2A** and **Figure 2.2B**), suggesting that the ectopically expressed wild type RAD51AP1 protein in *RAD51AP1* KO cells is fully functional. AP1KO-S2D cells respond to MMC in the same manner as AP1KO-WT cells. In contrast, when two different clones of RAD51AP1-S2A expressing *RAD51AP1* KO cells (AP1KO-S2A-1 and AP1KO-S2A-2) were challenged with MMC, their survival was similar to the response of *RAD51AP1* KO cells (**Figure 4.2A**). These results suggest that phosphorylation of S277 and/or S282 is important for the function of the RAD51AP1 protein and for the protection of HeLa

cells from MMC-induced DNA damage. Our preliminary results also show that MMC exposure of cells expressing either S277A or S282A single RAD51AP1 mutants does not affect the sensitivity of cells (data not shown). This highlights that phosphorylation of either S277 or S282 residue is sufficient for normal function of RAD51AP1.

RAD51AP1 KO cells expressing RAD51AP1-S2A show a more pronounced G2/M arrest after MMC

To further examine the impact of the non-phosphorylatable RAD51AP1-S2A in cells after MMC, we assessed cell cycle progression in *RAD51AP1* KO cells and cells expressing AP1KO-WT, AP1KO-S2A or AP1KO-S2D. In the absence of MMC, all cell lines proceeded similarly through the cell cycle, with the exception of AP1KO-S2A-2 cells which showed a smaller fraction of cells present in G2/M phase (**Figure 4.2B**). Twenty-four hours after release from MMC, *RAD51AP1* KO, AP1KO-WT and AP1KO-S2A-1 cells are accumulated at G2/M phase. In contrast, AP1KO-S2A-2 cells are accumulated in S phase rather than G2/M phase. AP1KO-S2D cells also are accumulated at G2/M phase, comparable to AP1KO-WT and *RAD51AP1* KO cells (**Figure 4.2C)**. At 72 hours post-treatment, *RAD51AP1* KO, AP1KO-WT and AP1KO-S2D were able to proceed through mitosis and enter the following cell cycle, while both AP1KO-S2A-1 and AP1KO-S2A-2 cells remained arrested in G2/M phase (**Figure 4.2D**). These results suggest that phosphorylation S277 and/or S282 is required for timely repair of DNA damage and progression of cells through the cell cycle.

RAD51AP1 KO cells expressing RAD51AP1-S2A show increased sensitivity to olaparib

We chose to assess if the RAD51AP1 phospho-mutants affect the resistance of cells to olaparib. *RAD51AP1* KO cells and cells ectopically expressing RAD51AP1 wild-type and phospho-mutants were chronically exposed to olaparib while plated for colony formation. *RAD51AP1* KO cells exhibit a higher sensitivity to olaparib compared to AP1KO-WT cells, the sensitivity of which to olaparib is similar to that of HeLa cells (**Figure 4.2E and Figure S2.1H**). Sensitivity to olaparib of AP1KO-S2D cells is comparable to that of AP1KO-WT cells. In contrast, *RAD51AP1* KO cells expressing AP1-S2A exhibit greatly decreased survival after olaparib and are more sensitive than *RAD51AP1* KO cells (**Figure 4.2E**). Recently,

a second clone of *RAD51AP1* KO cell expressing AP1KO-S2A has also been tested, and this clone exhibits the same sensitivity to olaparib as AP1-S2A-1 (data not shown).

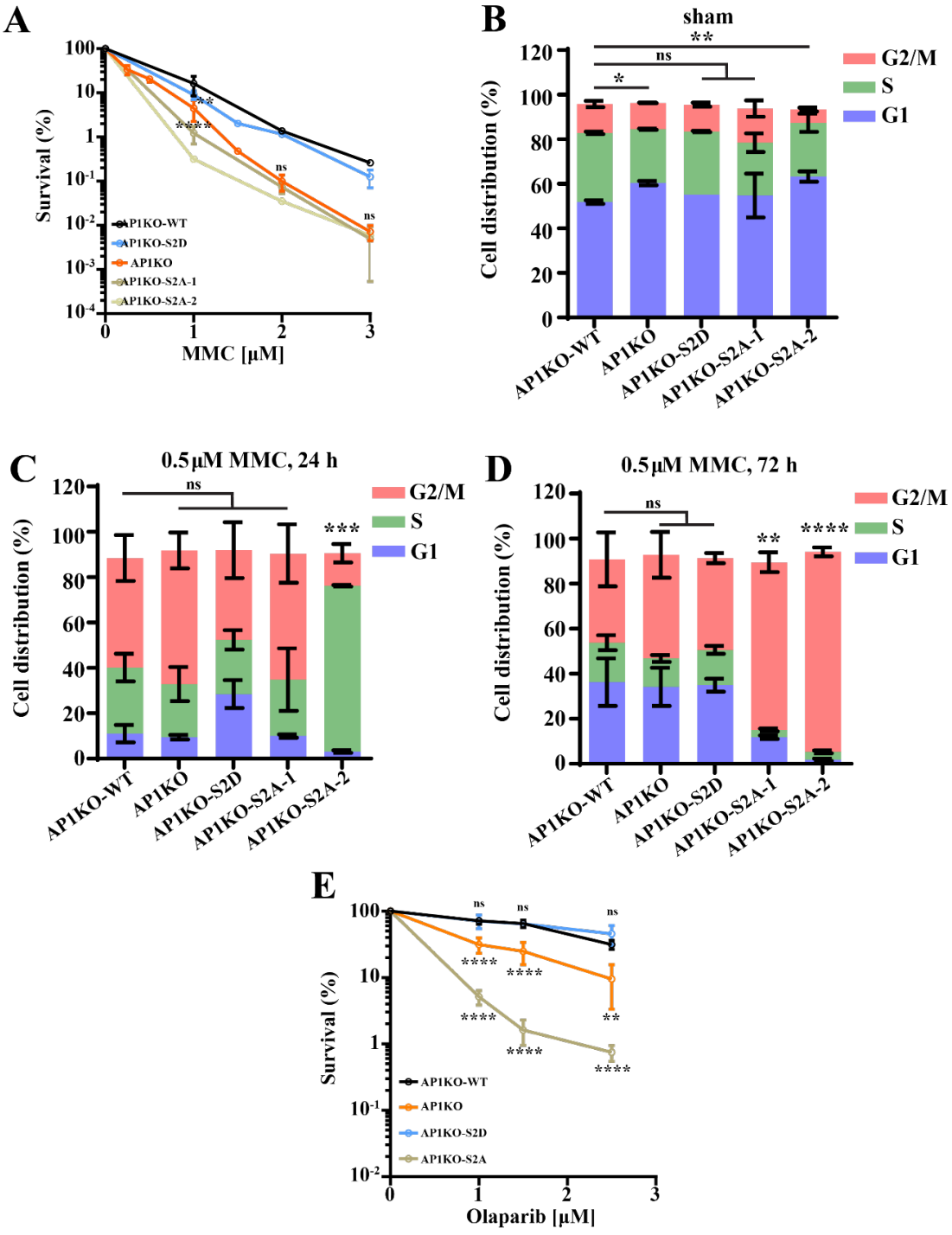

Figure 4.2. Phosphorylation of RAD51AP1 is essential for protection from DNA damage. (A) Results from clonogenic survival assays after MMC in *RAD51AP1* KO cells and AP1KO-WT, AP1KO-S2D and AP1KO-S2A cells

(note: two different clones were tested S2A-1, S2A-2). For AP1KO-WT, AP1KO-S2D, AP1KO and AP1KO-S2A-1 data points are the means from 2 independent experiments ± 1SD. **, $p<0.01$, ****, $p<0.0001$, ns, not significant; two-way ANOVA analysis (Dunnett's multiple comparisons test). For AP1KO-S2A-2 data points are the means from 3 technical replicates. **(B)** Average percentage of cells in G1, S and G2/M cell cycle phases without MMC treatment. **(C)** As described in panel **(B)**, 24 hours after treatment with 0.5 μM MMC for 2 hours. **(D)** As described in panels **(B)** and **(C),** 72 hours after treatment with MMC. Bars are the means from 2 independent experiments ± 1SD. *, $p<0.05$, **, $p<0.01$, ***, $p<0.001$, ****, $p<0.0001$, ns, not significant; one-way ANOVA analysis (Tukey's multiple comparisons test) **(E)** Results from clonogenic survival assays after chronic olaparib treatment of *RAD51AP1* KO cells and AP1KO-WT, AP1KO-S2D and AP1KO-S2A cells. Data are the means from 3 independent experiments ± 1SD. **, $p<0.01$, ****, $p<0.0001$, ns, not significant; two-way ANOVA analysis (Dunnett's multiple comparisons test). [Data by Neelam Sharma and Platon Selemenakis]

RAD51AP1 KO cells expressing RAD51AP1-S2A show increased sensitivity to replication stress

Next, we sought to assess the effect of RAD51AP1-S2A/S2D expression in DNA replication fork progression. Similar to the approach described in **Section 2.3**, we used the single-molecule DNA fiber assay and labeled exponentially growing cells first with CldU. We then exposed cells to HU and finally labeled with IdU. Replication fork restart after HU treatment was determined by measuring the length of IdU tracts. In the absence of HU, IdU tract lengths were not significantly different between *RAD51AP1* KO cells (data from **Section 2.3**) and AP1KO-WT, AP1KO-S2D, and AP1KO-S2A cells ($p>0.9999$) (**Figure 4.3A** and **Table S4.1**) Upon exposure to HU, *RAD51AP1* KO cells (data from **Section 2.3**) showed significantly impaired replication fork restart compared to AP1KO-WT cells ($p=0.0013$). Replication fork restart in AP1KO-S2D was similar to that of AP1KO-WT cells ($p=0.3733$). In contrast, replication fork restart was greatly impaired in AP1KO-S2A cells ($p<0.0001$) (**Figure 4.3B** and **Table S4.2**). This suggests that phosphorylation of S277 and/or S282 plays a critical role in RAD51AP1 function and the response of human cells to replication stress.

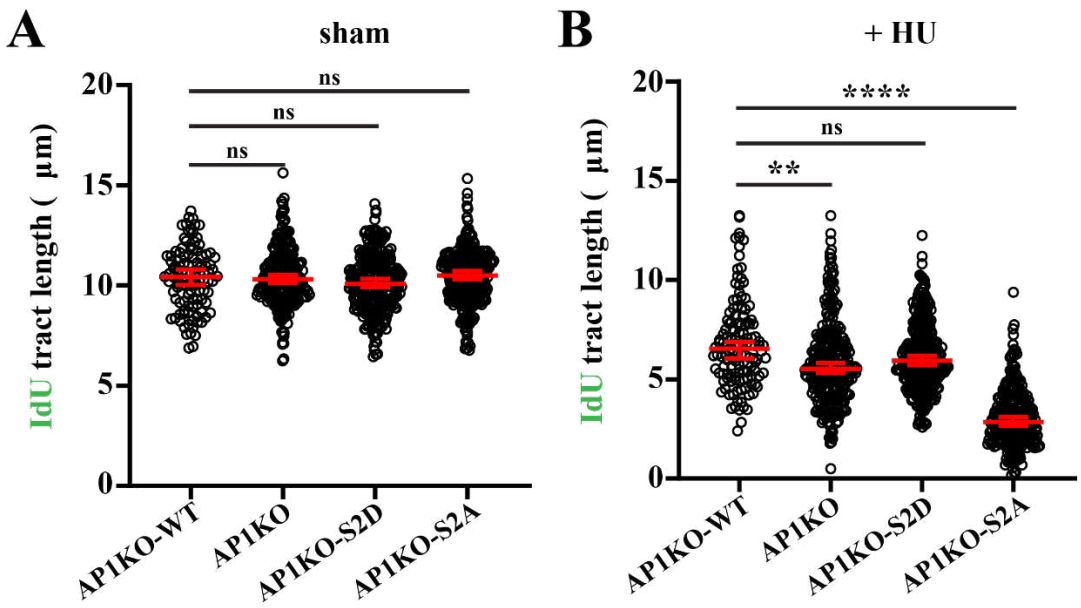

Figure 4.3. Phosphorylation of RAD51AP1 is crucial for the protection of HeLa cells from replication stress. **(A)** Median IdU (green) tract lengths in cells without treatment. **(B)** As described in panel **(A)**, after treatment with 4mM HU. Bars are medians from 2 independent experiments ± 95% CI. Per experiment and condition 100-150 fibers were analyzed. **, $p<0.01$, ****, $p<0.0001$; Kruskal-Wallis test (Dunn's multiple comparisons test). [Data by Neelam Sharma, Elena Pires and Platon Selemenakis]

4.4. Discussion

HR is a cell-cycle dependent pathway, and its DNA repair capacity is restricted to late S and G2 phase where the sister chromatid is present as a template for DNA repair synthesis (Kadyk and Hartwell 1992; Takata et al. 1998). The majority of genes involved in HR are transcriptionally regulated throughout the cell cycle and upon DNA damage (Krejci et al. 2012; Tkach et al. 2012). *RAD51AP1* as well as *RAD51* are two such genes that are differentially expressed throughout the cell cycle with their transcripts and gene products peaking in S phase and remaining throughout G2 phase (Henson et al. 2006). RAD51AP1 is found to undergo post-translational modifications after induced DNA damage, such as phosphorylation (Beli et al. 2012; Elia et al. 2015; Wagner et al. 2016). In this study, we raised the question of the functional role of residues S277 and S282 in RAD51AP1, which are located within its C-terminal DNA binding domain. We

speculated that phosphorylation of S277 and/or S282 may regulate the function of RAD51AP1 in human cells.

We found that *RAD51AP1* KO cells expressing the phospho-mimetic mutant RAD51AP1-S2D did not exhibit any phenotype different from AP1KO-WT cells. An explanation of this observation could be that the phosphorylation may activate the protein. Therefore, RAD51AP1-S2D being active at all times may work in favor of RAD51AP1's immediate action on DNA damage. Previous proteomic studies have shown S277 and S282 are phosphorylated upon exposure of cells to IR (Beli et al. 2012; Elia et al. 2015), supporting the notion that phosphorylation of S277 and/or S282 indeed is DNA damage-induced and primes RAD51AP1 for optimal function in HR. In contrast, AP1KO-S2A mutant cells - overall - behave similar to *RAD51AP1* KO cells, suggesting that modification of S277 and/or S282 in RAD51AP1 is important for the activity of the protein after induced DNA damage.

In addition, we noted that AP1KO-S2A cells are more sensitive to the PARPi olaparib than *RAD51AP1* KO cells (**Figure 4.2E**). Therefore, it seems that the inability of RAD51AP1 to not get phosphorylated at these residues is worse than its absence. Also, it is surprising that we do not observe the same phenotype after MMC treatment. One explanation of these data might be that, because cells are chronically exposed to olaparib but acutely to MMC, the consequences of non-functional RAD51AP1 are more pronounced after olaparib. Also, the difference may stem from the observed interaction between RAD51AP1 and PARP-1. A recent proteomic analysis found that RAD51AP1 interacts with PARP1 upon exposure to HU (Wagner et al. 2016). We also found that RAD51AP1-WT, -S2D and -S2A can bind to PARP-1 (data not shown). Hence, greater sensitivity of AP1KO-S2A to olaparib could derive from the fact that RAD51AP1 still can bind to PARP-1, but the failure to become phosphorylated may impact the recruitment of proteins involved in downstream steps of the pathway.

In summary, our findings shed light on the cellular function of RAD51AP1 protein and the significance of S277 and S282 as potential phosphorylation sites for HR regulation.

4.5. Future Directions

While our findings show the importance of S277 and S282 for the regulation of RAD51AP1 during HR, it would be of great interest to identify the kinases responsible for phosphorylating the S277 and S282 residues in RAD51AP1. RAD51AP1 possesses residues that are targets for phosphorylation by ATM and ATR kinases (Matsuoka et al. 2007; Bennetzen et al. 2010; Beli et al. 2012; Elia et al. 2015; Wagner et al. 2016). In addition, a recent study identified two phosphorylation sites that reside within the RAD51AP1's RAD51-binding domain and that are targets of CDK1 or NEK1 (Bisteau et al. 2020). CDKs phosphorylate serine or threonine residues that are part of SP or TP motifs. S277 is part of an SP motif (^{277}SPSA^{280}), and therefore we speculate that a CDK might be responsible for the phosphorylation of S277. It would be interesting to investigate which CDK is responsible for the phosphorylation of this residue. One way to test for this is to perform *in vitro* kinase assays with recombinant wild type and mutant RAD51AP1, as described in a recent study that identified RAD51AP1 as a target of both NEK1 and CDK1 (Bisteau et al. 2020). Using different kinases and radiolabelled ATP, we may be able to detect any difference in phosphorylation between RAD51AP1-WT and -S2A. Another option would be to perform immunoprecipitation and perform a proteomic analysis to identify all potential candidates for kinases that bind to RAD51AP1-WT and -S2A.

The second residue (S282) is not part of any known phosphorylation consensus motif. Possibly the second phosphorylation site is induced by the adjacent S277. Perhaps this phosphorylation occurs to signal for ubiquitination or SUMOylation of RAD51AP1. Both SUMOylation and ubiquitination are tightly connected to phosphorylation (Stehmeier and Muller 2009; Nguyen et al. 2013).We speculate that residue K252 (isoform 2), found to be both ubiquitinated and sumoylated (Barroso-Gonzalez et al. 2019) is modified upon phosphorylation of the adjacent S277 residue. To investigate this, we could analyze if the single and double S277A and S282A mutants are sumoylated and ubiquitinylated differently than wild type RAD51AP1.

REFERENCES

Alexeev A, Mazin A, Kowalczykowski SC. 2003. Rad54 protein possesses chromatin-remodeling activity stimulated by the Rad51-ssDNA nucleoprotein filament. *Nat Struct Biol* **10**: 182-186.

Ali RMM, McIntosh SA, Savage KI. 2020. Homologous recombination deficiency in breast cancer: Implications for risk, cancer development, and therapy. *Genes Chromosomes Cancer*.

Allers T, Lichten M. 2001. Differential timing and control of noncrossover and crossover recombination during meiosis. *Cell* **106**: 47-57.

Aylon Y, Liefshitz B, Kupiec M. 2004. The CDK regulates repair of double-strand breaks by homologous recombination during the cell cycle. *EMBO J* **23**: 4868-4875.

Bae SH, Choi E, Lee KH, Park JS, Lee SH, Seo YS. 1998. Dna2 of Saccharomyces cerevisiae possesses a single-stranded DNA-specific endonuclease activity that is able to act on double-stranded DNA in the presence of ATP. *J Biol Chem* **273**: 26880-26890.

Barroso-Gonzalez J, Garcia-Exposito L, Hoang SM, Lynskey ML, Roncaioli JL, Ghosh A, Wallace CT, de Vitis M, Modesti M, Bernstein KA et al. 2019. RAD51AP1 Is an Essential Mediator of Alternative Lengthening of Telomeres. *Mol Cell* **76**: 11-26 e17.

Beli P, Lukashchuk N, Wagner SA, Weinert BT, Olsen JV, Baskcomb L, Mann M, Jackson SP, Choudhary C. 2012. Proteomic investigations reveal a role for RNA processing factor THRAP3 in the DNA damage response. *Mol Cell* **46**: 212-225.

Bennetzen MV, Larsen DH, Bunkenborg J, Bartek J, Lukas J, Andersen JS. 2010. Site-specific phosphorylation dynamics of the nuclear proteome during the DNA damage response. *Mol Cell Proteomics* **9**: 1314-1323.

Bianchi V, Pontis E, Reichard P. 1986. Changes of deoxyribonucleoside triphosphate pools induced by hydroxyurea and their relation to DNA synthesis. *J Biol Chem* **261**: 16037-16042.

Bianco PR, Bradfield JJ, Castanza LR, Donnelly AN. 2007. Rad54 oligomers translocate and cross-bridge double-stranded DNA to stimulate synapsis. *J Mol Biol* **374**: 618-640.

Bisteau X, Lee J, Srinivas V, Lee JHS, Niska-Blakie J, Tan G, Yap SYX, Hom KW, Wong CK, Chae J et al. 2020. The Greatwall kinase safeguards the genome integrity by affecting the kinome activity in mitosis. *Oncogene* **39**: 6816-6840.

Bochum S, Berger S, Martens UM. 2018. Olaparib. *Recent Results Cancer Res* **211**: 217-233.

Bridges AE, Ramachandran S, Pathania R, Parwal U, Lester A, Rajpurohit P, Morera DS, Patel N, Singh N, Korkaya H et al. 2020. RAD51AP1 deficiency reduces tumor growth by targeting stem cell self-renewal. *Cancer Res*.

Bryant HE, Schultz N, Thomas HD, Parker KM, Flower D, Lopez E, Kyle S, Meuth M, Curtin NJ, Helleday T. 2005. Specific killing of BRCA2-deficient tumours with inhibitors of poly(ADP-ribose) polymerase. *Nature* **434**: 913-917.

Budzowska M, Kanaar R. 2009. Mechanisms of dealing with DNA damage-induced replication problems. *Cell Biochem Biophys* **53**: 17-31.

Bugreev DV, Mazina OM, Mazin AV. 2006. Rad54 protein promotes branch migration of Holliday junctions. *Nature* **442**: 590-593.

Bugreev DV, Rossi MJ, Mazin AV. 2011. Cooperation of RAD51 and RAD54 in regression of a model replication fork. *Nucleic Acids Res* **39**: 2153-2164.

Bunting SF, Callen E, Kozak ML, Kim JM, Wong N, Lopez-Contreras AJ, Ludwig T, Baer R, Faryabi RB, Malhowski A et al. 2012. BRCA1 functions independently of homologous recombination in DNA interstrand crosslink repair. *Mol Cell* **46**: 125-135.

Bunting SF, Callen E, Wong N, Chen HT, Polato F, Gunn A, Bothmer A, Feldhahn N, Fernandez-Capetillo O, Cao L et al. 2010. 53BP1 inhibits homologous recombination in Brca1-deficient cells by blocking resection of DNA breaks. *Cell* **141**: 243-254.

Calderon IL, Contopoulou CR, Mortimer RK. 1983. Isolation and characterization of yeast DNA repair genes. *Current Genetics* **7**: 93-100.

Campeau E, Ruhl VE, Rodier F, Smith CL, Rahmberg BL, Fuss JO, Campisi J, Yaswen P, Cooper PK, Kaufman PD. 2009. A versatile viral system for expression and depletion of proteins in mammalian cells. *PLoS One* **4**: e6529.

Ceballos SJ, Heyer WD. 2011. Functions of the Snf2/Swi2 family Rad54 motor protein in homologous recombination. *Biochim Biophys Acta* **1809**: 509-523.

Chen H, Lisby M, Symington LS. 2013. RPA coordinates DNA end resection and prevents formation of DNA hairpins. *Mol Cell* **50**: 589-600.

Chudasama D, Bo V, Hall M, Anikin V, Jeyaneethi J, Gregory J, Pados G, Tucker A, Harvey A, Pink R et al. 2018. Identification of cancer biomarkers of prognostic value using specific gene regulatory networks (GRN): a novel role of RAD51AP1 for ovarian and lung cancers. *Carcinogenesis* **39**: 407-417.

Collins I, Newlon CS. 1994. Meiosis-specific formation of joint DNA molecules containing sequences from homologous chromosomes. *Cell* **76**: 65-75.

Conrad S, Kunzel J, Lobrich M. 2011. Sister chromatid exchanges occur in G2-irradiated cells. *Cell Cycle* **10**: 222-228.

Crickard JB, Moevus CJ, Kwon Y, Sung P, Greene EC. 2020. Rad54 Drives ATP Hydrolysis-Dependent DNA Sequence Alignment during Homologous Recombination. *Cell* **181**: 1380-1394 e1318.

Cukras S, Lee E, Palumbo E, Benavidez P, Moldovan GL, Kee Y. 2016. The USP1-UAF1 complex interacts with RAD51AP1 to promote homologous recombination repair. *Cell Cycle* **15**: 2636-2646.

Davies OR, Pellegrini L. 2007. Interaction with the BRCA2 C terminus protects RAD51-DNA filaments from disassembly by BRC repeats. *Nat Struct Mol Biol* **14**: 475-483.

Dhingra N, Zhao X. 2019. Intricate SUMO-based control of the homologous recombination machinery. *Genes Dev* **33**: 1346-1354.

Dray E, Dunlop MH, Kauppi L, San Filippo J, Wiese C, Tsai MS, Begovic S, Schild D, Jasin M, Keeney S et al. 2011. Molecular basis for enhancement of the meiotic DMC1 recombinase by RAD51 associated protein 1 (RAD51AP1). *Proc Natl Acad Sci U S A* **108**: 3560-3565.

Dray E, Etchin J, Wiese C, Saro D, Williams GJ, Hammel M, Yu X, Galkin VE, Liu D, Tsai MS et al. 2010. Enhancement of RAD51 recombinase activity by the tumor suppressor PALB2. *Nat Struct Mol Biol* **17**: 1255-1259.

Dunlop MH, Dray E, Zhao W, San Filippo J, Tsai MS, Leung SG, Schild D, Wiese C, Sung P. 2012. Mechanistic insights into RAD51-associated protein 1 (RAD51AP1) action in homologous DNA repair. *J Biol Chem* **287**: 12343-12347.

Edwards SL, Brough R, Lord CJ, Natrajan R, Vatcheva R, Levine DA, Boyd J, Reis-Filho JS, Ashworth A. 2008. Resistance to therapy caused by intragenic deletion in BRCA2. *Nature* **451**: 1111-1115.

Elia AE, Boardman AP, Wang DC, Huttlin EL, Everley RA, Dephoure N, Zhou C, Koren I, Gygi SP, Elledge SJ. 2015. Quantitative Proteomic Atlas of Ubiquitination and Acetylation in the DNA Damage Response. *Mol Cell* **59**: 867-881.

Elstrodt F, Hollestelle A, Nagel JH, Gorin M, Wasielewski M, van den Ouweland A, Merajver SD, Ethier SP, Schutte M. 2006. BRCA1 mutation analysis of 41 human breast cancer cell lines reveals three new deleterious mutants. *Cancer Res* **66**: 41-45.

Esashi F, Christ N, Gannon J, Liu Y, Hunt T, Jasin M, West SC. 2005. CDK-dependent phosphorylation of BRCA2 as a regulatory mechanism for recombinational repair. *Nature* **434**: 598-604.

Essers J, Hendriks RW, Swagemakers SM, Troelstra C, de Wit J, Bootsma D, Hoeijmakers JH, Kanaar R. 1997. Disruption of mouse RAD54 reduces ionizing radiation resistance and homologous recombination. *Cell* **89**: 195-204.

Evers B, Jonkers J. 2006. Mouse models of BRCA1 and BRCA2 deficiency: past lessons, current understanding and future prospects. *Oncogene* **25**: 5885-5897.

Faraoni I, Graziani G. 2018. Role of BRCA Mutations in Cancer Treatment with Poly(ADP-ribose) Polymerase (PARP) Inhibitors. *Cancers (Basel)* **10**.

Farmer H, McCabe N, Lord CJ, Tutt AN, Johnson DA, Richardson TB, Santarosa M, Dillon KJ, Hickson I, Knights C et al. 2005. Targeting the DNA repair defect in BRCA mutant cells as a therapeutic strategy. *Nature* **434**: 917-921.

Feng J, Hu J, Xia Y. 2019. Identification of RAD54 homolog B as a promising therapeutic target for breast cancer. *Oncol Lett* **18**: 5350-5362.

Fong PC, Boss DS, Yap TA, Tutt A, Wu P, Mergui-Roelvink M, Mortimer P, Swaisland H, Lau A, O'Connor MJ et al. 2009. Inhibition of poly(ADP-ribose) polymerase in tumors from BRCA mutation carriers. *N Engl J Med* **361**: 123-134.

Foster ER, Downs JA. 2005. Histone H2A phosphorylation in DNA double-strand break repair. *FEBS J* **272**: 3231-3240.

Galkin VE, Esashi F, Yu X, Yang S, West SC, Egelman EH. 2005. BRCA2 BRC motifs bind RAD51-DNA filaments. *Proc Natl Acad Sci U S A* **102**: 8537-8542.

Game JC, Mortimer RK. 1974. A genetic study of x-ray sensitive mutants in yeast. *Mutat Res* **24**: 281-292.

Gonzalez R, Silva JM, Dominguez G, Garcia JM, Martinez G, Vargas J, Provencio M, Espana P, Bonilla F. 1999. Detection of loss of heterozygosity at RAD51, RAD52, RAD54 and BRCA1 and BRCA2 loci in breast cancer: pathological correlations. *Br J Cancer* **81**: 503-509.

Gottipati P, Vischioni B, Schultz N, Solomons J, Bryant HE, Djureinovic T, Issaeva N, Sleeth K, Sharma RA, Helleday T. 2010. Poly(ADP-ribose) polymerase is hyperactivated in homologous recombination-defective cells. *Cancer Res* **70**: 5389-5398.

Goyal N, Rossi MJ, Mazina OM, Chi Y, Moritz RL, Clurman BE, Mazin AV. 2018. RAD54 N-terminal domain is a DNA sensor that couples ATP hydrolysis with branch migration of Holliday junctions. *Nature Communications* **9**.

Hamad H, Mangla A. 2020. Lymphocytosis. in *StatPearls*, Treasure Island (FL).

Hanahan D, Weinberg RA. 2011. Hallmarks of cancer: the next generation. *Cell* **144**: 646-674.

Heeke AL, Pishvaian MJ, Lynce F, Xiu J, Brody JR, Chen WJ, Baker TM, Marshall JL, Isaacs C. 2018. Prevalence of Homologous Recombination-Related Gene Mutations Across Multiple Cancer Types. *JCO Precis Oncol* **2018**.

Helleday T. 2010. Homologous recombination in cancer development, treatment and development of drug resistance. *Carcinogenesis* **31**: 955-960.

Hendriks IA, Lyon D, Young C, Jensen LJ, Vertegaal AC, Nielsen ML. 2017. Site-specific mapping of the human SUMO proteome reveals co-modification with phosphorylation. *Nat Struct Mol Biol* **24**: 325-336.

Henson SE, Tsai SC, Malone CS, Soghomonian SV, Ouyang Y, Wall R, Marahrens Y, Teitell MA. 2006. Pir51, a Rad51-interacting protein with high expression in aggressive lymphoma, controls mitomycin C sensitivity and prevents chromosomal breaks. *Mutat Res* **601**: 113-124.

Heyer WD, Li X, Rolfsmeier M, Zhang XP. 2006. Rad54: the Swiss Army knife of homologous recombination? *Nucleic Acids Res* **34**: 4115-4125.

Hill SJ, Clark AP, Silver DP, Livingston DM. 2014. BRCA1 pathway function in basal-like breast cancer cells. *Mol Cell Biol* **34**: 3828-3842.

Hiramoto T, Nakanishi T, Sumiyoshi T, Fukuda T, Matsuura S, Tauchi H, Komatsu K, Shibasaki Y, Inui H, Watatani M et al. 1999. Mutations of a novel human RAD54 homologue, RAD54B, in primary cancer. *Oncogene* **18**: 3422-3426.

Hwang JC, Sung WW, Tu HP, Hsieh KC, Yeh CM, Chen CJ, Tai HC, Hsu CT, Shieh GS, Chang JG et al. 2015. The Overexpression of FEN1 and RAD54B May Act as Independent Prognostic Factors of Lung Adenocarcinoma. *PLoS One* **10**: e0139435.

Ira G, Pellicioli A, Balijja A, Wang X, Fiorani S, Carotenuto W, Liberi G, Bressan D, Wan L, Hollingsworth NM et al. 2004. DNA end resection, homologous recombination and DNA damage checkpoint activation require CDK1. *Nature* **431**: 1011-1017.

Jaskelioff M, Van Komen S, Krebs JE, Sung P, Peterson CL. 2003. Rad54p is a chromatin remodeling enzyme required for heteroduplex DNA joint formation with chromatin. *J Biol Chem* **278**: 9212-9218.

Jensen RB, Carreira A, Kowalczykowski SC. 2010. Purified human BRCA2 stimulates RAD51-mediated recombination. *Nature* **467**: 678-683.

Kadyk LC, Hartwell LH. 1992. Sister chromatids are preferred over homologs as substrates for recombinational repair in Saccharomyces cerevisiae. *Genetics* **132**: 387-402.

Keung MY, Wu Y, Badar F, Vadgama JV. 2020. Response of Breast Cancer Cells to PARP Inhibitors Is Independent of BRCA Status. *J Clin Med* **9**.

Keung MYT, Wu Y, Vadgama JV. 2019. PARP Inhibitors as a Therapeutic Agent for Homologous Recombination Deficiency in Breast Cancers. *J Clin Med* **8**.

Kirshner M, Rathavs M, Nizan A, Essers J, Kanaar R, Shiloh Y, Barzilai A. 2009. Analysis of the relationships between ATM and the Rad54 paralogs involved in homologous recombination repair. *DNA Repair (Amst)* **8**: 253-261.

Klein HL. 1997. RDH54, a RAD54 homologue in Saccharomyces cerevisiae, is required for mitotic diploid-specific recombination and repair and for meiosis. *Genetics* **147**: 1533-1543.

Kovalenko OV, Golub EI, Bray-Ward P, Ward DC, Radding CM. 1997. A novel nucleic acid-binding protein that interacts with human rad51 recombinase. *Nucleic Acids Res* **25**: 4946-4953.

Kovalenko OV, Wiese C, Schild D. 2006. RAD51AP2, a novel vertebrate- and meiotic-specific protein, shares a conserved RAD51-interacting C-terminal domain with RAD51AP1/PIR51. *Nucleic Acids Res* **34**: 5081-5092.

Krejci L, Altmannova V, Spirek M, Zhao X. 2012. Homologous recombination and its regulation. *Nucleic Acids Res* **40**: 5795-5818.

Kuznetsov SG, Haines DC, Martin BK, Sharan SK. 2009. Loss of Rad51c leads to embryonic lethality and modulation of Trp53-dependent tumorigenesis in mice. *Cancer Res* **69**: 863-872.

Lamoliatte F, McManus FP, Maarifi G, Chelbi-Alix MK, Thibault P. 2017. Uncovering the SUMOylation and ubiquitylation crosstalk in human cells using sequential peptide immunopurification. *Nat Commun* **8**: 14109.

Landry JJ, Pyl PT, Rausch T, Zichner T, Tekkedil MM, Stutz AM, Jauch A, Aiyar RS, Pau G, Delhomme N et al. 2013. The genomic and transcriptomic landscape of a HeLa cell line. *G3 (Bethesda)* **3**: 1213-1224.

Lee Bi BI, Nguyen LH, Barsky D, Fernandes M, Wilson DM, 3rd. 2002. Molecular interactions of human Exo1 with DNA. *Nucleic Acids Res* **30**: 942-949.

Lee JH, Paull TT. 2005. ATM activation by DNA double-strand breaks through the Mre11-Rad50-Nbs1 complex. *Science* **308**: 551-554.

Li S, Xuan Y, Gao B, Sun X, Miao S, Lu T, Wang Y, Jiao W. 2018. Identification of an eight-gene prognostic signature for lung adenocarcinoma. *Cancer Manag Res* **10**: 3383-3392.

Liang F, Longerich S, Miller AS, Tang C, Buzovetsky O, Xiong Y, Maranon DG, Wiese C, Kupfer GM, Sung P. 2016. Promotion of RAD51-Mediated Homologous DNA Pairing by the RAD51AP1-UAF1 Complex. *Cell Rep* **15**: 2118-2126.

Liang F, Miller AS, Longerich S, Tang C, Maranon D, Williamson EA, Hromas R, Wiese C, Kupfer GM, Sung P. 2019. DNA requirement in FANCD2 deubiquitination by USP1-UAF1-RAD51AP1 in the Fanconi anemia DNA damage response. *Nat Commun* **10**: 2849.

Liang F, Miller AS, Tang C, Maranon D, Williamson EA, Hromas R, Wiese C, Zhao W, Sung P, Kupfer GM. 2020. The DNA-binding activity of USP1-associated factor 1 is required for efficient RAD51-mediated homologous DNA pairing and homology-directed DNA repair. *J Biol Chem* **295**: 8186-8194.

Lim DS, Hasty P. 1996. A mutation in mouse rad51 results in an early embryonic lethal that is suppressed by a mutation in p53. *Mol Cell Biol* **16**: 7133-7143.

Lim G, Chang Y, Huh WK. 2020. Phosphoregulation of Rad51/Rad52 by CDK1 functions as a molecular switch for cell cycle-specific activation of homologous recombination. *Sci Adv* **6**: eaay2669.

Lisby M, Barlow JH, Burgess RC, Rothstein R. 2004. Choreography of the DNA damage response: spatiotemporal relationships among checkpoint and repair proteins. *Cell* **118**: 699-713.

Liu J, Ede C, Wright WD, Gore SK, Jenkins SS, Freudenthal BD, Todd Washington M, Veaute X, Heyer WD. 2017. Srs2 promotes synthesis-dependent strand annealing by disrupting DNA polymerase delta-extending D-loops. *Elife* **6**.

Ludwig T, Chapman DL, Papaioannou VE, Efstratiadis A. 1997. Targeted mutations of breast cancer susceptibility gene homologs in mice: lethal phenotypes of Brca1, Brca2, Brca1/Brca2, Brca1/p53, and Brca2/p53 nullizygous embryos. *Genes Dev* **11**: 1226-1241.

Mah LJ, El-Osta A, Karagiannis TC. 2010. gammaH2AX: a sensitive molecular marker of DNA damage and repair. *Leukemia* **24**: 679-686.

Maranon DG, Sharma N, Huang Y, Selemenakis P, Wang M, Altina N, Zhao W, Wiese C. 2020. NUCKS1 promotes RAD54 activity in homologous recombination DNA repair. *J Cell Biol* **219**.

Martin RW, Orelli BJ, Yamazoe M, Minn AJ, Takeda S, Bishop DK. 2007. RAD51 up-regulation bypasses BRCA1 function and is a common feature of BRCA1-deficient breast tumors. *Cancer Res* **67**: 9658-9665.

Maser RS, Monsen KJ, Nelms BE, Petrini JH. 1997. hMre11 and hRad50 nuclear foci are induced during the normal cellular response to DNA double-strand breaks. *Mol Cell Biol* **17**: 6087-6096.

Mason-Osann E, Terranova K, Lupo N, Lock YJ, Carson LM, Flynn RL. 2020. RAD54 promotes alternative lengthening of telomeres by mediating branch migration. *EMBO Rep* **21**: e49495.

Mason JM, Dusad K, Wright WD, Grubb J, Budke B, Heyer WD, Connell PP, Weichselbaum RR, Bishop DK. 2015. RAD54 family translocases counter genotoxic effects of RAD51 in human tumor cells. *Nucleic Acids Res* **43**: 3180-3196.

Masuda-Sasa T, Imamura O, Campbell JL. 2006. Biochemical analysis of human Dna2. *Nucleic Acids Res* **34**: 1865-1875.

Matsuda M, Miyagawa K, Takahashi M, Fukuda T, Kataoka T, Asahara T, Inui H, Watatani M, Yasutomi M, Kamada N et al. 1999. Mutations in the RAD54 recombination gene in primary cancers. *Oncogene* **18**: 3427-3430.

Matsuoka S, Ballif BA, Smogorzewska A, McDonald ER, 3rd, Hurov KE, Luo J, Bakalarski CE, Zhao Z, Solimini N, Lerenthal Y et al. 2007. ATM and ATR substrate analysis reveals extensive protein networks responsive to DNA damage. *Science* **316**: 1160-1166.

Mazin AV, Alexeev AA, Kowalczykowski SC. 2003. A novel function of Rad54 protein. Stabilization of the Rad51 nucleoprotein filament. *J Biol Chem* **278**: 14029-14036.

Mazin AV, Bornarth CJ, Solinger JA, Heyer WD, Kowalczykowski SC. 2000. Rad54 protein is targeted to pairing loci by the Rad51 nucleoprotein filament. *Mol Cell* **6**: 583-592.

Mazin AV, Mazina OM, Bugreev DV, Rossi MJ. 2010. Rad54, the motor of homologous recombination. *DNA Repair (Amst)* **9**: 286-302.

Mazina OM, Rossi MJ, Thomaa NH, Mazin AV. 2007. Interactions of human rad54 protein with branched DNA molecules. *J Biol Chem* **282**: 21068-21080.

McAndrew EN, McManus KJ. 2017. The enigmatic oncogene and tumor suppressor-like properties of RAD54B: Insights into genome instability and cancer. *Genes Chromosomes Cancer* **56**: 513-523.

Meng X, Zhao X. 2017. Replication fork regression and its regulation. *FEMS Yeast Res* **17**.

Messiaen S, Le Bras A, Duquenne C, Barroca V, Moison D, Dechamps N, Doussau M, Bauchet AL, Guerquin MJ, Livera G et al. 2013. Rad54 is required for the normal development of male and female germ cells and contributes to the maintainance of their genome integrity after genotoxic stress. *Cell Death Dis* **4**: e774.

Mimitou EP, Symington LS. 2008. Sae2, Exo1 and Sgs1 collaborate in DNA double-strand break processing. *Nature* **455**: 770-774.

Mizuta R, LaSalle JM, Cheng HL, Shinohara A, Ogawa H, Copeland N, Jenkins NA, Lalande M, Alt FW. 1997. RAB22 and RAB163/mouse BRCA2: proteins that specifically interact with the RAD51 protein. *Proc Natl Acad Sci U S A* **94**: 6927-6932.

Modesti M, Budzowska M, Baldeyron C, Demmers JA, Ghirlando R, Kanaar R. 2007. RAD51AP1 is a structure-specific DNA binding protein that stimulates joint molecule formation during RAD51-mediated homologous recombination. *Mol Cell* **28**: 468-481.

Nguyen LK, Kolch W, Kholodenko BN. 2013. When ubiquitination meets phosphorylation: a systems biology perspective of EGFR/MAPK signalling. *Cell Commun Signal* **11**: 52.

Obama K, Satoh S, Hamamoto R, Sakai Y, Nakamura Y, Furukawa Y. 2008. Enhanced expression of RAD51 associating protein-1 is involved in the growth of intrahepatic cholangiocarcinoma cells. *Clin Cancer Res* **14**: 1333-1339.

Olivieri M, Cho T, Alvarez-Quilon A, Li K, Schellenberg MJ, Zimmermann M, Hustedt N, Rossi SE, Adam S, Melo H et al. 2020. A Genetic Map of the Response to DNA Damage in Human Cells. *Cell* **182**: 481-496 e421.

Parplys AC, Kratz K, Speed MC, Leung SG, Schild D, Wiese C. 2014. RAD51AP1-deficiency in vertebrate cells impairs DNA replication. *DNA Repair (Amst)* **24**: 87-97.

Parplys AC, Zhao W, Sharma N, Groesser T, Liang F, Maranon DG, Leung SG, Grundt K, Dray E, Idate R et al. 2015. NUCKS1 is a novel RAD51AP1 paralog important for homologous recombination and genome stability. *Nucleic Acids Res* **43**: 9817-9834.

Pathania R, Ramachandran S, Mariappan G, Thakur P, Shi H, Choi JH, Manicassamy S, Kolhe R, Prasad PD, Sharma S et al. 2016. Combined Inhibition of DNMT and HDAC Blocks the Tumorigenicity of Cancer Stem-like Cells and Attenuates Mammary Tumor Growth. *Cancer Res* **76**: 3224-3235.

Paull TT, Rogakou EP, Yamazaki V, Kirchgessner CU, Gellert M, Bonner WM. 2000. A critical role for histone H2AX in recruitment of repair factors to nuclear foci after DNA damage. *Curr Biol* **10**: 886-895.

Perera JR, Glasunov AV, Glaser VM, Boreiko AV. 1988. Repair of double-strand breaks in plasmid DNA in the yeast Saccharomyces cerevisiae. *Mol Gen Genet* **213**: 421-424.

Petukhova G, Stratton S, Sung P. 1998. Catalysis of homologous DNA pairing by yeast Rad51 and Rad54 proteins. *Nature* **393**: 91-94.

Petukhova G, Sung P, Klein H. 2000. Promotion of Rad51-dependent D-loop formation by yeast recombination factor Rdh54/Tid1. *Genes Dev* **14**: 2206-2215.

Petukhova G, Van Komen S, Vergano S, Klein H, Sung P. 1999. Yeast Rad54 promotes Rad51-dependent homologous DNA pairing via ATP hydrolysis-driven change in DNA double helix conformation. *J Biol Chem* **274**: 29453-29462.

Pires E, Sharma N, Selemenakis P, Wu B, Huang Y, Zhao W, Wiese C. 2020. RAD51AP1 mediates RAD51 activity through nucleosome interaction. *bioRxiv*: 2020.2012.2017.421636.

Pires E, Sung P, Wiese C. 2017. Role of RAD51AP1 in homologous recombination DNA repair and carcinogenesis. *DNA Repair (Amst)* **59**: 76-81.

Poti A, Gyergyak H, Nemeth E, Rusz O, Toth S, Kovacshazi C, Chen D, Szikriszt B, Spisak S, Takeda S et al. 2019. Correlation of homologous recombination deficiency induced mutational signatures with sensitivity to PARP inhibitors and cytotoxic agents. *Genome Biol* **20**: 240.

Prado F. 2018. Homologous Recombination: To Fork and Beyond. *Genes (Basel)* **9**.

Qiu HZ, Huang J, Xiang CC, Li R, Zuo ED, Zhang Y, Shan L, Cheng X. 2020. Screening and Discovery of New Potential Biomarkers and Small Molecule Drugs for Cervical Cancer: A Bioinformatics Analysis. *Technol Cancer Res Treat* **19**: 1533033820980112.

Rasio D, Murakumo Y, Robbins D, Roth T, Silver A, Negrini M, Schmidt C, Burczak J, Fishel R, Croce CM. 1997. Characterization of the human homologue of RAD54: a gene located on chromosome 1p32 at a region of high loss of heterozygosity in breast tumors. *Cancer Res* **57**: 2378-2383.

Reginato G, Cejka P. 2020. The MRE11 complex: A versatile toolkit for the repair of broken DNA. *DNA Repair (Amst)* **91-92**: 102869.

Riaz N, Blecua P, Lim RS, Shen R, Higginson DS, Weinhold N, Norton L, Weigelt B, Powell SN, Reis-Filho JS. 2017. Pan-cancer analysis of bi-allelic alterations in homologous recombination DNA repair genes. *Nat Commun* **8**: 857.

Rijkers T, Van Den Ouweland J, Morolli B, Rolink AG, Baarends WM, Van Sloun PP, Lohman PH, Pastink A. 1998. Targeted inactivation of mouse RAD52 reduces homologous recombination but not resistance to ionizing radiation. *Mol Cell Biol* **18**: 6423-6429.

Ristic D, Wyman C, Paulusma C, Kanaar R. 2001. The architecture of the human Rad54-DNA complex provides evidence for protein translocation along DNA. *Proc Natl Acad Sci U S A* **98**: 8454-8460.

Rivina L, Davoren MJ, Schiestl RH. 2016. Mouse models for radiation-induced cancers. *Mutagenesis* **31**: 491-509.

Robison JG, Dixon K, Bissler JJ. 2007. Cell cycle-and proteasome-dependent formation of etoposide-induced replication protein A (RPA) or Mre11/Rad50/Nbs1 (MRN) complex repair foci. *Cell Cycle* **6**: 2399-2407.

Rogakou EP, Boon C, Redon C, Bonner WM. 1999. Megabase chromatin domains involved in DNA double-strand breaks in vivo. *J Cell Biol* **146**: 905-916.

Rossi MJ, Mazin AV. 2008. Rad51 protein stimulates the branch migration activity of Rad54 protein. *J Biol Chem* **283**: 24698-24706.

Russo A, Cordelli E, Salvitti T, Palumbo E, Pacchierotti F. 2018. Rad54/Rad54B deficiency is associated to increased chromosome breakage in mouse spermatocytes. *Mutagenesis* **33**: 323-332.

Sakai W, Swisher EM, Karlan BY, Agarwal MK, Higgins J, Friedman C, Villegas E, Jacquemont C, Farrugia DJ, Couch FJ et al. 2008. Secondary mutations as a mechanism of cisplatin resistance in BRCA2-mutated cancers. *Nature* **451**: 1116-1120.

Sarai N, Kagawa W, Fujikawa N, Saito K, Hikiba J, Tanaka K, Miyagawa K, Kurumizaka H, Yokoyama S. 2008. Biochemical analysis of the N-terminal domain of human RAD54B. *Nucleic Acids Res* **36**: 5441-5450.

Sartori AA, Lukas C, Coates J, Mistrik M, Fu S, Bartek J, Baer R, Lukas J, Jackson SP. 2007. Human CtIP promotes DNA end resection. *Nature* **450**: 509-514.

Schlacher K, Christ N, Siaud N, Egashira A, Wu H, Jasin M. 2011. Double-strand break repair-independent role for BRCA2 in blocking stalled replication fork degradation by MRE11. *Cell* **145**: 529-542.

Schlacher K, Wu H, Jasin M. 2012. A distinct replication fork protection pathway connects Fanconi anemia tumor suppressors to RAD51-BRCA1/2. *Cancer Cell* **22**: 106-116.

Schwacha A, Kleckner N. 1995. IDENTIFICATION OF DOUBLE HOLLIDAY JUNCTIONS AS INTERMEDIATES IN MEIOTIC RECOMBINATION. *Cell* **83**: 783-791.

Scully R, Chen J, Plug A, Xiao Y, Weaver D, Feunteun J, Ashley T, Livingston DM. 1997. Association of BRCA1 with Rad51 in mitotic and meiotic cells. *Cell* **88**: 265-275.

Scully R, Panday A, Elango R, Willis NA. 2019. DNA double-strand break repair-pathway choice in somatic mammalian cells. *Nat Rev Mol Cell Biol* **20**: 698-714.

Sharan SK, Morimatsu M, Albrecht U, Lim DS, Regel E, Dinh C, Sands A, Eichele G, Hasty P, Bradley A. 1997. Embryonic lethality and radiation hypersensitivity mediated by Rad51 in mice lacking Brca2. *Nature* **386**: 804-810.

Shinohara M, Gasior SL, Bishop DK, Shinohara A. 2000. Tid1/Rdh54 promotes colocalization of rad51 and dmc1 during meiotic recombination. *Proc Natl Acad Sci U S A* **97**: 10814-10819.

Silver DP, Livingston DM. 2012. Mechanisms of BRCA1 tumor suppression. *Cancer Discov* **2**: 679-684.

Singleton MR, Dillingham MS, Wigley DB. 2007. Structure and mechanism of helicases and nucleic acid translocases. *Annu Rev Biochem* **76**: 23-50.

Snow R. 1967. Mutants of yeast sensitive to ultraviolet light. *J Bacteriol* **94**: 571-575.

Solinger JA, Heyer WD. 2001. Rad54 protein stimulates the postsynaptic phase of Rad51 protein-mediated DNA strand exchange. *Proc Natl Acad Sci U S A* **98**: 8447-8453.

Solinger JA, Lutz G, Sugiyama T, Kowalczykowski SC, Heyer WD. 2001. Rad54 protein stimulates heteroduplex DNA formation in the synaptic phase of DNA strand exchange via specific interactions with the presynaptic Rad51 nucleoprotein filament. *J Mol Biol* **307**: 1207-1221.

Song H, Xia SL, Liao C, Li YL, Wang YF, Li TP, Zhao MJ. 2004. Genes encoding Pir51, Beclin 1, RbAp48 and aldolase b are up or down-regulated in human primary hepatocellular carcinoma. *World J Gastroenterol* **10**: 509-513.

Sonoda E, Sasaki MS, Buerstedde JM, Bezzubova O, Shinohara A, Ogawa H, Takata M, Yamaguchi-Iwai Y, Takeda S. 1998. Rad51-deficient vertebrate cells accumulate chromosomal breaks prior to cell death. *EMBO J* **17**: 598-608.

Spies J, Waizenegger A, Barton O, Sürder M, Wright William D, Heyer W-D, Löbrich M. 2016. Nek1 Regulates Rad54 to Orchestrate Homologous Recombination and Replication Fork Stability. *Molecular Cell* **62**: 903-917.

Stehmeier P, Muller S. 2009. Phospho-regulated SUMO interaction modules connect the SUMO system to CK2 signaling. *Mol Cell* **33**: 400-409.

Sung P, Klein H. 2006. Mechanism of homologous recombination: mediators and helicases take on regulatory functions. *Nat Rev Mol Cell Biol* **7**: 739-750.

Swagemakers SM, Essers J, de Wit J, Hoeijmakers JH, Kanaar R. 1998. The human RAD54 recombinational DNA repair protein is a double-stranded DNA-dependent ATPase. *J Biol Chem* **273**: 28292-28297.

Swisher EM, Sakai W, Karlan BY, Wurz K, Urban N, Taniguchi T. 2008. Secondary BRCA1 mutations in BRCA1-mutated ovarian carcinomas with platinum resistance. *Cancer Res* **68**: 2581-2586.

Taglialatela A, Alvarez S, Leuzzi G, Sannino V, Ranjha L, Huang JW, Madubata C, Anand R, Levy B, Rabadan R et al. 2017. Restoration of Replication Fork Stability in BRCA1- and BRCA2-Deficient Cells by Inactivation of SNF2-Family Fork Remodelers. *Mol Cell* **68**: 414-430 e418.

Takata M, Sasaki MS, Sonoda E, Morrison C, Hashimoto M, Utsumi H, Yamaguchi-Iwai Y, Shinohara A, Takeda S. 1998. Homologous recombination and non-homologous end-joining pathways of DNA double-strand break repair have overlapping roles in the maintenance of chromosomal integrity in vertebrate cells. *EMBO J* **17**: 5497-5508.

Tan TL, Essers J, Citterio E, Swagemakers SM, de Wit J, Benson FE, Hoeijmakers JH, Kanaar R. 1999. Mouse Rad54 affects DNA conformation and DNA-damage-induced Rad51 foci formation. *Curr Biol* **9**: 325-328.

Tanaka K, Hiramoto T, Fukuda T, Miyagawa K. 2000. A novel human rad54 homologue, Rad54B, associates with Rad51. *J Biol Chem* **275**: 26316-26321.

Tanaka K, Kagawa W, Kinebuchi T, Kurumizaka H, Miyagawa K. 2002. Human Rad54B is a double-stranded DNA-dependent ATPase and has biochemical properties different from its structural homolog in yeast, Tid1/Rdh54. *Nucleic Acids Res* **30**: 1346-1353.

Tanori M, Casciati A, Berardinelli F, Leonardi S, Pasquali E, Antonelli F, Tanno B, Giardullo P, Pannicelli A, Babini G et al. 2017. Synthetic lethal genetic interactions between Rad54 and PARP-1 in mouse development and oncogenesis. *Oncotarget* **8**: 100958-100974.

Tkach JM, Yimit A, Lee AY, Riffle M, Costanzo M, Jaschob D, Hendry JA, Ou J, Moffat J, Boone C et al. 2012. Dissecting DNA damage response pathways by analysing protein localization and abundance changes during DNA replication stress. *Nat Cell Biol* **14**: 966-976.

Toone WM, Aerne BL, Morgan BA, Johnston LH. 1997. Getting started: regulating the initiation of DNA replication in yeast. *Annu Rev Microbiol* **51**: 125-149.

Tsuzuki T, Fujii Y, Sakumi K, Tominaga Y, Nakao K, Sekiguchi M, Matsushiro A, Yoshimura Y, MoritaT. 1996. Targeted disruption of the Rad51 gene leads to lethality in embryonic mice. *Proc Natl Acad Sci U S A* **93**: 6236-6240.

Van Komen S, Petukhova G, Sigurdsson S, Stratton S, Sung P. 2000. Superhelicity-driven homologous DNA pairing by yeast recombination factors Rad51 and Rad54. *Mol Cell* **6**: 563-572.

Van Komen S, Petukhova G, Sigurdsson S, Sung P. 2002. Functional cross-talk among Rad51, Rad54, and replication protein A in heteroduplex DNA joint formation. *J Biol Chem* **277**: 43578-43587.

Wagner SA, Oehler H, Voigt A, Dalic D, Freiwald A, Serve H, Beli P. 2016. ATR inhibition rewires cellular signaling networks induced by replication stress. *Proteomics* **16**: 402-416.

Wang H, Shi LZ, Wong CC, Han X, Hwang PY, Truong LN, Zhu Q, Shao Z, Chen DJ, Berns MW et al. 2013. The interaction of CtIP and Nbs1 connects CDK and ATM to regulate HR-mediated double-strand break repair. *PLoS Genet* **9**: e1003277.

Wang L, Liang C, Li F, Guan D, Wu X, Fu X, Lu A, Zhang G. 2017a. PARP1 in Carcinomas and PARP1 Inhibitors as Antineoplastic Drugs. *Int J Mol Sci* **18**.

Wang W, Daley JM, Kwon Y, Krasner DS, Sung P. 2017b. Plasticity of the Mre11-Rad50-Xrs2-Sae2 nuclease ensemble in the processing of DNA-bound obstacles. *Genes Dev* **31**: 2331-2336.

Wesoly J, Agarwal S, Sigurdsson S, Bussen W, Van Komen S, Qin J, van Steeg H, van Benthem J, Wassenaar E, Baarends WM et al. 2006. Differential contributions of mammalian Rad54 paralogs to recombination, DNA damage repair, and meiosis. *Mol Cell Biol* **26**: 976-989.

Wiese C, Dray E, Groesser T, San Filippo J, Shi I, Collins DW, Tsai MS, Williams GJ, Rydberg B, Sung P et al. 2007. Promotion of homologous recombination and genomic stability by RAD51AP1 via RAD51 recombinase enhancement. *Mol Cell* **28**: 482-490.

Wiwanitkit V. 2007. Structure of human BRCA2-RAD51 by molecular docking study. *Arch Gynecol Obstet* **276**: 625-627.

Wright WD, Heyer WD. 2014. Rad54 functions as a heteroduplex DNA pump modulated by its DNA substrates and Rad51 during D loop formation. *Mol Cell* **53**: 420-432.

Yasuhara T, Suzuki T, Katsura M, Miyagawa K. 2014. Rad54B serves as a scaffold in the DNA damage response that limits checkpoint strength. *Nat Commun* **5**: 5426.

Yu DS, Sonoda E, Takeda S, Huang CL, Pellegrini L, Blundell TL, Venkitaraman AR. 2003. Dynamic control of Rad51 recombinase by self-association and interaction with BRCA2. *Mol Cell* **12**: 1029-1041.

Yuan J, Chen J. 2010. MRE11-RAD50-NBS1 complex dictates DNA repair independent of H2AX. *J Biol Chem* **285**: 1097-1104.

Yuan SS, Lee SY, Chen G, Song M, Tomlinson GE, Lee EY. 1999. BRCA2 is required for ionizing radiation-induced assembly of Rad51 complex in vivo. *Cancer Res* **59**: 3547-3551.

Zafar F, Seidler SB, Kronenberg A, Schild D, Wiese C. 2010. Homologous recombination contributes to the repair of DNA double-strand breaks induced by high-energy iron ions. *Radiat Res* **173**: 27-39.

Zhang Z, Fan HY, Goldman JA, Kingston RE. 2007. Homology-driven chromatin remodeling by human RAD54. *Nat Struct Mol Biol* **14**: 397-405.

Zhao H, Gao Y, Chen Q, Li J, Ren M, Zhao X, Yue W. 2020. RAD51AP1 promotes progression of ovarian cancer via TGF-beta/Smad signalling pathway. *J Cell Mol Med*.

Zhao W, Steinfeld JB, Liang F, Chen X, Maranon DG, Jian Ma C, Kwon Y, Rao T, Wang W, Sheng C et al. 2017. BRCA1-BARD1 promotes RAD51-mediated homologous DNA pairing. *Nature* **550**: 360-365.

Zhou Q, Huang J, Zhang C, Zhao F, Kim W, Tu X, Zhang Y, Nowsheen S, Zhu Q, Deng M et al. 2020. The bromodomain containing protein BRD-9 orchestrates RAD51-RAD54 complex formation and regulates homologous recombination-mediated repair. *Nat Commun* **11**: 2639.

Zhu Z, Chung WH, Shim EY, Lee SE, Ira G. 2008. Sgs1 helicase and two nucleases Dna2 and Exo1 resect DNA double-strand break ends. *Cell* **134**: 981-994.

Zhuang L, Zhang Y, Meng Z, Yang Z. 2020. Oncogenic Roles of RAD51AP1 in Tumor Tissues Related to Overall Survival and Disease-Free Survival in Hepatocellular Carcinoma. *Cancer Control* **27**: 1073274820977149.

CHAPTER TWO

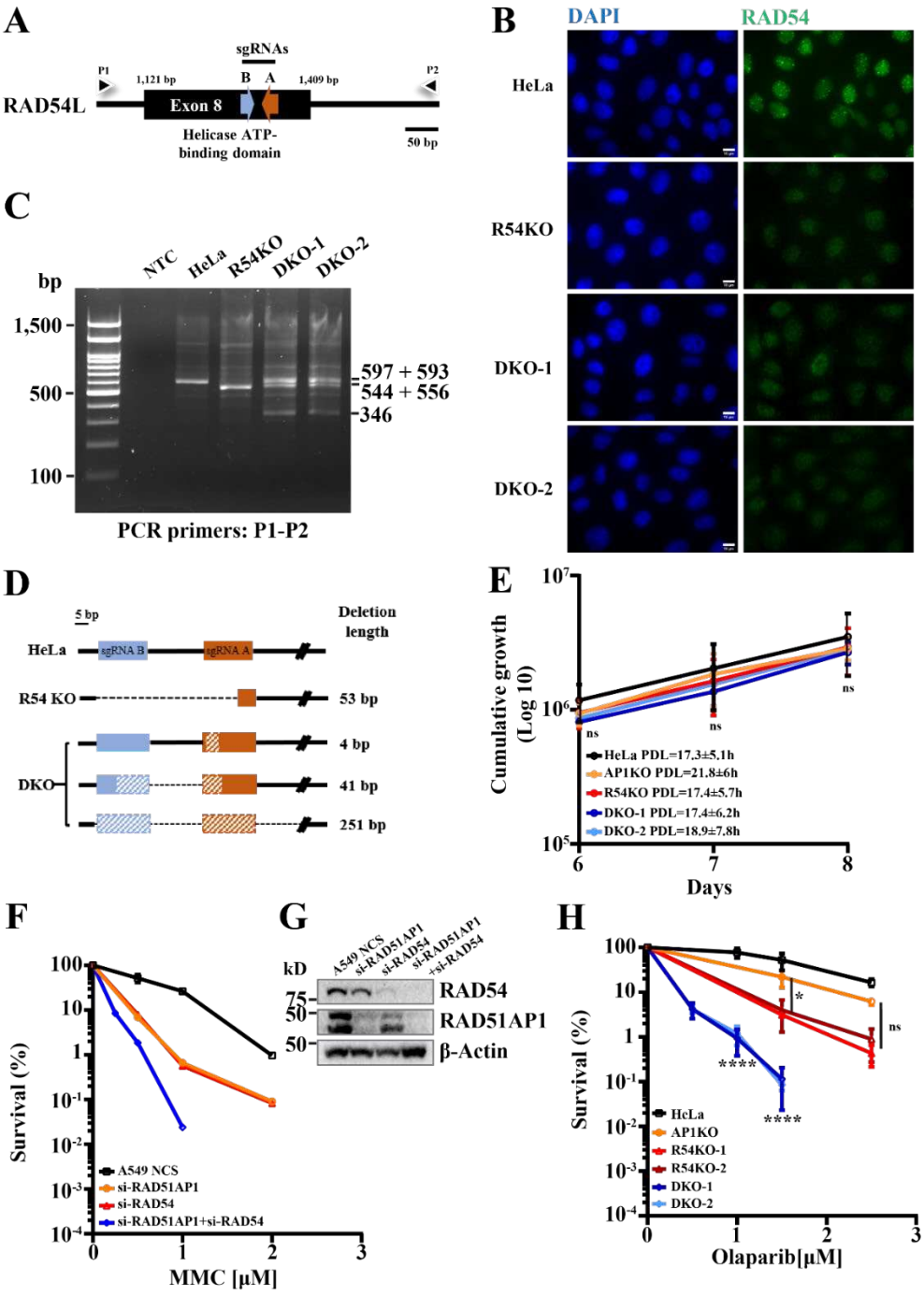

Figure S2.1. Characterization of *RAD51AP1* KO, *RAD54* KO and DKO cells. (A) Schematic of exon 8 and adjacent introns of the human *RAD54* gene with the locations of the sgRNA targeting sequences (see

Table S2.1) and PCR primers (see **Table S2.2**). **(B)** Representative micrographs showing RAD54 foci in HeLa cells, a clonal isolate lacking *RAD54,* and two clonal isolates lacking both *RAD51AP1* and *RAD54* (DKO-1 and DKO-2). Scale bars, 10 μm. **(C)** Representative agarose gel of PCR products obtained from genomic DNA of KO cells using primers P1-P2. **(D)** Schematics of the one *RAD54* KO allele detected in *RAD54* KO cells and the three alleles detected in DKO cells. PCR products from panel **(C)** were purified and amplified by topoisomerase based cloning and sequenced. **(E)** Growth curves of untreated cells. Data points are the means of 3 independent experiments ± 1SD. ns, not significant; two-way ANOVA analysis (Tukey's multiple comparisons test). **(F)** Results from clonogenic survival assays after acute MMC treatment of A549 cells with RAD51AP1 and/or RAD54 depletion. Data points are the means of 3 technical replicates. **(G)** Western blots of whole cell extracts confirming the knockdown of RAD51AP1 and/or RAD54 in A549 cells. The signal of β-actin serves as a loading control. **(H)** Results from clonogenic survival assays after chronic olaparib treatment in cells lacking *RAD51AP1* and/or *RAD54*. Data points are the means from 3 independent experiments ± 1SD. *, $p<0.05$, ***, $p<0.001$, ****, $p<0.0001$, ns, not significant; two-way ANOVA analysis (Dunnett's multiple comparisons test).

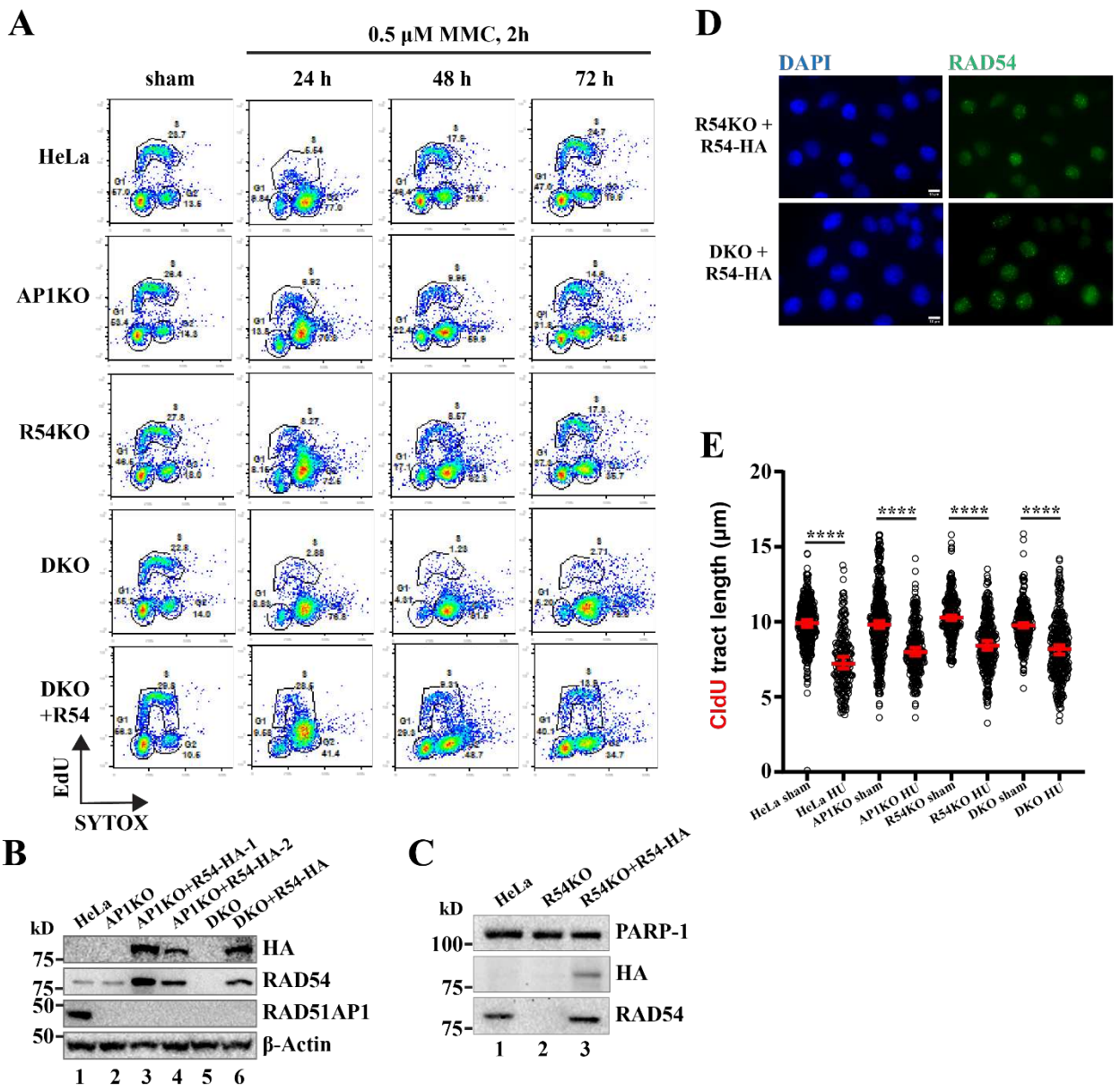

Figure S2.2. Characterization of *RAD51AP1* KO, *RAD54* KO and DKO cells and cells with ectopic RAD54-HA.

(A) Representative flow cytometry dot-plots displaying the distribution of cells in cell cycle phases with and without MMC. **(B)** Western blots of whole extracts to show ectopic expression of RAD54-HA. The signal of β-actin serves as loading control. **(C)** Representative micrographs showing RAD54 foci in *RAD54* KO and DKO cells expressing ectopic RAD54-HA. Scale bars, 10 μm. **(D)** Median CldU (red) tract lengths in cells with or without 4 mM HU. Bars are the medians from 2 independent experiments ±95% CI. *, p<0.05, ***, p<0.001, ****, p<0.0001, ns, not significant; Kruskal-Wallis test (Dunn's multiple comparisons test).

Table S2.1. List of sgRNA sequences used to target Cas9-nic to exon 8 of *RAD54*.

Name	**Target**	**Sequence (listed 5′- 3′)**
sgRNA A	*RAD54* Exon 8	GCCTGGTGAAGAACTGGTAC
sgRNA B	*RAD54* Exon 8	CGGAGGGAGGATCCAACCTC

Table S2.2. List of primer sequences used to amplify the fragment of *RAD54* flanking the sgRNAs.

Primer	**Target**	**Sequence (listed 5′- 3′)**	**Product Length (bp)**
P1	*RAD54 intron*	AGACTACCATCCCTGGGACA	597
P2	*RAD54* intron	TGTTCCCTTTACACCTTTTCTGTTG	

Table S2.3. Median IdU tract lengths with 95% CI under unperturbed conditions (i.e., sham), and *p*-values comparing to DKO cells.

	HeLa sham	**AP1KO sham**	**R54KO sham**	**DKO sham**
Median	9.946	10.33	10.03	9.421
Lower 95% CI	9.803	10.14	9.872	9.149
Upper 95% CI	10.14	10.54	10.2	9.588
***p*-value**	<0.0001	<0.0001	0.0002	-

Table S2.4. Median IdU tract lengths with 95% CI after HU and *p*-values comparing to DKO cells.

	HeLa HU	AP1KO HU	R54KO HU	DKO HU
Median	6.056	5.528	6.905	3.155
Lower 95% CI	5.834	5.322	6.587	2.942
Upper 95% CI	6.385	5.836	7.239	3.305
***p*-value**	<0.0001	<0.0001	<0.0001	-

Table S2.5. Median CldU tract lengths with 95% CI after sham and HU and *p*-values comparing sham to HU.

	HeLa sham	HeLa HU	AP1KO sham	AP1KO HU	R54KO sham	R54KO HU	DKO sham	DKO HU
Median	9.926	7.229	10.12	8.013	10.28	8.424	9.771	8.191
Lower 95% CI	9.679	6.887	9.895	7.761	10.12	8.16	9.629	7.848
Upper 95% CI	10.12	7.675	10.33	8.268	10.43	8.741	9.931	8.446
***p*-value**	<0.0001		<0.0001		<0.0001		<0.0001	

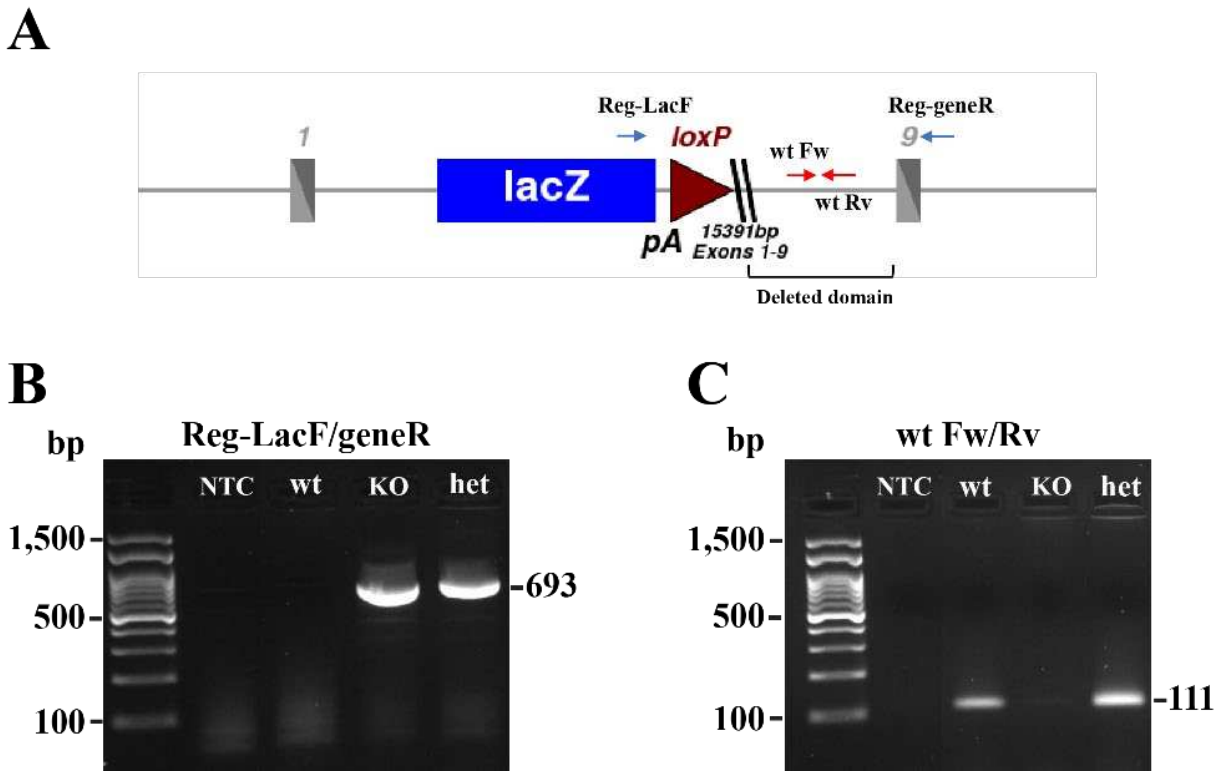

Figure S3.1. Genotyping of *Rad51ap1*$^{+/+}$, *Rad51ap1*$^{+/-}$ and *Rad51ap1*$^{-/-}$ mice. (A) *Rad51ap1*$^{tm1.1(KOMP)Vlcg}$ construct depicting the 15.4 kbp deleted sequence of *Rad51ap1* gene, and the location of the two primer sets used to amplify the wt (wt Fw/Rv) and KO (Reg-LacF/geneR) allele. **(B)** Representative agarose gel analyzing the amplified total DNA from tail snips using primers Reg-LacF/geneR. **(C)** Representative agarose gel analyzing the amplified total DNA from tail snips using primers wt Fw/Rv.

Table S3. 1. List of primer sequences used to amplify wt and KO *Rad51ap1* alleles

Primer	Target	Sequence (listed 5´- 3´)	Product Length (bp)
Reg-LacF	*Rad51ap1* KO allele	ACTTGCTTTAAAAAACCTCCCACA	693
Reg-geneR	*Rad51ap1* KO allele	TACACTAACCACCTGTCCCATGTAGG	
wt Fw	*Rad51ap1* wt allele	GAAGGTTCAGAAAGTGATCCTGA	111
wt Rv	*Rad51ap1* wt allele	TGCAGGTTTCTTCTGCACTG	

Table S4.1. Median IdU tract lengths with 95% CI under unperturbed conditions (i.e., sham), and *p*-values compared to AP1KO-WT.

	AP1KO-WT sham	**AP1KO sham**	**AP1KO-S2D sham**	**AP1KO-S2A sham**
Median	**10.426**	**10.311**	**10.082**	**10.499**
Lower 95% CI	**10.034**	**10.270**	**9.947**	**10.288**
Upper 95% CI	**10.642**	**10.626**	**10.273**	**10.580**
***p*-value**	**-**	**>0.9999**	**>0.9999**	**>0.9999**

Table S4.2. Median IdU tract lengths with 95% CI after HU, and *p*-values compared to AP1KO-WT.

	AP1KO-WT HU	**AP1KO HU**	**AP1KO-S2D HU**	**AP1KO-S2A HU**
Median	**6.552**	**5.528**	**5.937**	**2.844**
Lower 95% CI	**6.411**	**5.587**	**5.963**	**2.886**
Upper 95% CI	**7.180**	**6.098**	**6.337**	**3.235**
***p*-value**	**-**	**0.0013**	**0.3733**	**<0.0001**